Optical Camera Communication Based Li-Fi Systems for Enabling Internet of Optical Things for Smart Buildings

by

Babar HUSSAIN

A Thesis Submitted to

The Hong Kong University of Science and Technology
in Partial Fulfillment of the Requirements for
the Degree of Doctor of Philosophy
in the Department of Electronic and Computer Engineering

August 2021, Hong Kong

i

Authorization

I hereby declare that I am the sole author of the thesis.

I authorize the Hong Kong University of Science and Technology to lend this thesis to other institutions or individuals for the purpose of scholarly research.

I further authorize the Hong Kong University of Science and Technology to reproduce the thesis by photocopying or by other means, in total or in part, at the request of other institutions or individuals for the purpose of scholarly research.

Signature redacted

Babar HUSSAIN

August 2021

Optical Camera Communication Based Li-Fi Systems for Enabling Internet of Optical Things for Smart Buildings

by

Babar HUSSAIN

This is to certify that I have examined the above PhD thesis and have found that it is complete and satisfactory in all respects, and that any and all revisions required by

the thesis examination committee have been made. Signature redacted

Prof. C. Patrick YUE, ECE Department (Thesis Supervisor)
Signature redacted

Prof. Andrew POON (Head of ECE Department)

Thesis Examination Committee:

- Prof. C. Patrick YUE (Supervisor), Department of Electronic and Computer Engineering
- 2. Prof. Weichuan YU, Department of Electronic and Computer Engineering
- 3. Prof. Abhishek Kumar SRIVASTAVA, Department of Electronic and Computer Engineering
- 4. Prof. Lilong CAI, Department of Mechanical and Aerospace Engineering
- Prof. Hao-chung KUO (External Examiner), Department of Photonics, National Yang
 Ming Chiao Tung University

Department of Electronic and Computer Engineering,
The Hong Kong University of Science and Technology
August 2021

To my family

Acknowledgements

I would like to begin with thanking my supervisor, Prof. C. Patrick Yue, who took me under his wing as a Master's student and guided me through to the PhD. He shared wonderful ideas with me that kept me motivated and helped me broaden my horizons. Under his supervision, I learned extremely valuable lessons both in and outside the lab that will continue to help me in my future endeavors.

I am also very thankful to Prof. Weichuan Yu, Prof. Abhishek Kumar Srivastava, Prof. Lilong Cai, and Prof. Hao-chung Kuo for being my thesis examination committee members. They spent their precious time going through my research work and provided invaluable comments and suggestions to help me improve my thesis.

Additionally, I am thankful to my colleagues, both in and outside of my research group, for extending their technical support whenever needed and being wonderful friends and teammates. The list includes, but is not limited to, Dr. Xianbo Li, Dr. Wang Li, Mr. Sam Wang, Dr. Khawaja Qasim Maqbool, Dr. Weimin Shi, Ms. Xuan Wu, Mr. Jian Kang, Ms. Bo Xu, Mr. Fredrick Hong, Ms. Yiru Wang, Mr. Rehan Azmat, Mr. Fuzhan Chen, Ms. Tianxin Min, Ms. Zilu Liu, Mr. Chongyun Zhang and Ms. Xinyi Liu. I should also acknowledge the technical and logistics support from ECE lab technicians Mr. Raymond Wong, and Mr. Frederick Kwok.

I would like to thank my colleagues from LiPHY, Johnny, Rheaa, and Duncan, for their contribution towards software application front-end development and testing, and Dr. Jeff Qiu for his support in Bluetooth firmware development.

I would also like to acknowledge the support that I received from our industrial partners, including Prosperity Lamps and Components Limited, Daikan International Co. Ltd., Infineon Technologies HK Ltd., Play More Ltd., and Maphive Technology Ltd., for their support in providing hardware samples, access to their software platforms, and sharing their industrial know-how to help us improve our design and make it market ready.

Further thanks go to Ms. Tania Wilmshurst for helping me proofread my thesis.

Thanks also to my Pakistani friends, Dr. Faheem Mushtaq, Dr. Asad Iqbal, Dr. Irfan Haider Abidi, Dr. Usman Majeed, Dr. Kishwar Khan and all Eagle-Shaheen members, for the time and fun we had together and for the everlasting sweet memories of their friendship.

To my brother, Dr. Waseem Akhtar, I would like to express my gratitude for putting me on this journey and showing me the importance of pursuing a PhD through his own example. His help and guidance have been an indispensable part of shaping my career.

Lastly, I am very thankful to my family members, especially my mother, for their unconditional love and support.

Table of Contents

Acknowledgements	v
List of Figures	x
List of Tables	xv
Abstract	xvi
CHAPTER 1 Introduction to VLC Systems and their Applications	1
1.1 Introduction to VLC	1
1.2 Types of VLC Systems Based on a Receiver	2
1.2.1 High-Data-Rate VLC Systems using PDs	2
1.2.2 Low-Data-Rate VLC Systems Using Cameras	4
1.3 Visible Light Communication Standard	5
1.4 Applications of Visible Light Communication	8
1.4.1 Location-based Services	9
1.4.2 Augmented Reality and Virtual Reality	11
1.4.3 Robotics	12
1.5 Thesis Organization	13
1.6 References	14
CHAPTER 2 Enabling VLC in LED Lighting and Signage	18
2.1 Related Works	18
2.2 Light Intensity Modulation	20
2.3 Supply and Connectivity for VLC Modulator	21
2.4 Constant Current and Constant Voltage Lighting	22
2.5 Constant Voltage and Constant Current Control	23
2.6 A Universal VLC Modulator Design	24
2.6.1 Voltage Level Conversion and Regulation	24
2.6.2 Voltage Step-down Conversion using Zener Diode	25
2.6.3 Hardware Prototype Design	26
2.7 Bluetooth-based Wireless Control	28
2.7.1 System Architecture	28
2.7.2 VLC Control Signal Generation	29
2.7.3 Flowchart of Configuration	30
2.8 The Effect of Modulation on CC LED Drivers	31
2.8.1 Output Voltage Range of CC LED Drivers and its Impact on LED Brightness	33

2.9 The Effect of Modulation on CV LED Drivers	35
2.10 Methods to Compensate for Brightness Drop in CV LED Drivers	36
2.10.1 Using a Higher Power Supply	37
2.10.2 Using a DC-DC Boost Converter	37
2.10.3 Reducing the Current Limiting Resistors on LED Strips	38
2.10.4 Using a Higher Duty Cycle Digital Coding Scheme	39
2.10.5 Using a Turn-Off Resistor	40
2.11 Impact of Light Modulation on Reliability and Quality of Lighting	41
2.12 References	45
CHAPTER 3 VLC Receiver Design Using CMOS Image Sensor	48
3.1 CMOS Image Sensor for VLC	
3.2 Related Works	49
3.3 VLC Receiver Implementation on Smartphone Camera	52
3.4 Optical Model of Camera for OCC	55
3.5 Choosing an Optimum Modulation Frequency	57
3.6 Choosing Optimum Capture Resolution	59
3.7 Light Shape Dependency on the Detection Performance	60
3.8 Light Color Dependency on the Detection Performance	62
3.9 Dependency on Smartphone Models	64
3.10 OCC System Design Guidelines	
3.11 References	69
CHAPTER 4 Smart Lighting and Displays	73
4.1 Smart Lighting	73
4.1.1 Existing Solutions on Smart Lighting Control	73
4.1.2 VLC-enabled Smart Lighting and Control	75
4.1.3 Smart Lighting Installation and Mapping	76
4.1.4 Smart Lighting with VLC for Location-based Services	78
4.2 Smart Displays	78
4.2.1 Enabling VLC in LCD Displays	80
4.2.2 Design of LCD Display-based VLC System	81
4.2.3 OCC-based Receiver Design for Display	82
4.2.4 Retrofitting an LCD Display Module	82
4.2.5 Experimental Results	84
4.2.6 Sensitivity comparison between LCD display and LED light	84

4.2.7 Dependency of Detection Performance on Display Content and Communication Distance	e 85
4.3 References	86
CHAPTER 5 VLC and PDR-based High Accuracy Indoor Navigation	87
5.1 Introduction	87
5.2 Related Work	89
5.2.1 VLP with PDR	89
5.2.2 Stride-Length Estimation	90
5.2.3 Heading Angle Estimation	91
5.3 Methodology	93
5.3.1 System Overview	93
5.3.2 Dead Reckoning	94
5.3.3 Visible Light Positioning	97
5.3.4 Stride-Length Estimation	99
5.3.5 Heading Angle Correction	103
5.3.6 Software Integration	107
5.4 Experiment and Evaluation	108
5.4.1 Visible Light Positioning	109
5.4.2 Step-Length Estimation	110
5.4.3 Heading Angle Correction	111
5.4.4 Computation Timing	112
5.4.5 Indoor Navigation Performance	113
5.5 Summary	114
5.6 References	115
CHAPTER 6 Conclusion, Future Work and Publications	121
6.1 Summary of Contributions	
6.2 Future Work	122
6.2.1 Indoor Farming Control and Management using VLC integrated Smart Grow Lights	122
6.2.2 Smart Home Appliance Control and Location-Based Access	
6.3 Publications	124
6.3.1 Works under review	124
6.3.2 Published	124

List of Figures

Figure 1.1 LED lighting, signage, and displays as access points
Figure 1.2 A VLC transceiver system with PD-based receiver
Figure 1.3 LiFi providing internet connectivity through indoor lighting [3]
Figure 1.4 A VLC transceiver system with camera-based receiver
Figure 1.5 Using camera to receive information from advertisement display
Figure 1.6 Network topologies in IEEE 802.15.7 standard
Figure 1.7 Modulation domain spectrum of IEEE 802.15.7 PHY
Figure 1.8 Applications of optical wireless communication (OWC) [11]9
Figure 1.9 VLC-enabled position tracking in VR headset
Figure 1.10 VLC-enabled AR
Figure 1.11 Robots can be accurately localized in multi-room and multi-floor buildings through globally
unique VLC-integrated smart LED lights
Figure 2.1 An LED light driven by an LED driver (a) without a modulator (b) with a modulator20
Figure 2.2 Connecting VLC modulator between LED driver and LED light: (a) Option 1: No external
AC needed. Step down LED VDD using on-board LDO; (b) Option 2: Use AC-DC adapter on-board to
convert from external AC
Figure 2.3 Using external PWM dimming control of LED driver for VLC modulation
Figure 2.4 Categories of LED lighting. (a) General lighting using CC LED drivers. (b) Signage and
light boxes using CV LED drivers
Figure 2.5 (a) CV regulation. (b) CC regulation
Figure 2.6 VLC modulator block diagram
Figure 2.7 Voltage level conversation consideration for different LED drivers
Figure 2.8 Adding Zener diode for voltage drop before LDO
Figure 2.9 Block-level schematic of VLC modulator
Figure 2.10 Assembled prototype of VLC modulator
Figure 2.11 The overall architecture of the BLE SoC-based wireless control and iBeacon
Figure 2.12 VLC control signal generation: (a) conventional approach, (b) proposed approach29

Figure 2.13 Flow chart of BLE configuration for setting VLC data and iBeacon	30
Figure 2.14 The effect of modulation on CC LED drivers	31
Figure 2.15 Setup for measuring the effect of modulation on LED driver	32
Figure 2.16 The measured waveform of various CC LED drivers under modulation	32
Figure 2.17 The effect of modulation on a single-stage PFC LED driver	33
Figure 2.18 An example of a modulated LED driver operating near its peak output power	34
Figure 2.19 The effect of modulation on CV LED drivers	35
Figure 2.20 The block diagram of the measurement setup for measuring the effect of modulation	n on CV
LED driver	36
Figure 2.21 The measured current output of the LED driver with and without modulation	36
Figure 2.22 Operating LED luminaire at higher supply voltage to compensate for the drop in bridge	ightness
due to modulation	37
Figure 2.23 Addition of a DC-DC boost converter for brightness drop compensation	38
Figure 2.24 Current limiting resistor modification to compensate for brightness drop	39
Figure 2.25 Extending the period of highs (1s) in digital modulation signals to improve the bri	ightness
of the luminaire	39
Figure 2.26 Using a turn-off resistor for brightness drop compensation	40
Figure 2.27 LED current waveform showing the effect of turn-off resistor on degree of modula	tion.41
Figure 2.28 Power consumption variation during long-term reliability test	43
Figure 2.29 Light intensity variation during long-term reliability test	43
Figure 2.30 Color temperature variation during long-term reliability test	44
Figure 2.31 Chromaticity diagram indicating the deviation in X and Y coordinates during lo	ng-term
reliability test	44
Figure 3.1 A CMOS image sensor: (a) hardware architecture (b) capture timing	48
Figure 3.2 (a) Rolling shutter effect on a CMOS image sensor (b) pattern obtained from a mo	dulated
LED source using a smartphone	49
Figure 3.3 Related Works on OCC	50

Figure 3.4 Contributions of this chapter include the modeling of key system design parameter	ers for
building a practical OCC system for location-based information delivery applications	51
Figure 3.5 Signal processing block diagram of VLC receiver on smartphone	52
Figure 3.6 Image processing steps to decode VLC signal	53
Figure 3.7 VLC Data Packet Format	54
Figure 3.8 Relation between the distance of the object and ROI	55
Figure 3.9 Relation between number of pixels on ROI vs distance	56
Figure 3.10 Images of a round shaped LED light modulated at various frequencies	57
Figure 3.11 Measurement results of frequency and distance dependency on data rate	58
Figure 3.12 The relation between modulation frequency and camera exposure time	58
Figure 3.13 The comparison of optimum and low resolution captured images of light	59
Figure 3.14 Effect of resolution on computation time	60
Figure 3.15 Comparison of captured images of two shapes of modulated LED lights: (a) circuit	lar (b)
rectangular	60
Figure 3.16 Various shapes and sizes of lights used in the experiment	62
Figure 3.17 Measurement results of comparison of light shape and size dependency on det	tection
performance	62
Figure 3.18 Color temperatures of white LED used for general illumination [24]	63
Figure 3.19 Color dependency on communication distance	63
Figure 3.20 Comparison of received lux, grayscale intensity and maximum detection distan	ce for
various color filters	64
Figure 3.21 Detection performance comparison for various models	65
Figure 3.22 Comparison of image-scanning rate of various smartphones	66
Figure 3.23 Comparison of FOV and readout time (t _r) of ten different smartphone models	66
Figure 3.24 OCC system design flow	67
Figure 3.25 Comparison of various smartphone models based on calculated design parameter	rs and
measured performance values	69
Figure 4.1 State-of-the-art technologies for smart lighting systems	73

Figure 4.2 Smart lighting application diagram for lighting control
Figure 4.3 Smart lighting installation and mapping procedure
Figure 4.4 Location-based information delivery system using VLC in smart lighting
Figure 4.5 How VLC can be used to complement state-of-the-art in smart displays
Figure 4.6 Image of a VLC modulated LCD display captured using a CMOS camera under different
exposures8
Figure 4.7 VLC broadcast system using LCD
Figure 4.8 VLC signal detection using CMOS camera on mobile device
Figure 4.9 Retrofitting VLC in LCD module
Figure 4.10 Experiment setup for measuring the performance of LCD-based VLC system
Figure 4.11 Comparison of received signal from an LCD display and LED light
Figure 4.12 Effect of distance and display content on detection performance
Figure 5.1 System Overview: Combined usage of VLC AoA-based positioning and pedestrian dea
reckoning with cloud-controlled backend database to provide high-accuracy indoor localization9
Figure 5.2 Vertical acceleration waveform and smartphone holding state while walking9
Figure 5.3 Comparison of accelerometer waveform recorded from various Android devices9
Figure 5.4 Visible light positioning using optical camera communication: (a) image capture, (b)
processing steps
Figure 5.5 Using visible light positioning for measuring step size of a pedestrian9
Figure 5.6 Front camera view with its corresponding low-exposure image captured while the pedestria
is walking under the light and holding the phone in front, at two instances
Figure 5.7 Step size estimation via partially blocked FoV during pedestrian walking: (a) position
tracking during effective FoV, (b) FoV and height of ceiling
Figure 5.8 Rectangular lighting at commercial and industrial venues
Figure 5.9 Heading angle estimation from rectangular light shape
Figure 5.10 Image processing steps for heading angle correction: (a) grayscale converted image of
square downlight LED panel, (b) corner and median detection (c) corner angles w.r.t to smartphone axis
(d) estimated world orientation of corners and smartphone heading

Figure 5.11 Indoor navigation application architecture.	107
Figure 5.12 Square-shaped smart LED light mounted on an adjustable light pole	108
Figure 5.13 VLC AoA positioning accuracy measurement: (a) measurement setup, (b) cur	mulative
density function of positioning error.	109
Figure 5.14 Cumulative density function (CDF) of step size measurement error	110
Figure 5.15 Step length estimation experiment: (a) VLP tracking results at three different	walking
speeds, (b) setup	111
Figure 5.16 Heading angle estimation error due to camera tilt	111
Figure 5.17 VLC heading angle estimation: (a) cumulative density function of heading estimat	ion error
(b) measurement setup	112
Figure 5.18 VLC AoA algorithm computation time.	113
Figure 5.19 Measurement results of combined VLC and PDR combined algorithm in an area of	f 10 m x
10 m	114
Figure 6.1 VI.C-based Smart Farming System Architecture	122

List of Tables

Table 1.1 Comparison of PD- and camera-based VLC systems	5
Table 1.2 Summary of PHY V modulation, coding schemes and data rates	8
Table 1.3 Comparison of various technologies for location-based applications	10
Table 2.1 Supply options for various LED driver voltage ranges	26
Table 2.2 Selection of CC LED driver for a given power of LED load under modulation	34
Table 2.3 Comparsion of LED light with and without VLC modulator	42
Table 2.4 Long-term Reliability Test of LED luminaire with VLC modulator	42
Table 3.1 OCC system design sepecifications	68

Optical Camera Communication Based Li-Fi Systems for Enabling Internet of Optical Things for Smart Buildings

by

Babar HUSSAIN

Department of Electronic and Computer Engineering,
The Hong Kong University of Science and Technology
August 2021

Abstract

With the rapid growth in the number of smart devices and sensors, the internet of things (IoT) is driving the intelligent transformation of our living spaces. Two of the fundamental requirements for providing any intelligent service inside a smart building are connectivity and localization. However, existing radio frequency-based technologies are neither bandwidth-sufficient nor accurate enough to meet the ever-increasing demand of connectivity and location intelligence, respectively. Therefore, in this thesis, visible light communication (VLC), or Li-Fi is proposed as a solution to this two-fold problem. VLC utilizes the ubiquity of optical devices, which include lighting, signage, and displays, inside a smart building to provide connectivity and location intelligence. In the proposed system, location-based information is broadcasted using optical devices that can be captured by the CMOS image sensor of a smartphone or a robot using optical camera communication (OCC). The OCC-based Li-Fi link is combined with Bluetooth and a cloud-based data collection, processing, and management system to provide location-based services. The design and implementation of the system is divided into three parts.

In the first part, a universal VLC modulator design is presented that can enable VLC in a wide variety of LED lighting, signage, and displays. The modulator can support a wide input

voltage and power range and features a Bluetooth-based wireless control and iBeacon-based proximity sensing to support IoT connectivity and location-based geofencing. Experiments are conducted to verify the modulation function and its impact on the light intensity and reliability.

In the second part, a VLC receiver is implemented using a CMOS image sensor-based rolling shutter camera on a smartphone. The VLC signal is extracted and decoded from the captured images of the light using image processing techniques. The impact of various system parameters including light size, shape, color and smartphone camera hardware, on receiver's sensitivity and detection range is studied. Based on the analysis, practical OCC receiver design guidelines are established.

In the final part, a VLC- and Bluetooth-integrated smart lighting infrastructure is used to enable high-accuracy indoor localization in large-scale venues. The high-accuracy positioning provided by VLC is complemented with a long-range non-line-of-sight Bluetooth and pedestrian dead reckoning algorithm to provide a continuous and smooth indoor positioning experience in various indoor environments with varying densities of lighting.

CHAPTER 1 Introduction to VLC Systems and their Applications

1.1 Introduction to VLC

Rising concerns over energy conservation for a sustainable environment have been driving the research and development of energy-saving green technologies. As an energy-efficient, cost-effective and reliable illumination technology, solid-state lighting using LEDs is being deployed more and more ubiquitously to replace conventional fluorescent and incandescent lights. Due to their inherent fast response, LEDs can also be switched on and off rapidly to modulate lights for information transmission. As their modulation frequency is far beyond the flicker fusion threshold of the human eye, LEDs can be simultaneously utilized as light sources and visible light communication (VLC) access points for next-generation smart building infrastructure, as shown in Figure 1.1.

Compared with the traditional radio frequency (RF) wireless communication, VLC is advantageous in terms of its huge bandwidth in the THz range, license-free operation, no electromagnetic interference and high security due to line-of-sight (LOS) signal propagation. Thus, VLC can be used in places where RF communication is prohibited, for instance hospitals, airplanes etc. However, VLC suffers from the critical drawback that the data rate falls sharply as the distance increases, which in turn limits the communication range [1]. For these reasons, VLC is regarded as a promising technology to supplement conventional RF wireless communications, especially for near-field high-data-rate communications and location-based information delivery for internet of things (IoT) applications.

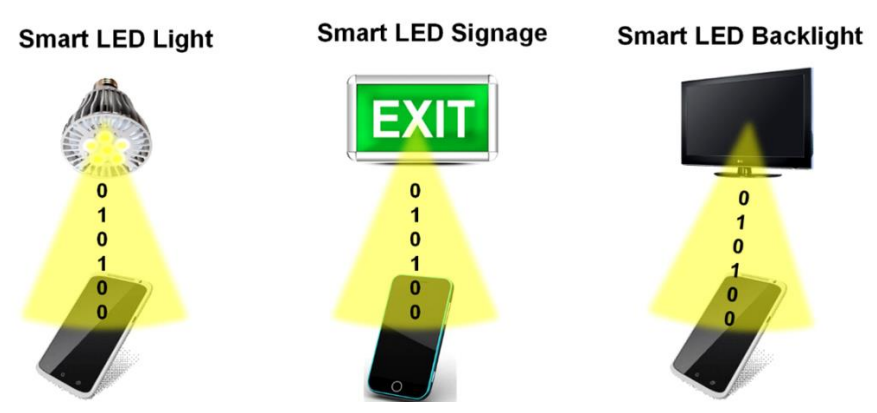


Figure 1.1 LED lighting, signage, and displays as access points

1.2 Types of VLC Systems Based on a Receiver

A complete VLC system, composed of a transmitter and a receiver, is shown in Figure 1.2. The transmitter typically includes a digital baseband, an analog front-end, an LED modulator, an LED driver and several LEDs, while the receiver consists of a photodiode (PD), transimpedance amplifier, filter and digital baseband. The transmitter varies the intensity of the light source at high speeds such that the human eye cannot observe the variation. Meanwhile, the VLC receiver detects the modulated light, converts it to electrical signal and then decodes the data. Various digital and analog modulations, channel and line coding schemes are typically employed to achieve a certain data rate with a target communication distance under specified channel conditions.

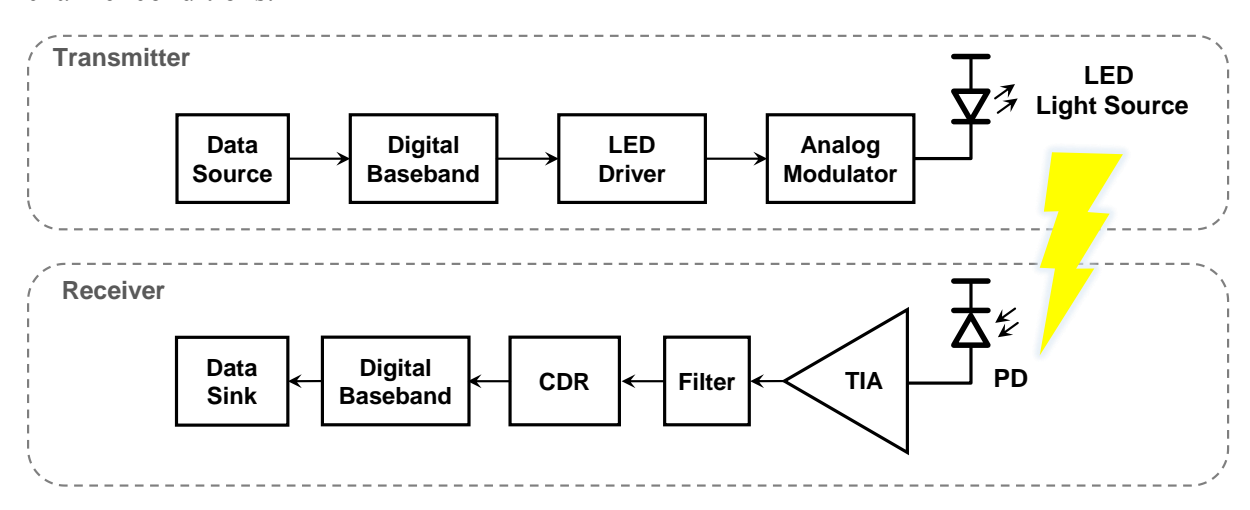


Figure 1.2 A VLC transceiver system with PD-based receiver

VLC systems can be divided into two broad categories from the perspective of the receiver hardware implementation and achievable data rates. The following sections describe each system in detail with their related applications.

1.2.1 High-Data-Rate VLC Systems using PDs

Generally, higher data rate systems use complex modulation schemes and bandwidth extension techniques to achieve such high transmission rates. In addition, a dedicated photodetector (PD)-based receiver with high sensitivity and maximum possible bandwidth is

used in these systems to ensure high data rates. The applications of such data rates enable high-speed data connectivity for two - way VLC, or LiFi applications [2], as shown in Figure 1.3.

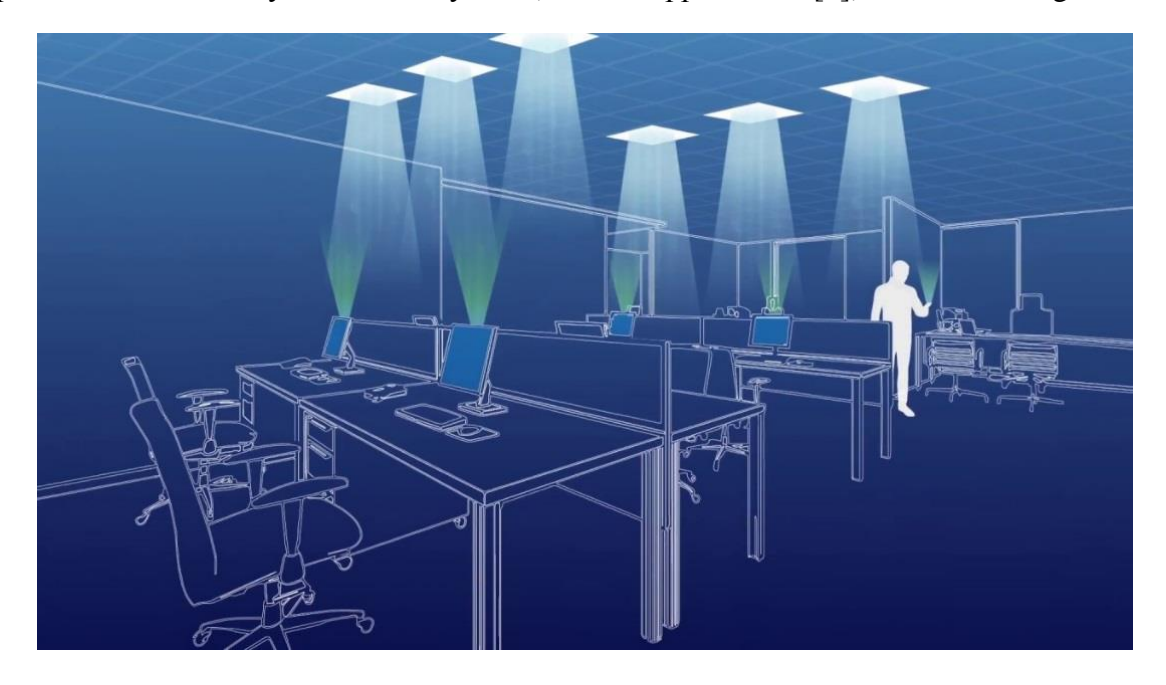


Figure 1.3 LiFi providing internet connectivity through indoor lighting [3]

For commercial white LEDs, data rates of up to 2 Gbps can be achieved using orthogonal frequency division multiplexing (OFDM) and equalization techniques [4]. Data rates can be further extended over 15 Gbps using a combination of red, green, blue and yellow (RGBY) LEDs, as demonstrated in [5]. In addition to the use of commercial LEDs, research on the use of custom-made gallium nitride µLEDs has achieved data rates of several Gbps [6]. However, these high-data-rate systems face many challenges from the perspective of practical system realization. One of the biggest hurdles in implementing a practical high-data-rate LiFi system is the lack of infrastructure support. For instance, there must be backhaul connectivity for LED lighting to connect to the internet backbone. In addition, there must be a channel for uplink on each LED light source to ensure duplex communication, as well as a full duplex receiver capable of transmitting and receiving the VLC signal on consumer devices, for example laptops, computers, smartphones etc. Such a requirement of external hardware on consumer devices is both costly and impractical.

1.2.2 Low-Data-Rate VLC Systems Using Cameras

Low-data-rate VLC systems use lower modulation speeds to enable low-data-rate communication using a camera as a receiver. This, so called, optical camera communication (OCC) uses either global shutter cameras [7], for example digital single-lens reflex (DSLR) cameras, or the rolling shutter camera of a smartphone [8]. The data rates of such systems are limited to a few kbps. Recently, support for camera communication has been included in the IEEE 802.15.7 standard on VLC [9]. A generic block diagram of an OCC system is shown in Figure 1.4.

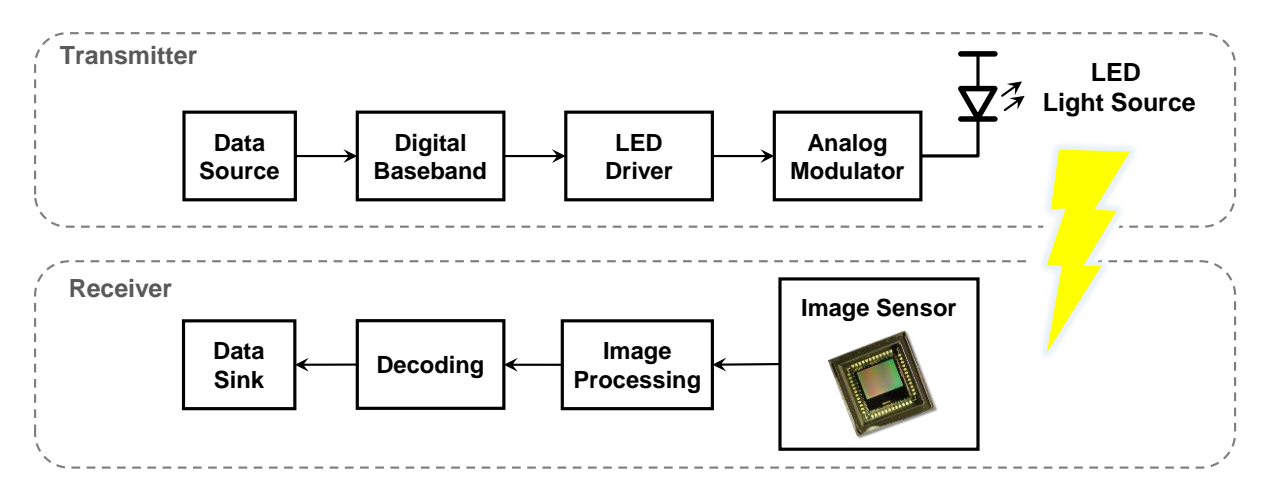


Figure 1.4 A VLC transceiver system with camera-based receiver

One of the major applications for OCC is in providing location-based information, which is the base for many other applications, including indoor positioning, augmented reality (AR), and virtual reality (VR), etc. In addition to its application in indoor lighting, enabling VLC on displays and signage allows it to broadcast information related to the displayed content, as shown in Figure 1.5.

A comparison of PD- and camera-based VLC systems is provided in Table 1.1. Nowadays, CMOS image sensors are available in many consumer electronic devices, including tablets, smartphones and notebooks, etc. This provides a great opportunity to implement OCC systems at a lower cost in comparison to PD-based systems and support a wider range of applications.

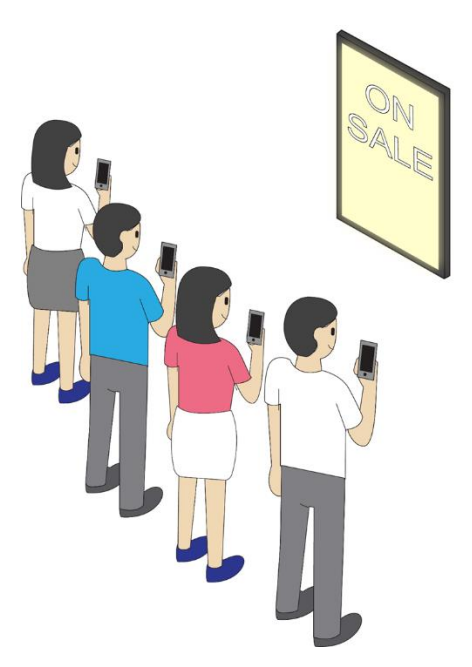


Figure 1.5 Using camera to receive information from advertisement display

Table 1.1 Comparison of PD- and camera-based VLC systems

Receiver Type	PD-based	Camera-based
Data rates	> 10 Gbps	< 10 kbps
Detection Range	Medium	High
Design Complexity	High	Low
Infrastructure	Low	High
Support		
Preferred Modulation	OFDM	OOK, FSK
Applications	Two-way data	IoT, Indoor
	connectivity (LiFi), Video	navigation, AR, VR, V2V,
	streaming, etc.	Smart displays etc.

1.3 Visible Light Communication Standard

The IEEE 802.15.7 standard [9] is developed by a working group of the IEEE 802 standards committee that is responsible for developing standards for wireless personal area networks (WPAN). The standard defines physical layers (PHY) and medium access control (MAC)

layers for short-range wireless optical communication using visible light. The scope of the standard covers the visible light spectrum from 380 nm to 780 nm and delivers data rates sufficient to support audio and video multimedia services. The standard supports three classes of devices, infrastructure, mobile and vehicle, which differ in their operation constraints, e.g. size, mobility, data rate and communication distance etc. Furthermore, the standard defines three network topologies for communication, namely, peer-to-peer, star and broadcast topologies, as illustrated in Figure 1.6. The peer-to-peer topology is VLC communication between two standard transceivers, while the star topology defines a method for communicating between multiple standard transceivers whose communication is coordinated via a coordinator, and the broadcast topology describes unidirectional communication through a single transmitting device to multiple receivers.

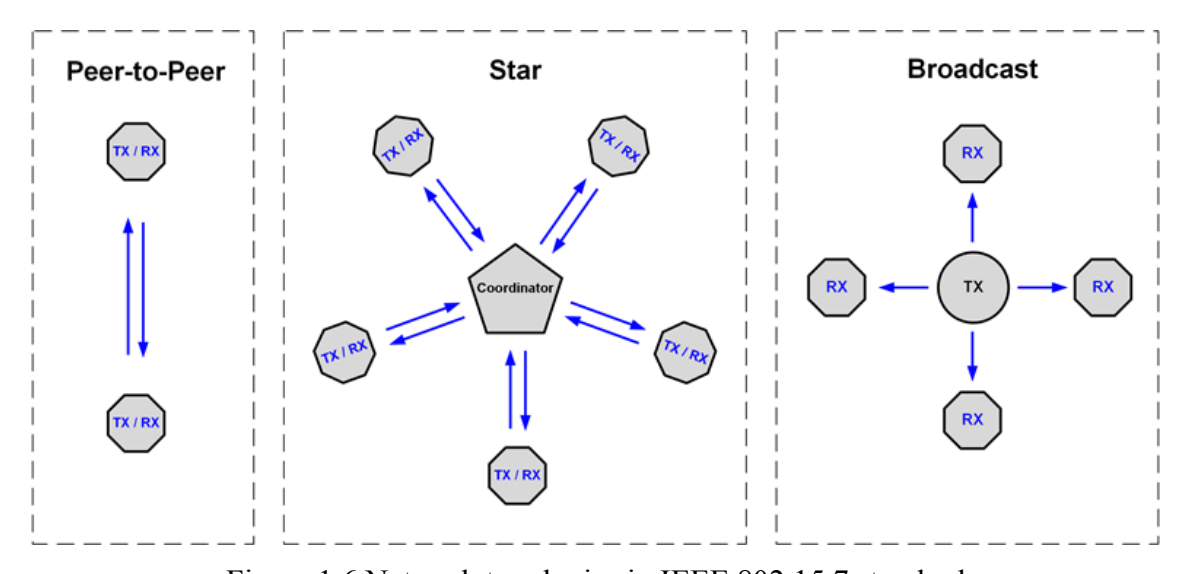


Figure 1.6 Network topologies in IEEE 802.15.7 standard

The modulation domain spectrum of IEEE 802.15.7, as shown in Figure 1.7, reveals the range of optical clock rates used in the PHY. The data rates of PHY I, which is mainly targeted to outdoor applications, range from 200 kHz to 400 kHz. PHY II and III are based on higher data rates of up to 96 Mbps and are suitable for transceiver systems that use a PD-based receiver. PHY IV, V, and VI were added in the 2018 revision of the standard to support OCC-based systems. PHY IV uses region of interest (ROI)-based signaling to receive the signal using either under-sampled capture for low-data-rate systems or oversampled capture for high-data-rate systems. Data rates of up to 22 kbps can be achieved if a high-frame-rate camera is used.

However, a limited data rate of a few bps is possible using low-frame-rate cameras. PHY V relies on rolling shutter sampling, and data rates can range from a few hundred bps to several kbps. PHY VI is based on screen-to-camera communication where the optical clock rate is usually equal to the display frame rate. However, thanks to the higher spatial density of the 2-dimensional pixels on the screen, data rates in the order of several hundreds of kbps can be achieved in PHY VI.

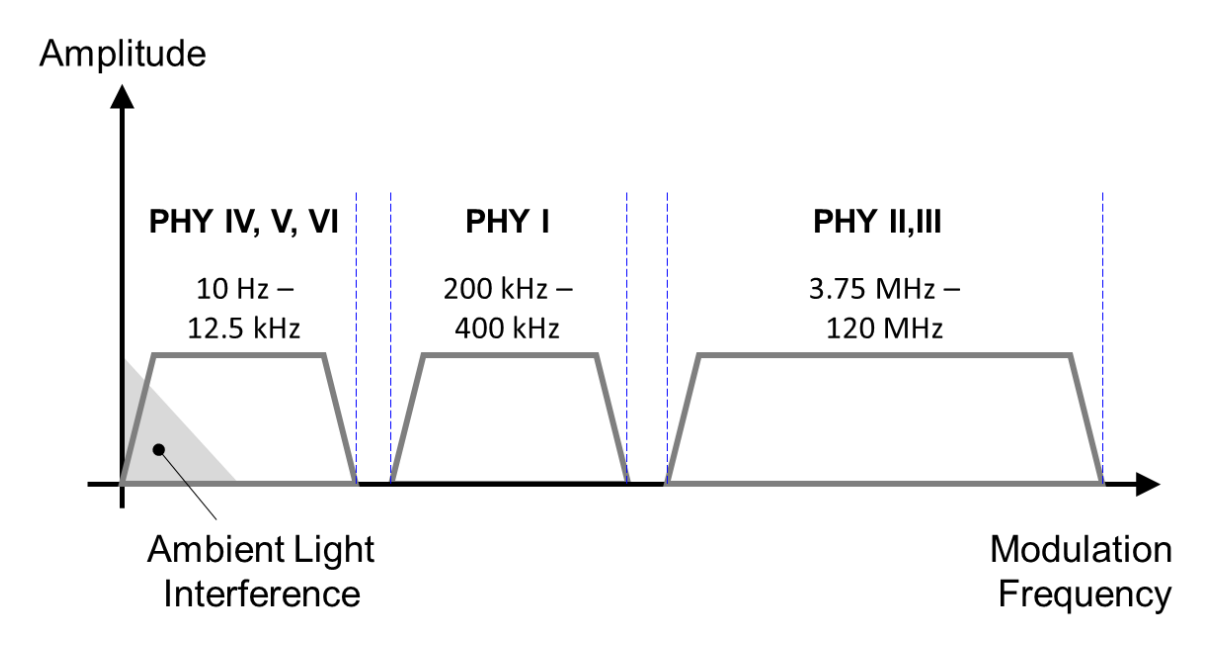


Figure 1.7 Modulation domain spectrum of IEEE 802.15.7 PHY

PHY V is considered most suitable for industrial and consumer applications as it requires CMOS image sensors as receivers, which are low cost and widely available in devices including, smartphones, robots, drones, automobiles, etc. In addition, simpler modulation schemes on the transmitter side can help to realize low-complexity and low-cost VLC systems. Furthermore, rolling shutter cameras can allow for a higher modulation frequency on the transmitter side, which helps to avoid the potential flicker problem. The modulation and coding schemes used in PHY V are rolling shutter frequency shift keying (RS-FSK), camera On-Off keying (C-OOK), camera m-ary frequency shift keying (CM-FSK), and mirror pulse modulation (MPM), as shown in Table 1.2. C-OOK provides a relatively higher data rate and can support a longer range. Therefore, it is the chosen modulation type in the proposed system design in this thesis, to be discussed in the subsequent chapters.

Table 1.2 Summary of PHY V modulation, coding schemes and data rates

Modulation	RLL code	Optical clock rate	FEC	Data rate
RS-FSK	None	30 Hz	XOR FEC	120 bps
C-OOK	Manchester/ 4B6B	2.2 kHz/ 4.4kHz	Inner Hamming code, Optional outer RS(15,11)	400 bps
CM-FSK	None	10 Hz	Optional Outer RS(15,11)	60 bps
MPM	None	12.5 kHz	Temporal error correction	5.71 kbps

1.4 Applications of Visible Light Communication

Visible light communication has applications both indoors and outdoors, as illustrated in Figure 1.8 [11]. Indoors, VLC finds its usage in large venues such as hospitals, train stations, airports, exhibition centers, shopping malls, industrial warehouses etc. In addition, VLC is suitable for smart home applications for controlling smart appliances. Outdoors, VLC can be used in transportation for communication between vehicles to vehicles and infrastructure (V2X) to support intelligent transportation systems (ITS) [12], and underwater expeditions [13]. Indoor applications of VLC, namely, location-based services, augmented reality (AR), virtual reality (VR), and robotics, are described in detail in the following sections.



Figure 1.8 Applications of optical wireless communication (OWC) [11]

1.4.1 Location-based Services

Positioning is the prerequisite to providing location-based services and applications. However, well-established outdoor positioning systems such as the Global Positioning System (GPS) and Global Navigation Satellite System (GLONASS) are not applicable to indoor scenarios due to the significant power attenuation from buildings. Therefore, various indoor positioning techniques have been developed that use ultrasound, radio frequency identification (RFID), and wireless local area network (WLAN) [14–17]. VLC is another disruptive technology, which enables LED light bulbs to be used as positioning beacons and to provide innovative location-based services. The relative location between the LEDs and the user devices is decided based on the features of the signals delivered from the LED beacons. Various methods have been investigated for location estimation through triangulation, including

received signal strength (RSS), time of arrival (TOA), and angle of arrival (AOA) [18–21]. RSS leverages the intensity of the received signal to find the location of the receiver, TOA is a positioning technique based on the arrival time of the received signal from different LED beacons, while AOA utilizes the angle at which the VLC signal is received to extract location information. Table 1.3 compares VLC to several other existing technologies for location-based applications in terms of the following features:

Table 1.3 Comparison of various technologies for location-based applications

Technology	Location Accuracy	Response Speed	Link Security	Detection Range	Energy Saving
VLC	~10 cm	High	High	Medium	High
RF	1~5 m	Low	Low	High	Low
NFC	N/A	High	High	Low	Medium
QR-code	N/A	Low	Low	Low	High

- (1) Location accuracy. Due to the line-of-sight characteristics of visible light, VLC potentially has higher location accuracy compared to RF-based indoor positioning techniques, such as WiFi and Bluetooth. The reported location accuracy using VLC is within 10 cm [18–21]. In contrast, the accuracy of RF-based indoor positioning systems range from 1 m to 5 m with a higher deployment cost [22, 23].
- (2) Response speed. Since the indoor illumination levels must reach the required values for various activities [22], the received VLC signal strength is usually strong enough for quick detection and processing. The case is similar for near-field communication (NFC) as the transmitter and receiver can communicate within a short distance. In RF systems, however, the multipath effects may degrade the signal-to-noise ratio of the receiver. In such cases, it will take a longer time to process the received signal. For a QR code, the time spent on the alignment between the scanner and the code also slows down the response speed.
- (3) Link security. Since visible light can be confined in a well-defined space, high security is guaranteed. For NFC, the limited communication distance also makes eavesdropping difficult. In contrast, an RF signal usually covers a wide range with an omnidirectional radiation

pattern, which results in a high risk of interception. Although the access range of a QR code is also limited, its visibility makes it easy to capture for illegal usage.

- (4) Detection range. The detection range of VLC based on smart lighting systems is limited to several meters due to the significant light intensity degradation with respect to distance, and the limited field of view of the light bulbs. Meanwhile, RF systems such as Wi-Fi can cover a distance of several tens of meters. In contrast, NFC only works within a very short distance of 10 cm, and the detection range of a QR code depends on the size of the pattern, which is very limited in most cases.
- (5) Energy saving. Since VLC takes advantage of existing lighting infrastructure for simultaneous communication purposes, minimum extra power is needed, saving a significant amount of energy compared to other active communication systems.

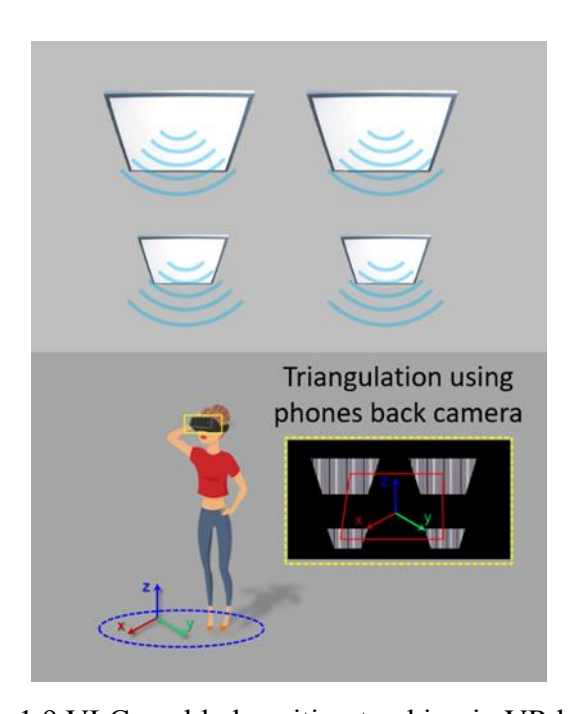


Figure 1.9 VLC-enabled position tracking in VR headset

1.4.2 Augmented Reality and Virtual Reality

VR enables the interaction between the user and the virtual world. In a VR system, position tracking has a great impact on the user experience, especially the immersion and the presence. Various position-tracking techniques have been developed for VR, including inertial tracking, acoustic tracking, optical tracking and others [23, 24]. VLC positioning techniques with high

accuracy are also applicable for VR applications. For example, the mobile phone of a VR user can work as an auxiliary positioning device to receive the beacon signal from ceiling LEDs via its camera, as shown in Figure 1.9. In some VR systems, optical tracking is achieved using predefined visible markers, and the camera on the head-mounted display identifies the markers and calculates the position [23]. Those visible markers can also be replaced with portable smart LED lights that are wirelessly programmable to facilitate system deployment.

AR is used to render virtual objects in the real world through mobile phone cameras. VLC can be easily employed in AR applications, as shown in Figure 1.10. In the figure, a light box in a shopping mall is enabled with VLC, and the AR information related to the product on the light box is broadcast in the form of a VLC ID. After detecting the transmitted VLC ID, the mobile phone will be able to access the AR content through ID translation and add it onto the screen.

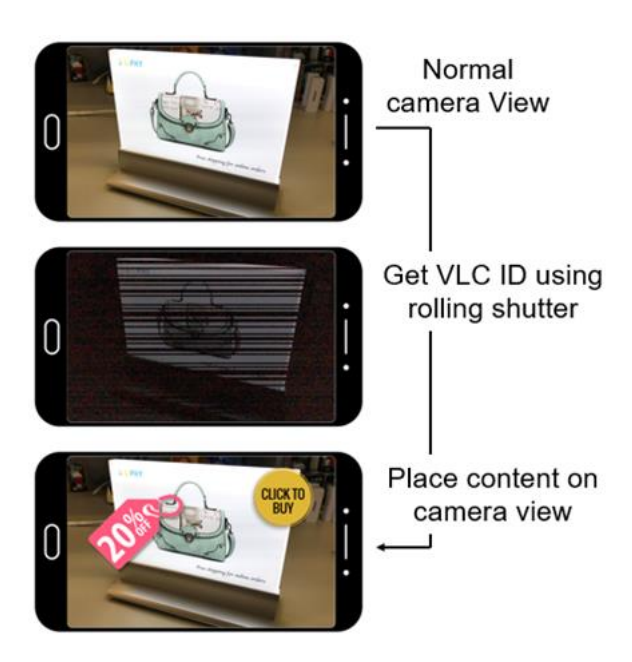


Figure 1.10 VLC-enabled AR

1.4.3 Robotics

Industry 4.0 transformation is driven by the connectivity between robots, sensors and a machine learning-based backend. A key driving factor for industrial automation is the capability of the robots, which includes mobility and connectivity with the IoT network.

Therefore, VLC presents great potential for realizing this transformation through VLC-integrated lighting. Smart LED lighting with IoT connectivity and location-based services could provide the infrastructure for a smart industrial building, as shown in Figure 1.11.

Currently, indoor robots use a combination of localization techniques, including inertial navigation, WiFi, and SLAM [25–27]. However, all these techniques suffer, either from limited accuracy or from a high computational cost. In addition, none of these localization methods provides a global location context. Thus, they can only be applied to small areas where each zone is physically distinctive from the others or location error may occur (particularly in SLAM). VLC in robotics can provide much higher accuracy of up to ~2 cm [28, 29] with a global scale, such that the robots can locate themselves accurately in a large multi-floor and multi-room building (Figure 1.11). In addition, a uniformly distributed network of VLC lighting in an industrial building can provide an IoT link for sensors and robots with high accessibility and low deployment cost.

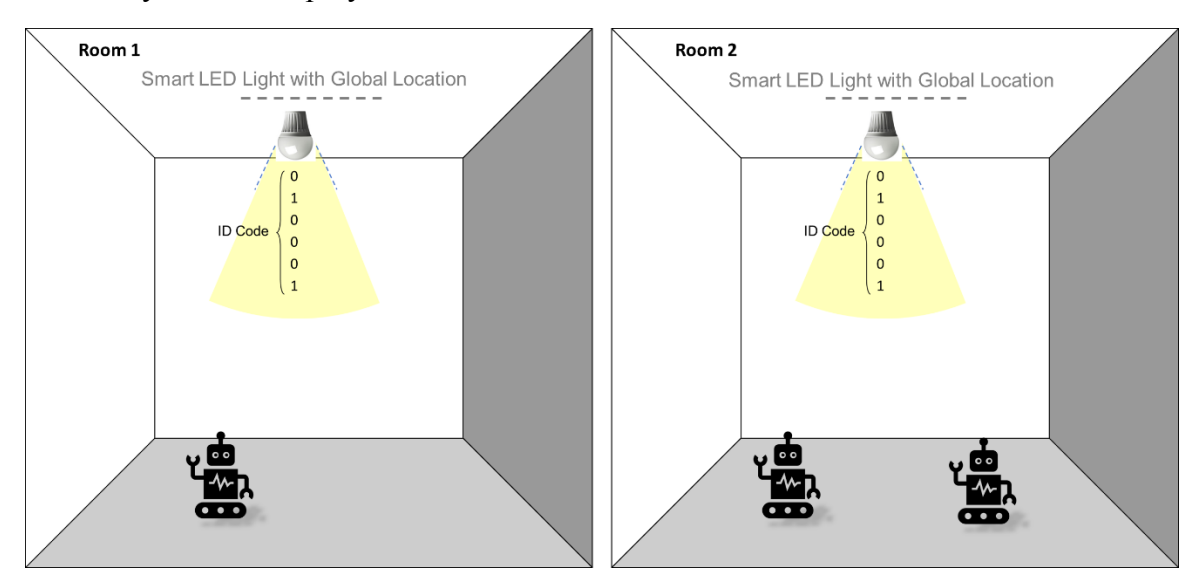


Figure 1.11 Robots can be accurately localized in multi-room and multi-floor buildings through globally unique VLC-integrated smart LED lights

1.5 Thesis Organization

The rest of the thesis is organized as follows. The design of a VLC transmitter system is discussed in Chapter 2. A universal VLC modulator design is presented that is integrated with Bluetooth-based wireless connectivity and supports various LED lighting and a wide range of

input power for LED drivers. Chapter 3 describes the use of a smartphone camera as a receiver and characterizes the performance of the communication link with respect to various types of lights, colors and smartphone models. Chapter 4 is focused on smart lighting and display applications of VLC. A smart LED lighting installation and control system is presented, followed by the implementation of OCC in LCD displays. Chapter 5 describes the implementation of a high-accuracy indoor positioning system using the transceiver system built in previous chapters. Finally, Chapter 6 concludes the thesis and gives an overview of future work.

1.6 References

- [1] A. Jovicic, J. Li, and T. Richardson, "Visible light communication: Opportunities, challenges and the path to market," *IEEE Communications Magazine*., vol. 51, no. 12, pp. 26–32, Dec. 2013.
- [2] H. Haas, L. Yin, Y.Wang, and C. Chen, "What is LiFi?," *J. Lightw. Technol.*, vol. 34, no. 6, pp. 1533–1544, Mar. 2016.
- [3] "What is LiFi", [Online], Available:

 https://www.youtube.com/watch?v=GkXyEgHRAcY
- [4] X. Huang et al., "2.0-Gb/s visible light link based on adaptive bit allocation OFDM of a single phosphorescent white LED," *IEEE Photon. J.*, vol. 7, no. 5, Oct. 2015, Art. no. 7904008.
- [5] R. Bian, I. Tavakkolnia and H. Haas, "15.73 Gb/s visible light communication with off-the-shelf LEDs," in *Journal of Lightwave Technology*, vol. 37, no. 10, pp. 2418-2424, May, 2019.
- [6] D. Tsonev et al., "A 3-Gb/s single-LED OFDM-based wireless VLC link using a gallium nitride μLED," *IEEE Photon. Technol. Lett.*, vol. 26, no. 7, pp. 637–640, Apr. 2014.

- [7] P. Luo, Z. Ghassemlooy, H. L. Minh, X. Tang, and H.-M. Tsai, "Undersampled phase shift ON-OFF keying for camera communication," in Proc. *6th Int. Conf. WCSP*, 2014, pp. 1–6.
- [8] H.-M. Tsai, H.-M. Lin, and H.-Y. Lee, "Demo: Rollinglight-universal camera communications for single LED," in Proc. *20th Annu. Int. Conf. Mobile Comput. Netw.*, 2014, pp. 317–320.
- [9] IEEE Standard for Local and Metropolitan Area Networks--Part 15.7: Short-Range Optical Wireless Communications IEEE Std 802.15.7-2018 (Revision of IEEE Std 802.15.7-2011) pp.1-407, 23 April 2019.
- [10] T. Nguyen, A. Islam, T. Hossan and Y. M. Jang, "Current status and performance analysis of optical camera communication technologies for 5G networks," in *IEEE Access*, vol. 5, pp. 4574-4594, 2017
- [12] M. Z. Chowdhury, M. T. Hossan, A. Islam, and Y. M. Jang, "A comparative survey of optical wireless technologies: Architectures and applications," *IEEE Access*, vol. 6, pp. 9819–9840, 2018.
- [12] A. Memedi and F. Dressler, "Vehicular visible light communications: A survey," in *IEEE Communications Surveys & Tutorials*, vol. 23, no. 1, pp. 161-181, First quarter 2021.
- [13] H. Kaushal and G. Kaddoum, "Underwater optical wireless communication," *IEEE Access*, vol. 4, pp. 1518 1547, 2016.
- [14] S. Holm, "Ultrasound positioning based on time-of-flight and signal strength," in International Conference on Indoor Positioning and Indoor Navigation (IPIN), 2012, pp. 1–6.
- [15] S. S. Saab and Z. S. Nakad, "A standalone RFID indoor positioning system using passive tags," *IEEE Transactions on Industrial Electronics*, vol. 58, no. 5, pp. 1961–1970, 2011.
- [16] C. Yang and H. Shao, "WiFi-based indoor positioning," *IEEE Communications Magazine*, vol. 53, no. 3, pp. 150-157, March 2015.

- [17] T. Bagosi and Z. Baruch, "Indoor localization by WiFi," in 2011 IEEE 7th

 International Conference on Intelligent Computer Communication and Processing,
 Cluj-Napoca, 2011, pp. 449-452.
- [18] Z. Zheng, L. Liu and W. Hu, "Accuracy of ranging based on DMT visible light communication for indoor positioning," *IEEE Photonics Technology Letters*, vol. 29, no. 8, pp. 679-682, Apr. 2017.
- [19] A. Wilkins, J. Veitch, B. Lehman, "A 3-D high accuracy positioning system based on visible light communication with novel positioning algorithm", *Optics Communications*, vol. 396, pp. 160-168, 2017.
- [20] T. Q. Wang, Y. A. Sekercioglu, A. Neild, and J. Armstrong, "Position accuracy of time-of-arrival based ranging using visible light with application in indoor localization systems," *J. Lightw. Technol.*, vol. 31, no. 20, pp. 3302–3308, Oct. 15, 2013.
- [21] A. Arafa, X. Jin, M. H. Bergen, R. Klukas, and J. F. Holzman, "Characterization of image receivers for optical wireless location technology," *IEEE Photon. Technol. Lett.*, vol. 27, no. 18, pp. 1923–1926, Sep. 15, 2015.
- [22] Illuminance Recommended Light Levels [Online]. Available:

 http://www.engineeringtoolbox.com/light-level-rooms-d_708.html
- [23] Y. Boger, "Overview of positional tracking technologies for virtual reality," Jun. 2014
 [Online]. Available: https://www.roadtovr.com/overview-of-positional-tracking-technologies-virtual-reality/
- [24] W. Fang *et al.*, "Real-time motion tracking for mobile augmented/virtual reality using adaptive visual-inertial fusion" *Sensors (Basel, Switzerland)*, vol. 17, no.5, pp. 1037, May. 2017.
- [25] J. Yi et al., "Kinematic modeling and analysis of skid-steered mobile robots with applications to low-cost inertial-measurement-unit-based motion estimation, *TEEE Transactions on Robotics*, vol. 25, no.5, pp. 1087-1097, 2009.

- [26] R. Miyagusuku, A. Yamashita and H. Asama, "Data information fusion from multiple access points for WiFi-based self-localization," *IEEE Robotics and Automation Letters*, vol. 4, no. 2, pp. 269-276, 2018.
- [27] S. Xu, W. Chou and H. Dong, "A robust indoor localization system integrating visual localization aided by CNN-based image retrieval with Monte Carlo localization," *Sensors*, vol. 19, no. 2, pp. 249, 2019.
- [28] W. Guan et al, "High-accuracy robot indoor localization scheme based on robot operating system using visible light positioning," *IEEE Photonics Journal*, vol. 12, no.2, pp. 1-16, 2020.
- [29] W. Guan, L. Huang, B. Hussain and C. Patrick Yue, "Robust robotic localization using visible light positioning and inertial fusion," *IEEE Sensors Journal*, doi: 10.1109/JSEN.2021.3053342.

CHAPTER 2 Enabling VLC in LED Lighting and Signage

A VLC transmitter system consists of a digital baseband, an LED driver, and an analogue modulator. The design of such transmitter system depends on several factors, including type of lighting source, output power, LED-driving method, required data rate, communication distance, and modulation scheme. Due to these considerations, a practical VLC transmitter system that meets the application requirements while keeping the design and deployment cost low, is a very challenging design problem and has been largely overlooked in the research community. This chapter tries to address this problem and presents the design and implementation details of a VLC modulator that can enable VLC transmission in a wide variety of existing LED lighting and signage for various applications, including location-based services, indoor positioning, internet-of-things (IoT) connectivity, etc.

2.1 Related Works

Several VLC transmitter systems have been reported in the literature and are discussed here as follows. A high-speed LED driver using the technique of sweeping remaining carriers is presented in [1]. The system can achieve a data rate of up to ~52 Mbps. However, it uses only a single LED and a total power of 33 mW, which makes it unsuitable for practical system deployment. In [2], a discrete power level stepping technique is used to design a VLC transmitter. The system employs infrared (IR) diodes with a power consumption of 40 mW per diode and total output power of ~1.5 W. A VLC transceiver with graphical user interface (GUI)-based software control, which produces 100 kbps data rate using a 4×4 LED array is presented in [3]. The system requires a computer with RS-232 to provide the transmission data. A VLC system using orthogonal frequency division multiplexing (OFDM) subcarrier grouping is presented in [8]. It requires individually driven LEDs with arbitrary waveform generator (AWG)-based control and achieves a communication distance of 120 cm.

Several works are focused on the LED driver design to support illumination and VLC. [4] presents a VLC transmitter using a burst mode LLC converter based on an LED array of 60×60 cm and powered by 80 W. The system achieves a data rate of 47 kbps at a distance of 10 m,

with an estimated lumen output of over 7000 lm. The system requires a non-standard 400 V input and is fed the input data through a field programmable gate array (FPGA). An LED driver to provide illumination control and VLC function using the VPPM scheme is reported in [9]. The driver can support 5.8 W of power with 450 lm output to provide a 2 Mb/s data rate at a 1 m communication distance. An LED driver with a similar power rating of 5 W and achieving 1 Mb/s is presented in [10], and uses a GaN device for switching. In [11] and [12], an LED driver design using LEDs as a replacement for freewheeling diodes is proposed. The system uses separate LEDs for communication and illumination, which makes the design complicated. A resonant switched-capacitor (RSC) DC-DC converter-based LED driver with VLC capability is demonstrated in [13]. The system achieves a data rate of 100 kb/s over a distance of 1 m by driving a load of 10 W. In [14], an LED driver design is presented that uses the phase of the ripple waveform of a buck converter to modulate VLC data. Similarly, an LED driver that is based on two DC-DC power converters is proposed in [15] to provide illumination and VLC functionality with improved efficiency. A dimmable LED driver that can perform power factor correction, VLC, and dimming is presented in [16]. It can achieve a data rate of 1.1 Mbps at a distance of 10 m with a power consumption of 20 W.

A few works have reported CMOS-integrated LED drivers with a VLC function [5–7]. A transmitter SoC based on the IEEE 802.15.7 standard is proposed in [5] and [6]. It integrates a VLC digital baseband and LED driver for portable applications. The system can achieve data rates of up to 266 kbps with 8 W power consumption and a communication distance of up to 2 m. In [8], an AC-input and inductor-less LED driver with VLC function is demonstrated, which can achieve an 8 Mbps data rate at 1 m distance. The regulation is based on individually controlled segments of LEDs, which makes the design unsuitable for a wider range of lighting devices and illumination applications.

In summary, all of the VLC transmitter designs discussed above are focused on either increasing the modulation bandwidth or improving the efficiency. However, there is no consideration of the practical implementation aspects, such as manufacturing cost of designing custom LED drivers, supporting a wide variety of luminaries with broad power ranges, the

impact of VLC on the reliability of the LED driver and the luminaire, or the quality of the lighting output in long-term usage. In addition, these systems do not examine how an LED driver could be connected to IoT infrastructure to become a part of the ambient intelligence in the context of smart buildings. Therefore, in this chapter, a VLC transmitter design is presented that takes into account all the aforementioned issues and provides a design with the following key characteristics:

- 1) Plug-n-play capability;
- 2) Low proportional power consumption;
- 3) Low implementation cost;
- 4) Fully integrated wireless control for IoT connectivity; and
- 5) Support for a wide variety of luminaries including constant current (CC)- and constant voltage (CV)-controlled lighting.

2.2 Light Intensity Modulation

An LED is a current-controlled device; i.e., the light produced by the LED is directly proportional to the amount of current flowing through it. Therefore, the power supply for an LED, usually referred to as the LED driver, is a circuit that regulates the current flowing through the LED. In order to modulate the light intensity with information, the current needs to be modulated, which requires insertion of a circuit called a modulator between the power supply and LED. This modulator circuit modulates the output current of the LED driver according to the modulation and encoding scheme required by the communication system.

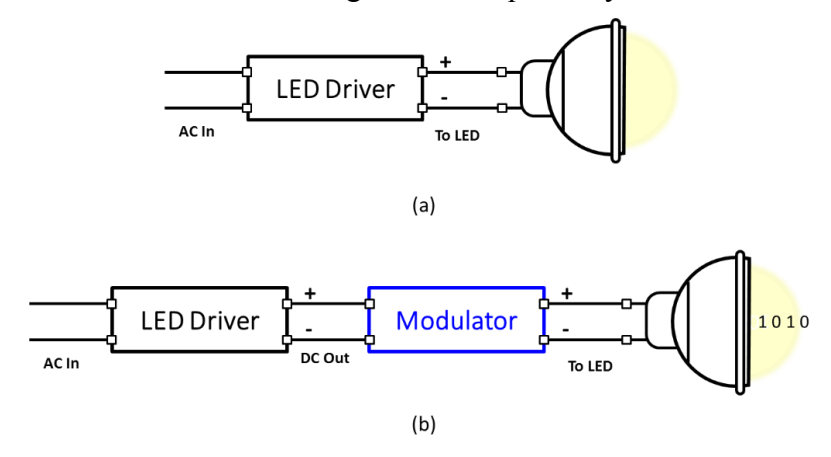


Figure 2.1 An LED light driven by an LED driver (a) without a modulator (b) with a modulator

2.3 Supply and Connectivity for VLC Modulator

With LED lighting being extensively used in both public and residential venues, enabling VLC requires a seamless retrofitting of required hardware, specifically, a modulator in the existing infrastructure. A very important practical consideration is how to power the modulator circuit since it features active circuit blocks that must be provided with an operating supply through the existing lighting hardware. There are two possible options, as shown in Figure 2.2. The modulator can either generate a power supply through the DC output of the LED driver directly and down-convert it using an LDO, or a modulator can be supplied with AC mains which go into the LED driver and have a built-in AC-DC adapter inside the modulator circuit block. Both of these configurations depend on the cost of the hardware and the size of the modulator circuit to fit a certain integration requirement.

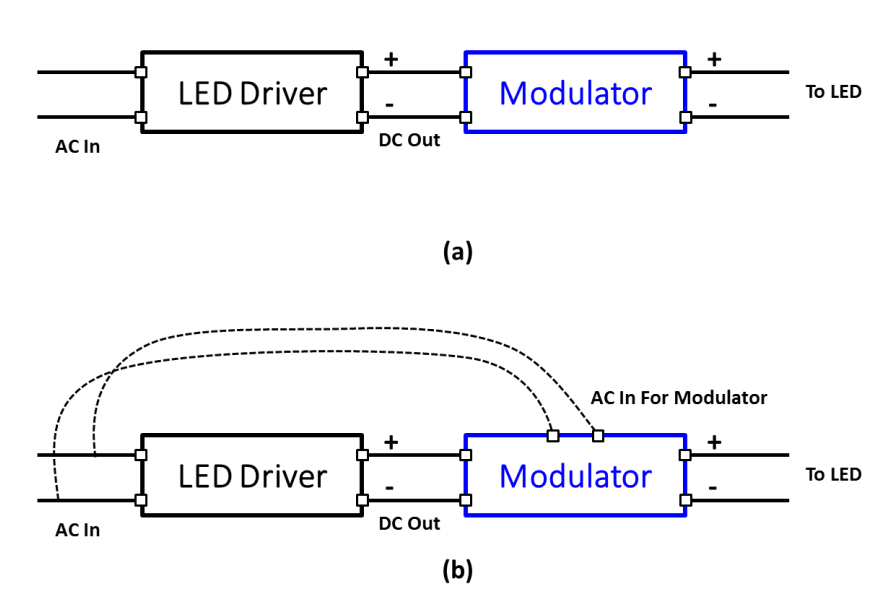


Figure 2.2 Connecting VLC modulator between LED driver and LED light: (a) Option 1: No external AC needed. Step down LED VDD using on-board LDO; (b) Option 2: Use AC-DC adapter on-board to convert from external AC

LED lighting supports several types of dimming, which include both analogue and digital forms. One of the digital methods to dim an LED light is using a pulse width modulation (PWM) control, i.e., controlling the duty cycle of a pulse signal that directly controls the turn ON and turn OFF time of the LED luminaire. This type of dimming control is provided as an external interface for LED drivers where the PWM signal can be externally fed to the driver. In order

to modulate the LED light with the VLC signal, the signal can be fed into the PWM control inputs of the LED driver, as shown in Figure 2.3. This type of VLC modulator does not need to have a power switch to modulate the LED light. However, it does need to have an on-board power supply to convert AC into a low-voltage-regulated DC to operate the microcontroller unit (MCU).

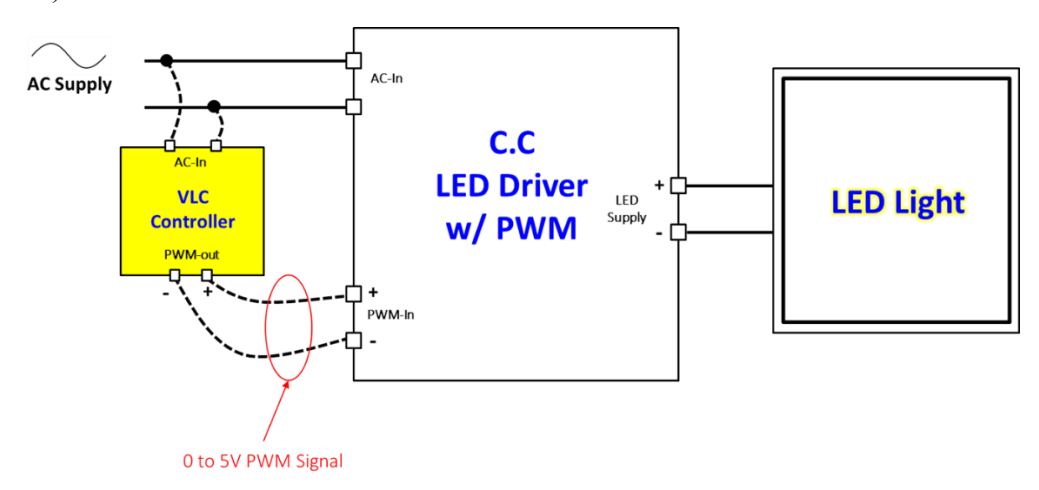


Figure 2.3 Using external PWM dimming control of LED driver for VLC modulation

2.4 Constant Current and Constant Voltage Lighting

LED lighting drivers are generally divided in two broad categories, namely, constant-current (CC) drives, which regulate output current and constant-voltage (CV) drives, which regulate output voltage (Figure 2.4). Since LEDs are inherently constant-current devices, with their light intensity directly proportional to the current, most general lighting, which includes light bulbs, tubelights, downlights, spotlights etc., is driven by constant-current supplies. In all of these general lighting types, the LED load is normally within a fixed range such that it can be driven by a CC output, with output voltage varying within a specified range. However, a CC driver cannot drive LED light boxes and signage, which comes in various sizes and loads. For such loads, the single driver is supposed to drive multiple loads of various power ratings and hence requires a CV supply such that the current regulation is done within the LED sign itself. For CV drivers, the number of loads and their power rating does not need to be known in advance and a driver can operate any number of loads as long as the total power is within the maximum output power of the CV LED driver.



Figure 2.4 Categories of LED lighting. (a) General lighting using CC LED drivers. (b) Signage and light boxes using CV LED drivers

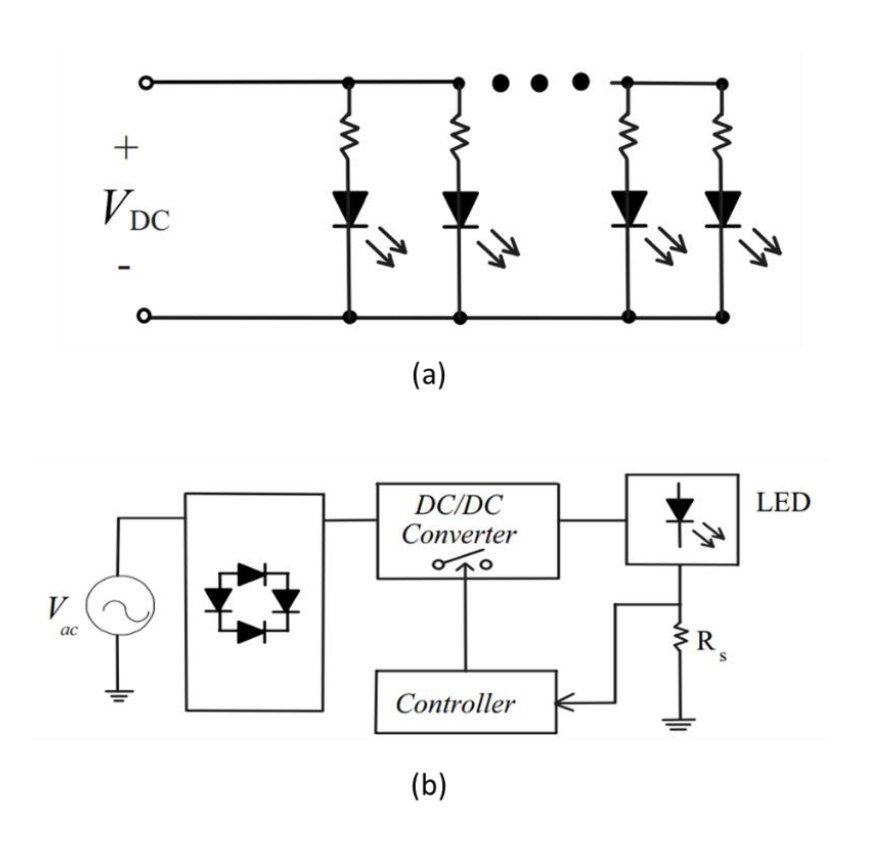


Figure 2.5 (a) CV regulation. (b) CC regulation

2.5 Constant Voltage and Constant Current Control

As described in the previous section, a CV LED load usually features current regulation circuitry within the lighting luminaire, whereas CC regulation is performed inside the CC LED driver, and the LEDs can be directly connected to the LED driver as multiple branches of seriesconnected LEDs, as shown in Figure 2.5. CV regulation circuit features an LED or a series of

LEDs with a current control resistor. The resistor value is chosen such that the series LED current flowing through the resistor causes a voltage drop across the resistor, which is equal to the difference of the supply voltage and LED operating voltage according to the I-V curve.

A CC led driver mainly features a DC-DC buck converter and a feedback control to regulate the amount of current by changing the duty cycle of the buck converter. Commercially available LED drivers, due to power consumption requirements for energy saving, must also feature a power factor correction (PFC) stage to improve the power efficiency of the overall system.

2.6 A Universal VLC Modulator Design

The block diagram of the proposed modulator circuit is shown in Figure 2.6. The modulator comprises a voltage level converter and regulator circuit to step down the LED supply voltage and provide a stable low voltage supply for the signal processing communication circuitry, which mainly features an MCU. The modulation and switch circuit is a combination of a driving circuit and a power device to modulate the current flowing through the LED according to the signal pattern produced by the communication block.

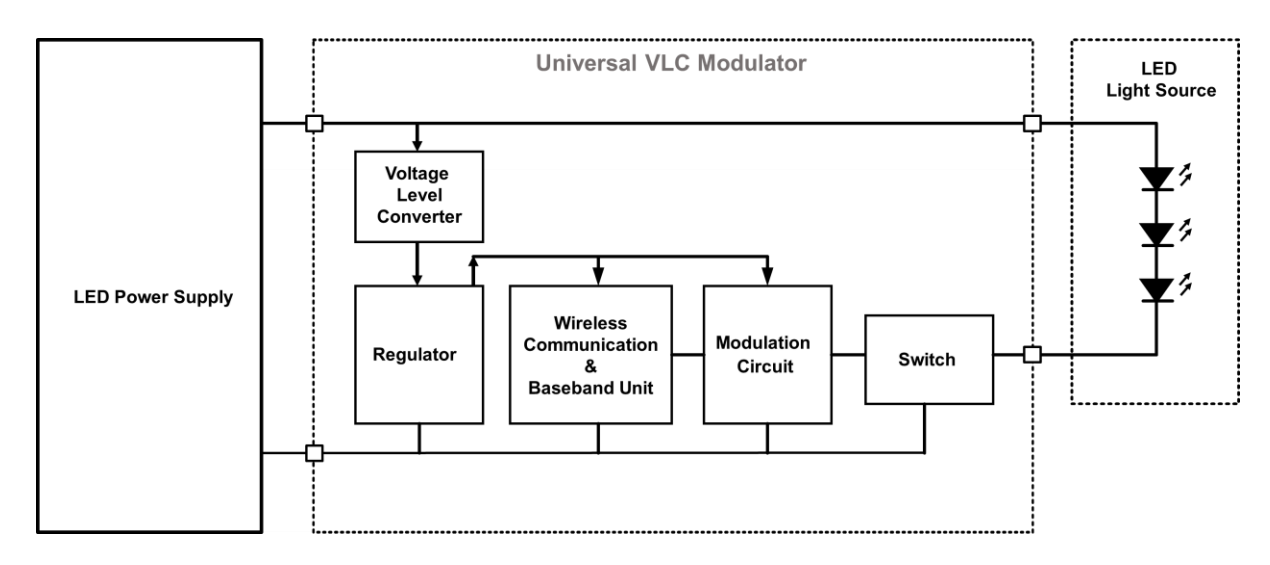


Figure 2.6 VLC modulator block diagram

2.6.1 Voltage Level Conversion and Regulation

A general LDO with a low voltage output of 3.3 - 5V usually has a maximum input voltage rating of up to 35 V. However, for medium-power-range general lighting driven by a CC LED

driver, the operating voltage can have a very wide operating range and can go as high as 60 V. In some cases, even though the LED operating voltage is well below the maximum output voltage of the LED driver, the open circuit voltage of the LED driver is always at its maximum. Therefore, it becomes quite challenging to design a supply circuit for the modulator, which can operate even when the LED is momentarily disconnected. In addition the output voltage is also modulated as the LED is turned Off and On, as shown in Figure 2.7. For this reason, a simple regulator cannot be used and a step down converter must be used before the regulator to produce a reliable supply to drive the communication and signal processing block of the modulator circuit. For CV LED drivers, on the other hand, since the voltage is either 12 or 24 V, a simpler circuit can be realized by only using a regulator to directly produce a regulated low-voltage supply for the modulator circuit.

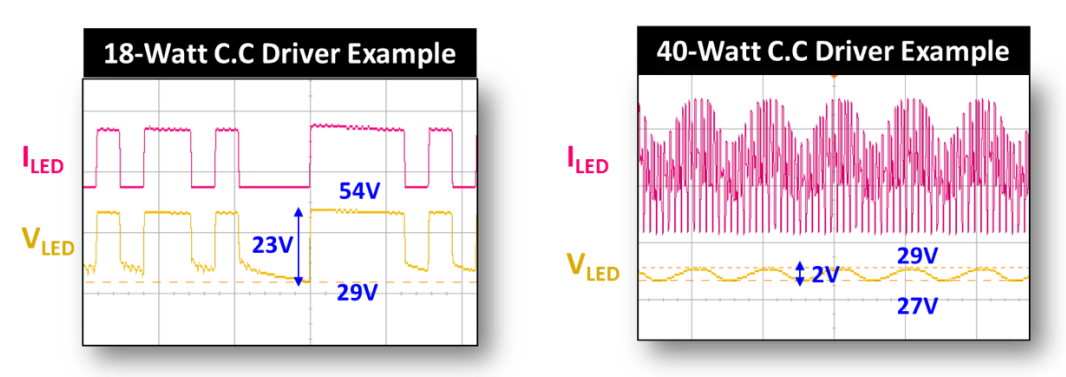


Figure 2.7 Voltage level conversation consideration for different LED drivers

2.6.2 Voltage Step-down Conversion using Zener Diode

A simple step down conversion is realized using a Zener diode, as shown in Figure 2.8. A Zener diode's fixed voltage drop can be used to subtract some of the high output voltage of the LED driver such that it brings down the input voltage of the LDO to within its allowable operating range. However, this method is not recommend for very high voltages as the required power rating of the Zener diode increases as the voltage drop across it increases. For higher voltages and better efficiency, a DC-DC converter must be used.

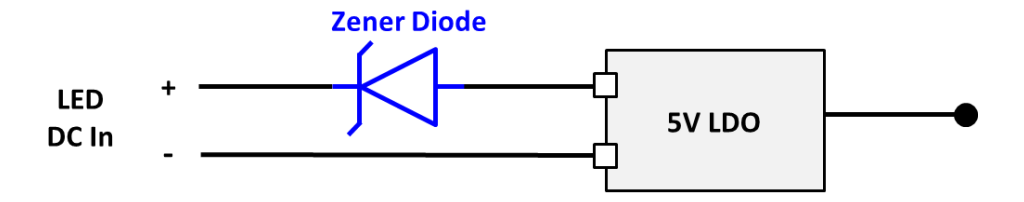


Figure 2.8 Adding Zener diode for voltage drop before LDO

Table 2.1 Supply options for various LED driver voltage ranges

Input LED Voltage Range	Options for use	
12 –24V	Use LDO directly	
24–45V	Use Zener Diode	
	DC/DC converter	
Higher than 45 V	or	
	use direct supply	

2.6.3 Hardware Prototype Design

The block level schematic of the proposed VLC modulator, which comprises two main modules, namely, a power supply module and a modulator module, is shown in Figure 2.9. The power supply module consists of a switch that can select between the on-board AC-DC supply that allows the modulator to be directly operated by AC mains or an LDO output, which converts the LED driver's DC output to a low-voltage output for driving the modulator circuit. Meanwhile, the modulator module consists of a Bluetooth Low Energy (BLE) controller board that features a BLE communication IC and MCU that allows for the modulator data output to be remotely programmed. The output of the controller board drives the driver IC that is connected to the power device to modulate the current of the LEDs according to the signal pattern generated by the controller board.

Figure 2.10 shows the hardware prototype of the VLC modulator featuring dual power supply input options. The dimensions are (L x W x H) 6 cm x 3 cm x 2.4 cm.

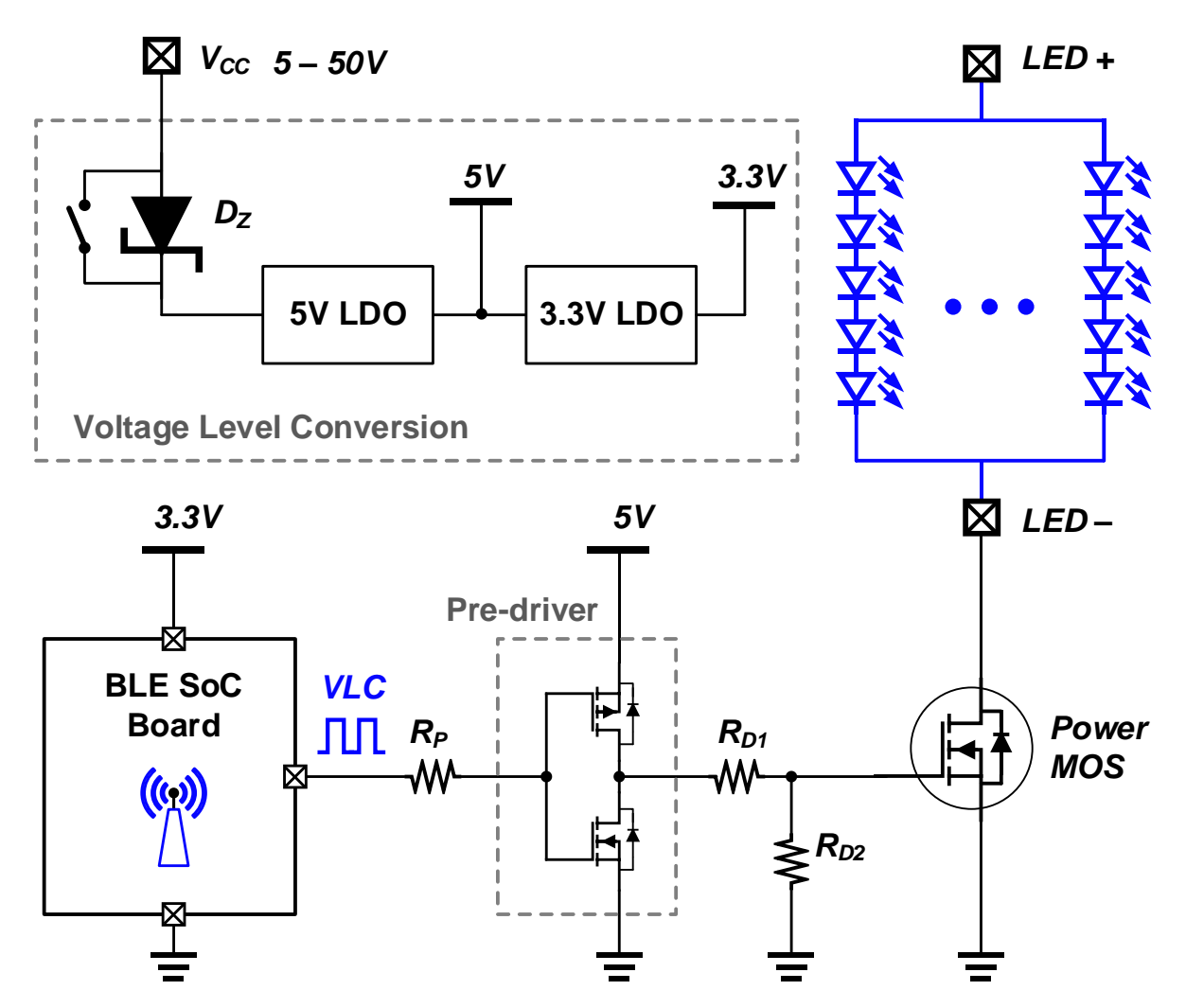


Figure 2.9 Block-level schematic of VLC modulator



Figure 2.10 Assembled prototype of VLC modulator

2.7 Bluetooth-based Wireless Control

Recently, Bluetooth has become a popular connectivity technology for IoT devices, including, smart home appliances, consumer devices such as wireless earphones, smart speakers, wristbands etc. Thanks to its compatibility with the most popular consumer devices, smartphones, Bluetooth will continue to be the prime choice of connectivity technology for IoT devices in the context of smart buildings and smart homes. In addition, with the release of the Bluetooth 5.0 standard, several new features, including precise localization and support for Mesh networking [17] have been added, which will further pave the way for industrial applications of Bluetooth to support large-scale deployment of IoT devices. Therefore, we propose to integrate a BLE system-on-chip (SoC) into the VLC modulator to upload data to the luminary and support wireless connectivity with other IoT devices in smart buildings. In addition, the BLE SoC also serves as an iBeacon [18] to continuously broadcast advertisement packets to nearby mobile devices and provide proximity-based applications.

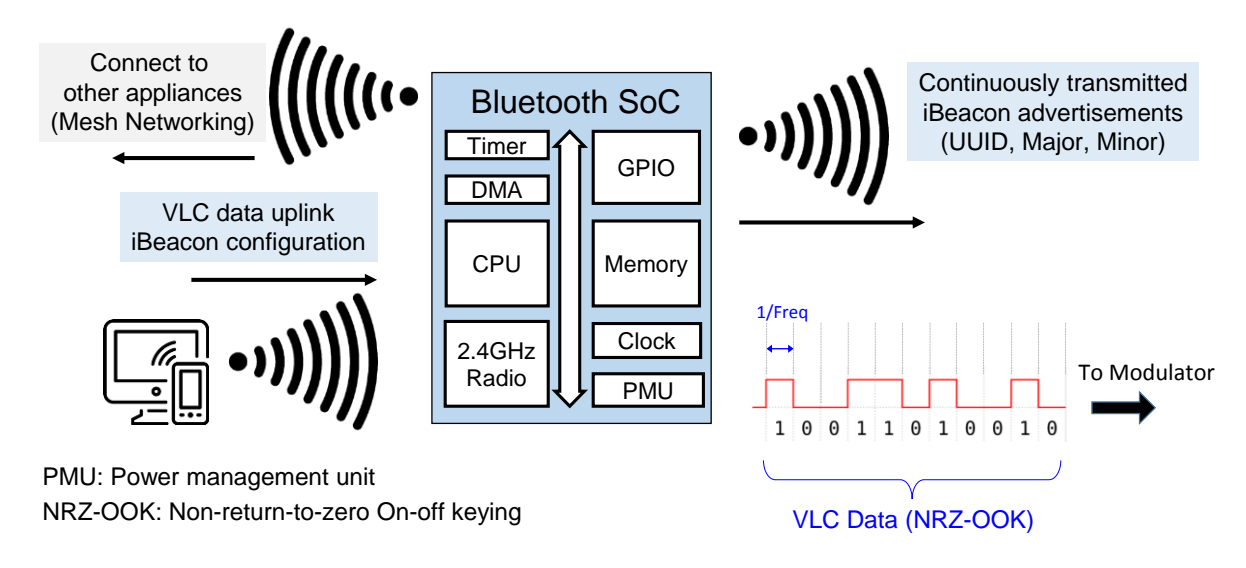


Figure 2.11 The overall architecture of the BLE SoC-based wireless control and iBeacon

2.7.1 System Architecture

The overall architecture of the system is shown in Figure 2.11. The processor, for instance 8051 in Ti/CC254x [19], ARM cortex-M0 in Dialog/DA1458x [20], memories (Flash, RAM, ROM), oscillators (Crystal and RC oscillators) and digital and analog peripheral blocks are

usually integrated on a chip. A radio, together with a modem and link controller, are used for BLE communication. Many SoCs have a DMA controller which can move data from a peripheral unit, such as the ADC, to the memory, or vice versa, with minimum CPU intervention, thus achieving high overall performance with good power efficiency. By utilizing the BLE SoC as the MCU of the controller, we can configure the VLC data/frequency as well as the iBeacon's parameters (UUID, Major, Minor, TX power etc.) through the BLE wireless channel. After configuration, the controller can continuously transmit iBeacon advertisements, and the VLC control signal is generated via one of the I/O pins of the Bluetooth SoC to modulate the LED current simultaneously. In addition to the VLC and iBeacon signal broadcasting, the newer generation of BLE also supports Mesh networking [17] to allow IoT connectivity with other nearby lighting devices and appliances.

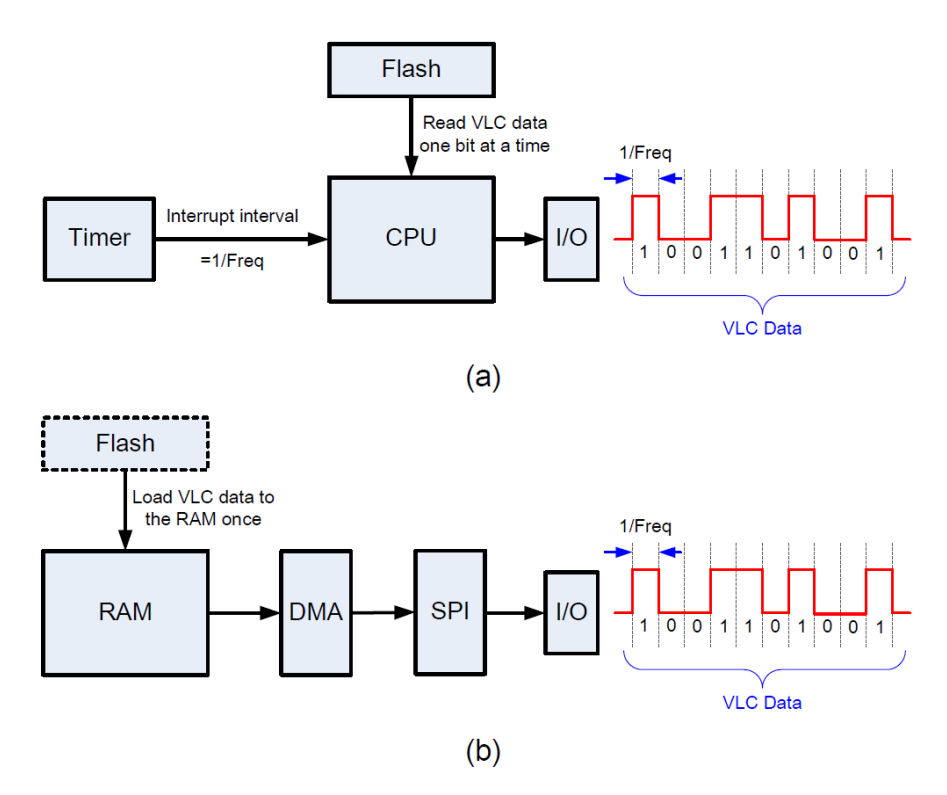


Figure 2.12 VLC control signal generation: (a) conventional approach, (b) proposed approach 2.7.2 VLC Control Signal Generation

An on-chip high-speed timer can be used to transmit VLC data. As shown in Figure 2.12 (a), the timer generates an interrupt signal within a specified time interval, as soon as the signal occurs, the processor reads the VLC data which has been stored in the flash one bit at a time

and transmits them in series via a selected pin. However, this is simple but not a good choice if we need to handle demanding applications and communication tasks in a short time frame.

Instead, the common serial peripheral interface (SPI) with DMA functionality is used in our proposed system, as shown in Figure 2.12 (b). The DMA controller is set to repeat mode, and the SPI frequency is adjusted according to the VLC bit duration. After being powered on, the stored VLC data are all loaded from Flash to a dedicated RAM area, the start address of which is configured as the source address of the DMA controller. Once triggered, the SPI module will start continuous VLC transmission without CPU intervention.

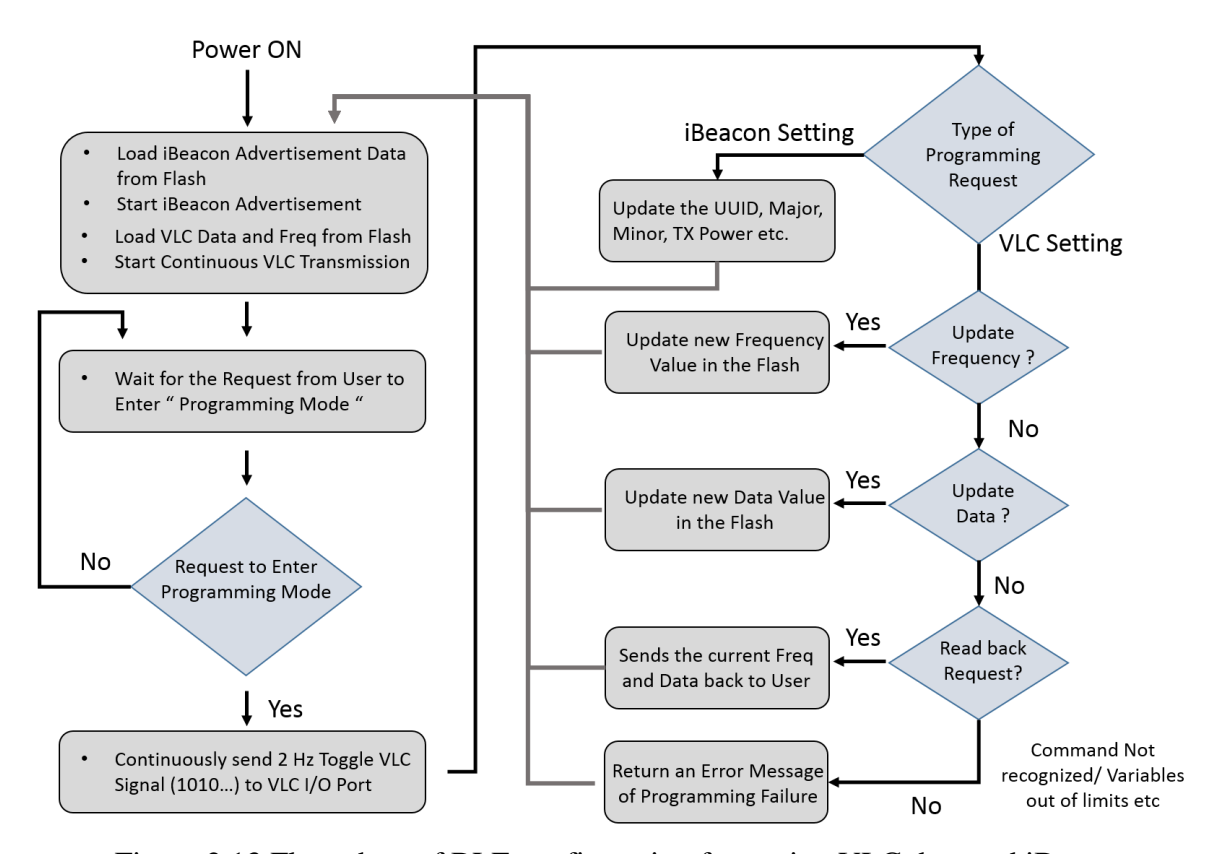


Figure 2.13 Flow chart of BLE configuration for setting VLC data and iBeacon

2.7.3 Flowchart of Configuration

A detailed flow chart of the whole wireless configuration for the iBeacon and VLC settings is presented in Figure 2.13. With the use of Bluetooth, these configurations can be controlled and managed via a smartphone or tablet running a dedicated application. Once the BLE SoC is powered on, it loads the iBeacon advertisement data, and VLC signal pattern from the flash memory and starts broadcasting iBeacon and VLC signals simultaneously, while waiting for

the controlling device to make the connection request. Once a controlling smartphone, or tablet establishes a connection with the BLE SoC, the device enters programming mode and starts to blink the light at a low frequency of ~2 Hz to indicate the activation of programming mode. The user can then choose to select either updating the iBeacon settings, or VLC settings including data and frequency as illustrated in the flowchart.

2.8 The Effect of Modulation on CC LED Drivers

One of the key considerations for VLC modulation is its impact on the brightness of the LED luminaire. In accordance with PWM dimming control, LED brightness intuitively drops when it is modulated with a VLC signal. However, in the case of a general CC LED driver, the peak current of the LED driver is increased such that the average current going through the LED is kept close to the rated current of the LED driver. In other words, if the LED is modulated with a 50% duty cycle VLC signal, the peak output current of the LED driver will double, as shown in Figure 2.14. This is because the current sensing circuit in the feedback control of the LED driver has a much lower response bandwidth than the modulation frequency of the LED, which ranges from tens of kHz to several MHz. Therefore, the current sensing circuit is only measuring the average amount of current that is given to the LED driver.

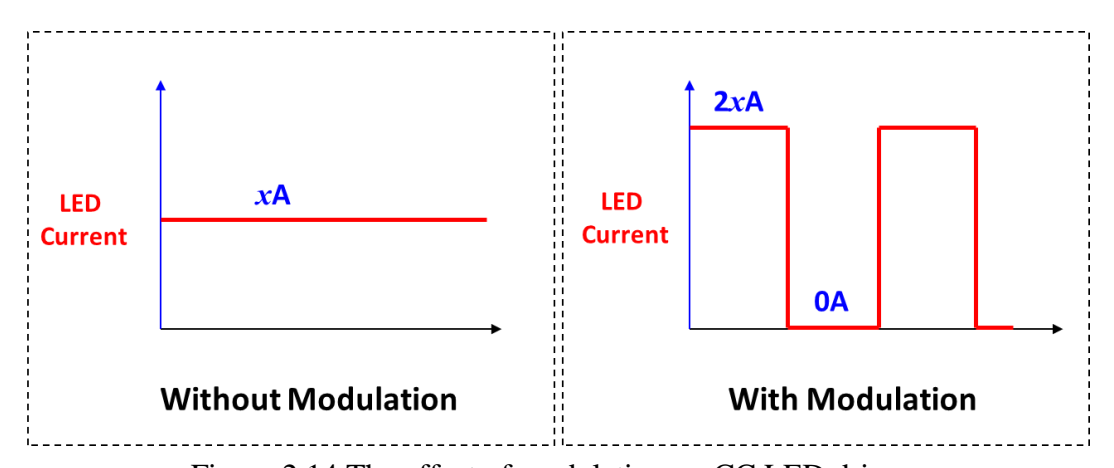


Figure 2.14 The effect of modulation on CC LED drivers

One very important aspect of this behavior is the voltage headroom of the LED driver. Since increasing the LED current to compensate for the modulation switching requires increasing the output voltage of the LED driver, the LED must not be operated near the maximum rated output

voltage of the LED driver as this will not leave room for a voltage increase and the brightness of the LED will drop. A general rule of thumb for selecting the LED driver is that the rated output power of the LED driver should be about 25% higher than the LED power.

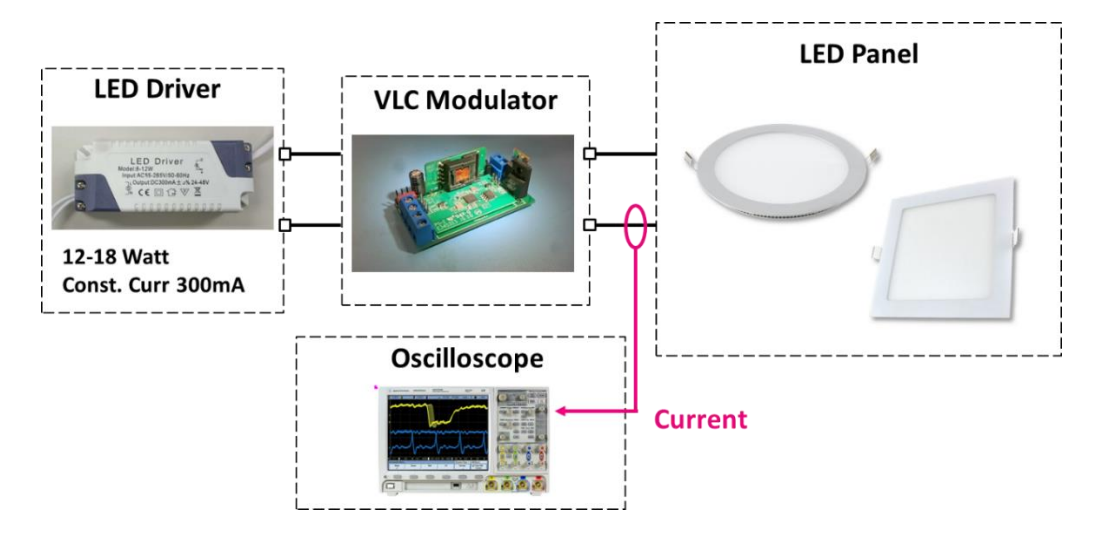


Figure 2.15 Setup for measuring the effect of modulation on LED driver



Figure 2.16 The measured waveform of various CC LED drivers under modulation

The measurement setup of a CC LED driver driving a range of LED lights from 12–18 W is shown in Figure 2.15. The modulator is put between the LED driver and LED light panels,

while the modulating current is measured using a current probe and oscilloscope. The measured current waveform of the LED panels for different wattages is shown in Figure 2.16. The unmodulated measured current is also shown, which is about 270 – 280 mA. It can be seen from the figure that the modulated current is almost double the unmodulated current for 9–18 W CC LED panels.

The effect of modulation on a single-stage PFC LED driver is measured and shown in Figure 2.17. The current waveform shows the output of the conventional single-stage PFC LED driver with and without modulation. The peak is pushed from 1.7A to 2.4A to compensate for the modulation and keep the average amount of current flowing through the LED the same.

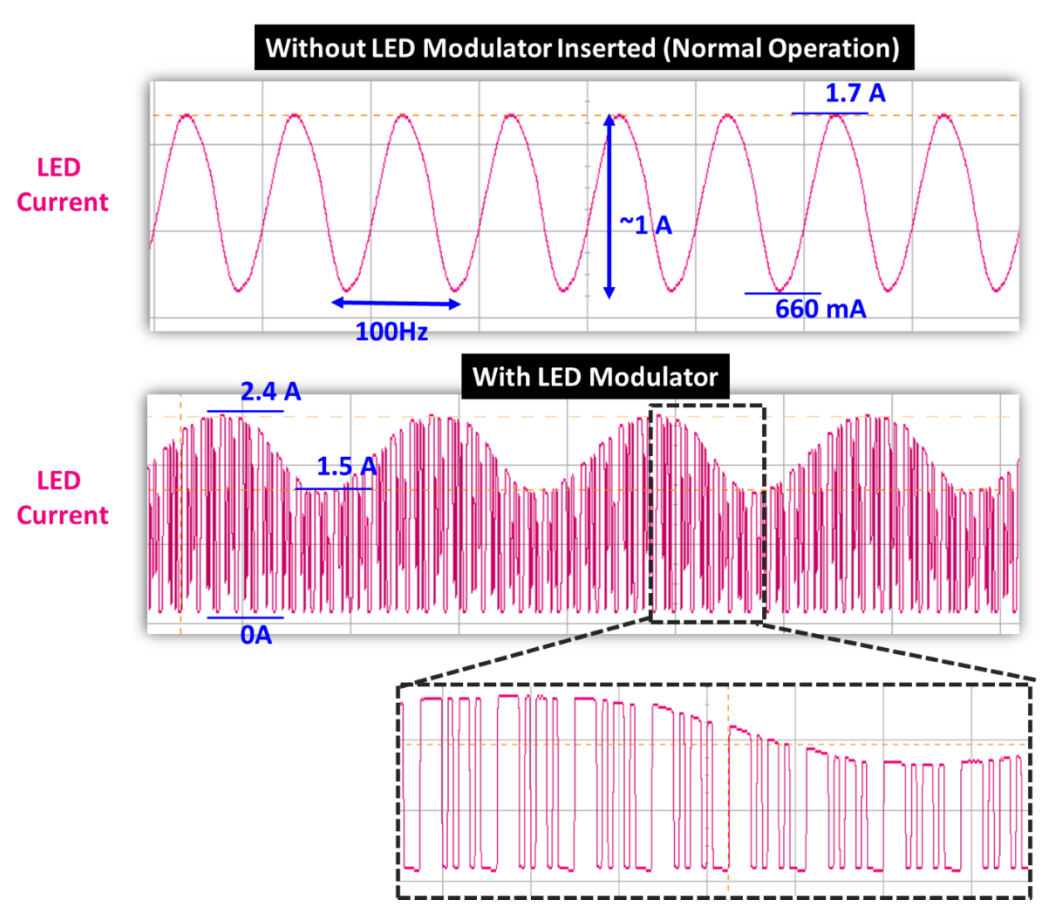


Figure 2.17 The effect of modulation on a single-stage PFC LED driver

2.8.1 Output Voltage Range of CC LED Drivers and its Impact on LED Brightness

Generally, LEDs driven with CC drivers do not exhibit any drop in brightness. However, when the output voltage of the LED is very close to the maximum range of the LED drivers,

the brightness drops because the driver cannot raise the voltage high enough to produce 2X the current in the LED, which is required for brightness drop compensation.

Figure 2.18 is an example of an LED driver where the I-V curve of the LED is extrapolated assuming a linear relationship of the current and voltage. It can be seen that, to produce twice of the peak current, the voltage must be increased beyond the maximum rating of the LED driver. This confirms that an LED driver must have voltage headroom while driving modulated LED lights in order to compensate for the drop in average current due to modulation.

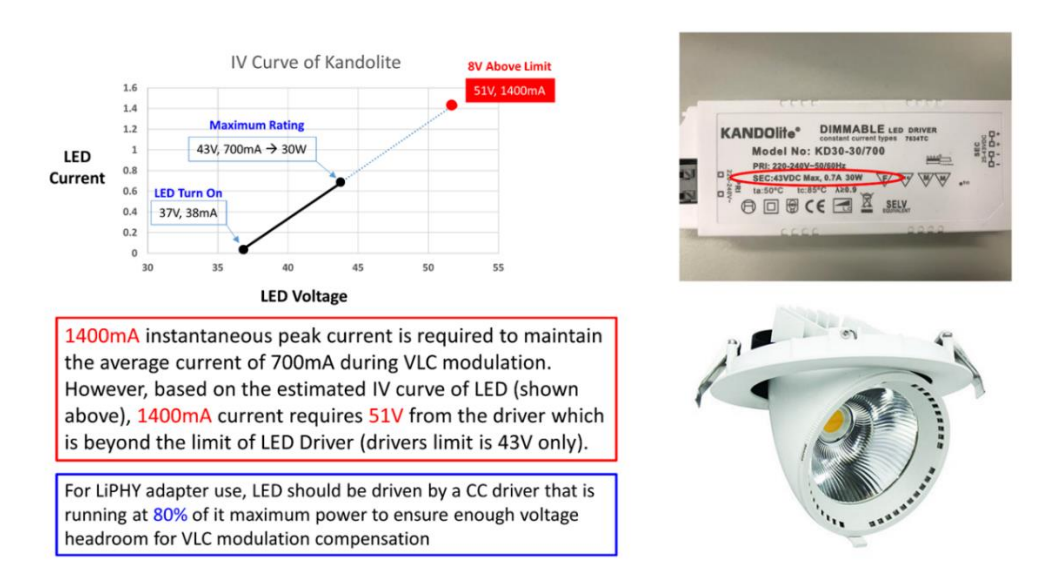


Figure 2.18 An example of a modulated LED driver operating near its peak output power

Table 2.2 gives examples of the minimum power rating of the CC LED driver that must be used with the corresponding power of the LED light to ensure that there is no drop in brightness after adding the modulator. A general rule of thumb is that the CC driver's maximum power rating must be at least 25% higher than the LED's power consumption to ensure there is no brightness drop.

Table 2.2 Selection of CC LED driver for a given power of LED load under modulation

LED Power Consumption	CC Driver Max Rating Required for VLC
10 W	12.5 W (CC 0.3 A, 42 V Max)
10 W	12.5 W (CC 0.7 A, 18 V Max)

20 W	25 W (CC 0.7 A, 36 V Max)
20 W	25 W (CC 1.4 A, 18 V Max)
30 W	37.5 W (CC 0.7 A, 54 V Max)
30 W	37.5 W (CC 1.4 A, 27 V Max)
40 W	50 W (CC 1.0 A, 50 V Max)
40 W	50 W (CC 2.0 A, 25 V Max)

2.9 The Effect of Modulation on CV LED Drivers

In contrast to CC drivers, CV drivers do not compensate for the modulation current as the current regulation is generally done on LED light signs using current control resistors. Therefore, modulating the output current of a CV LED driver reduces the amount of average current and hence brightness of the LEDs according to the duty cycle of the VLC modulation signal. As shown in Figure 2.19, the average current of an LED is reduced to half when modulated with a 50% duty cycle VLC signal.

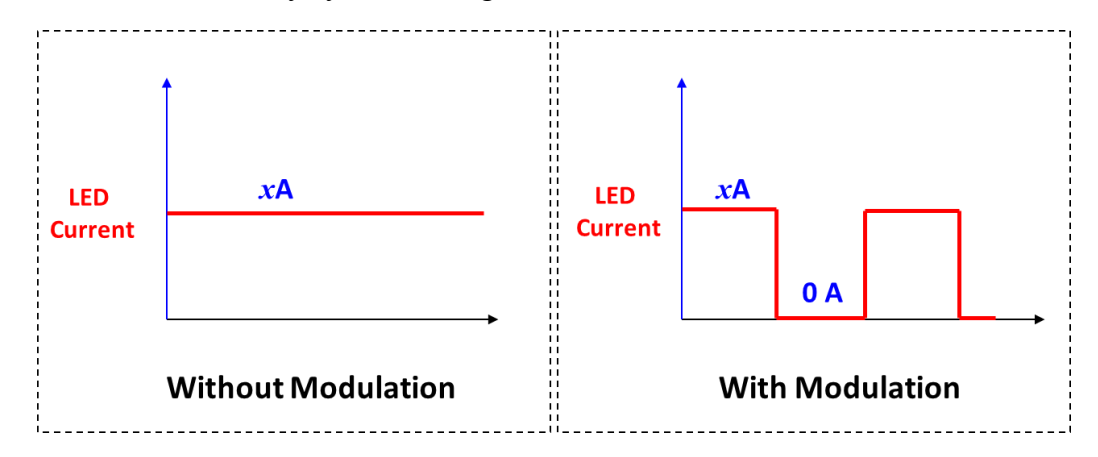


Figure 2.19 The effect of modulation on CV LED drivers

The setup for measuring the effect of modulation on a CV LED driver is shown in Figure 2.20. The block diagram shows a CV LED driver connected to an LED light box via a modulator. The current is measured using a current probe and oscilloscope, and the measured current waveform is shown in Figure 2.21. It can be observed that a DC current of 500 mA

without modulation is reduced to an average current of about 250 mA under a VLC signal with a 50% duty cycle, while the peak current remains about the same, i.e., 500 mA.

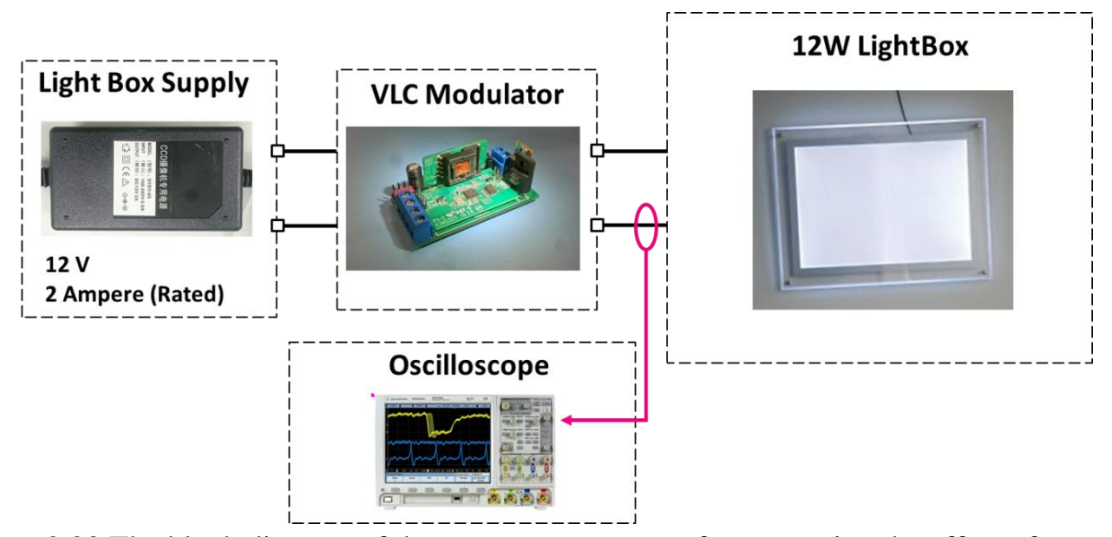


Figure 2.20 The block diagram of the measurement setup for measuring the effect of modulation on CV LED driver

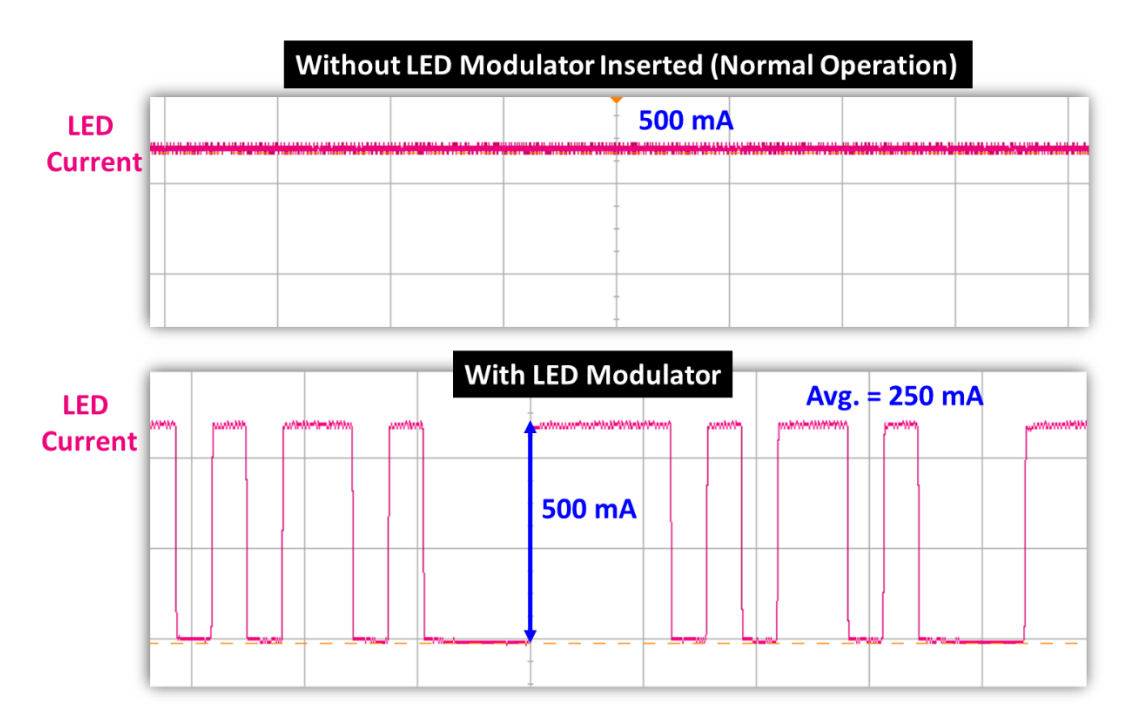


Figure 2.21 The measured current output of the LED driver with and without modulation

2.10 Methods to Compensate for Brightness Drop in CV LED Drivers

The brightness of an LED luminaire is directly proportional to the amount of average current flowing through the LEDs. As the modulation of LED current leads to a drop in average current and in turn reduces the brightness of the luminaire, the key to compensating for the brightness

drop is to increase the LED average current back to the rated level. Several methods can achieve this effect:

- 1) Using a higher voltage power supply
- 2) Using a DC-DC boost converter in the VLC modulator
- 3) Reducing current limiting resistors of LED strips/signage
- 4) Using a higher duty cycle digital coding scheme
- 5) Not fully turning off the LEDs by using a turn-off resistor

2.10.1 Using a Higher Power Supply

One very simple solution to compensate for the brightness drop caused by modulation is to increase the supply voltage of the luminaire such that the amount of peak current is doubled, as shown in Figure 2.22. However CV supplies are mostly a fixed voltage of 24 or 12V output. In addition, tunable supplies are relatively expensive and tuning must be performed every time the load is changed.

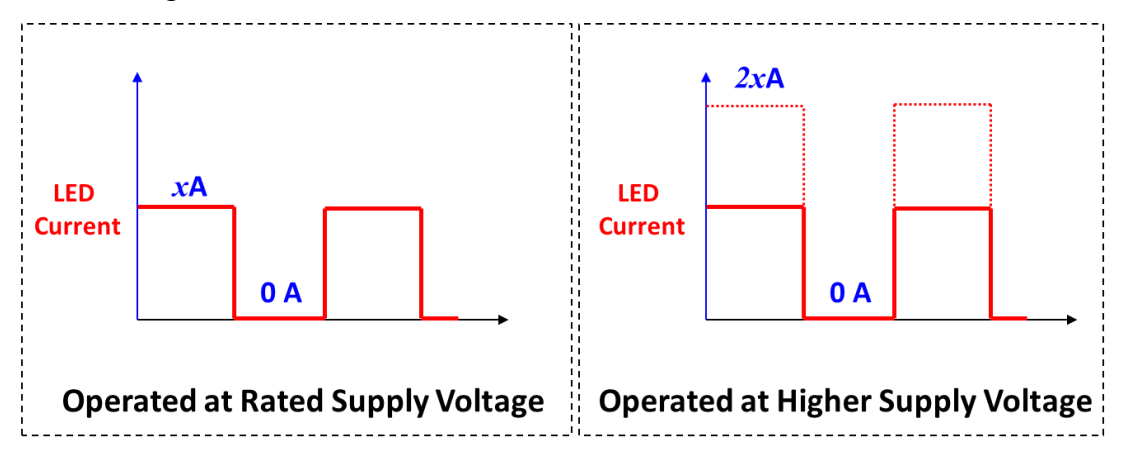


Figure 2.22 Operating LED luminaire at higher supply voltage to compensate for the drop in brightness due to modulation

2.10.2 Using a DC-DC Boost Converter

Another solution is to add a DC-DC boost converter to the modulator to boost the output voltage such that the current is increased in the LED. However, the boost converter must be tuned for different loads, which makes the operation tedious. In addition, the circuit complexity,

size and cost of the modulator will significantly increase. The concept of boost converter addition is illustrated in the modulator block diagram in Figure 2.23.

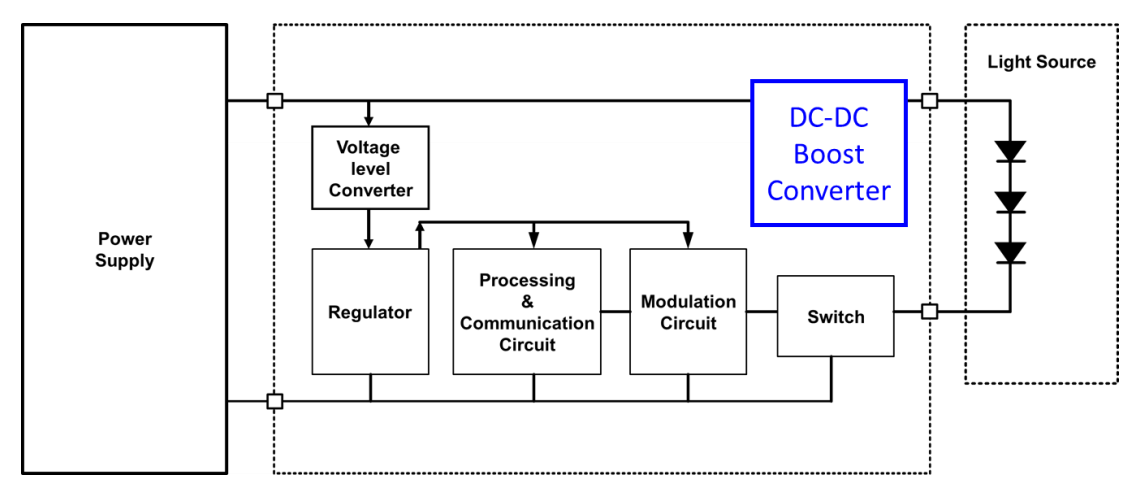


Figure 2.23 Addition of a DC-DC boost converter for brightness drop compensation

2.10.3 Reducing the Current Limiting Resistors on LED Strips

LED light strips are the most widely used type of load for CV signage and light boxes. These strips come with a series of LEDs with CC resistors, and these resistors' values can be modified to increase the current in the LEDs to compensate for brightness reduction. As shown in the measurement results in Figure 2.24, reducing the value of a series resistor from 680 Ohm to 330 Ohm for a 5 V LED strip, improves the brightness by up to 90%. Further reduction of the resistor value could also result in further improvement in brightness. However, such modification can be tedious to perform on existing LED strips. To solve this problem, LED strips can be custom designed for VLC applications at extra manufacturing cost.

LED Strip	Supply Voltage*	With VLC Modulator	Lux @50cm	
Original Strip with 680Ω Resistors	5.11V	NO	79.3 lx	
Original Strip with 680Ω Resistors	5.11V	YES	41.6 lx	→ 1.8x [‡]
New Strip with 330Ω Resistors	5.11V	No	143.9 lx	
New Strip with 330Ω Resistors	5.11V	YES	71.5 lx	

^{*} Supply Voltage is provided by 5V charging adapter that came with the Light.

^{# 1.8}x improvement of brightness by changing the resistor (without considering the Adapter)



Figure 2.24 Current limiting resistor modification to compensate for brightness drop 2.10.4 Using a Higher Duty Cycle Digital Coding Scheme

Brightness can also be improved by modifying the coding such that the overall duty cycle of the signal is increased. One simple method is illustrated in Figure 2.25 where the period of highs (binary 1) is increased x times to increase the duty cycle and hence brightness by (x/x+1)%. However, this method will reduce the coding efficiency and also increase the length of the binary code, which can affect the sensitivity and detection range of the communication link.

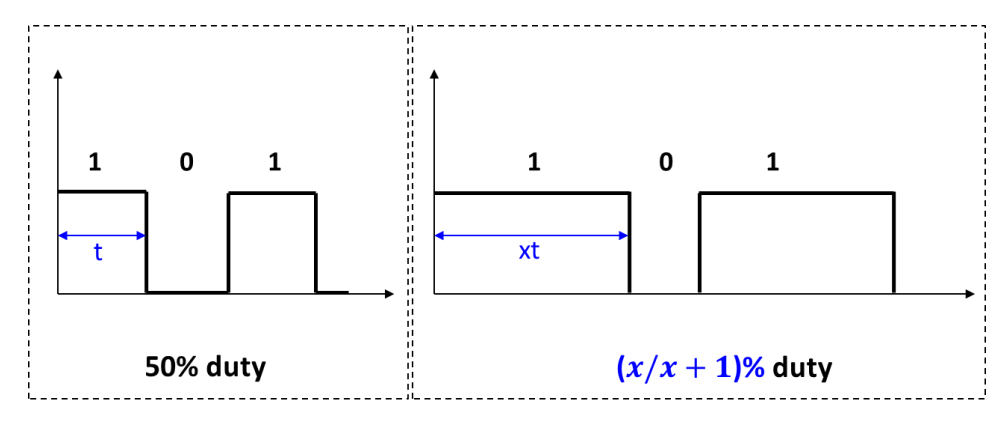


Figure 2.25 Extending the period of highs (1s) in digital modulation signals to improve the brightness of the luminaire

2.10.5 Using a Turn-Off Resistor

Instead of completely turning off the LEDs and reducing the current to 0 during the turn-off (binary 0) period of modulation, the LED current can be reduced to the amount where the brightness is significantly reduced but the LEDs are not entirely turned off. This way, the average amount of current flowing through the LEDs will become relatively higher in comparison to the case where the LEDs are entirely off during the turn-off period of modulation. This can be achieved using a current bypass resistor that is connected in parallel to the modulation switch, as shown in Figure 2.26. When the switch is opened, a reduced amount of current will flow through this resistor.

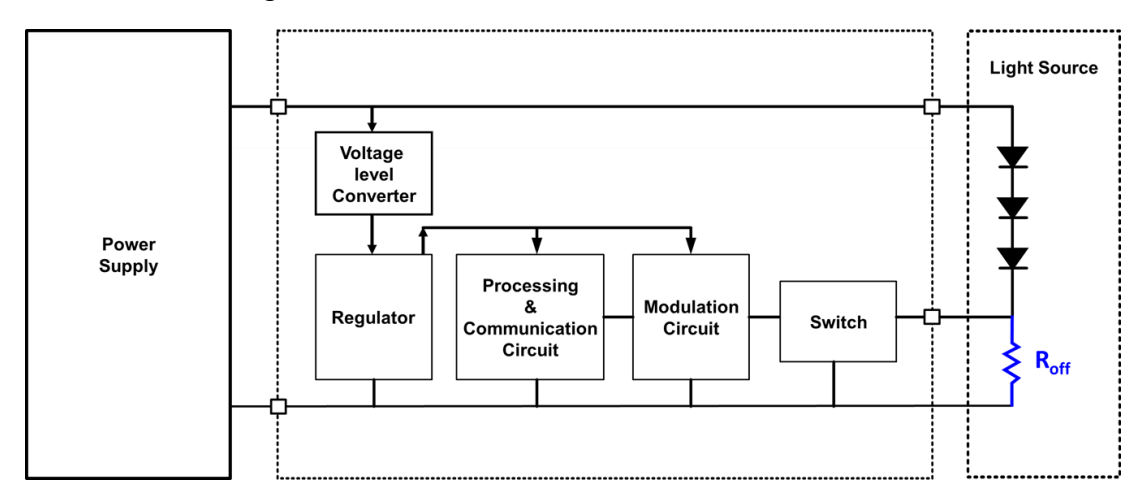


Figure 2.26 Using a turn-off resistor for brightness drop compensation

The degree of modulation is proportional to the value of the turn-off resistor. The higher the resistor value, the higher the modulation will be but lower the brightness. This brightness and modulation tradeoff must be made considering the sensitivity of the reception and brightness requirements. This method is very simple to implement. However the value of the resistor must be tuned to match various loads. In addition, even though the brightness is improved by using the turn-off resistor, it cannot be made equal to the original value as there must be some degree of modulation in the light in order for the communication link to work. The effect is illustrated in Figure 2.27.

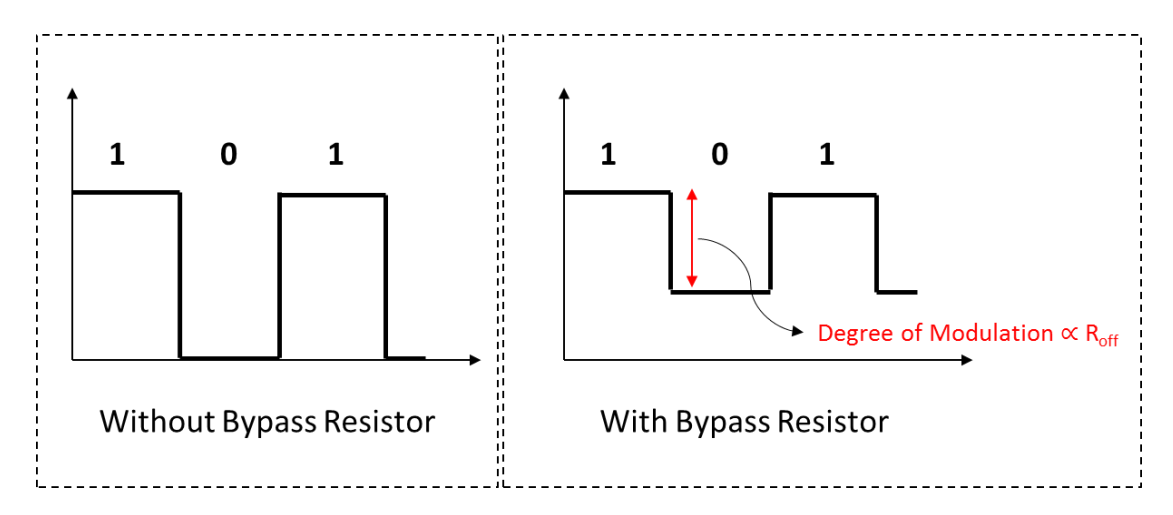


Figure 2.27 LED current waveform showing the effect of turn-off resistor on degree of modulation

2.11 Impact of Light Modulation on Reliability and Quality of Lighting

As discussed in the previous sections, the modulation current of a CC LED can rise to twice the amount of the original current instantaneously before falling to zero and then rising again. This sudden rise and fall in current could have a long-term impact on the reliability and lifetime of a luminaire and may affect the overall quality of lighting. In this section, we present the discussion and measurement results to verify that there are no noticeable performance impacts on the quality and reliability of lighting when operated with VLC modulation for a long time.

An LED's reliability is proportional to its junction temperature—the higher the temperature, the shorter the lifetime. Therefore, driving the LED at a current higher than the rated current, which results in an increase in the junction temperature [22], can reduce the lifetime of the LED. However, according to the results published in [21–23], if the higher current is supplied in the form of pulses with a duty cycle of 50% or less, the impact on the lifetime can be significantly reduced. As shown in the measurement results in [23], if the peak current of the LED is doubled while keeping a duty cycle of 50%, there is no noticeable impact on the lifetime of the LED. These results, in addition to the data provided in [21], verify that instantaneously overdriving LEDs at higher frequency PWM is a safe operation that does not increase the temperature of the LEDs, and hence it does not degrade the lifetime of the LEDs.

Table 2.3 Comparsion of LED light with and without VLC modulator

Parameter	With VLC Modulator	Without VLC Modulator	
Rated Current	500 mA		
Rated Power	18 Watt		
Measured Current	491 mA 493 mA		
Measured Voltage	40 V 37 V		
Measured Power	19.7 W	18.2 W	

A reliability test to verify the impact of VLC modulation on an LED light was conducted, measuring the power, lumen output and color temperature. The light used for the measurement was an Osram LED T8 ST8A-DC 18 W with 500 mA current [24]. Table 2.3 shows the initial measurement results with and without the VLC modulator. The measured current is identical for both cases, whereas the voltage and overall power consumption is slightly higher (~8%) in the former case due to the switching loss and the power consumed by the Bluetooth transmission in the modulator.

Table 2.4 Long-term Reliability Test of LED luminaire with VLC modulator

	Osram LED T8 ST8A-DC 18W @500mA with VLC modulator				
	Wattage Lumen CCT X Y				
0 Hours	22.32	1888.7	4003	0.3795	0.3735
100 Hours	22.31	1878.7	3989	0.3801	0.374
500 Hours	22.38	1940.1	3991	0.3797	0.3728
1000 Hours	22.53	1892.2	4000	0.3796	0.3735
2000 Hours	22.39	1990.1	3987	0.38	0.3733
3000 Hours	22.41	1934.3	3969	0.3809	0.3742
4000 Hours	22.3	1985.4	3998	0.3799	0.3744

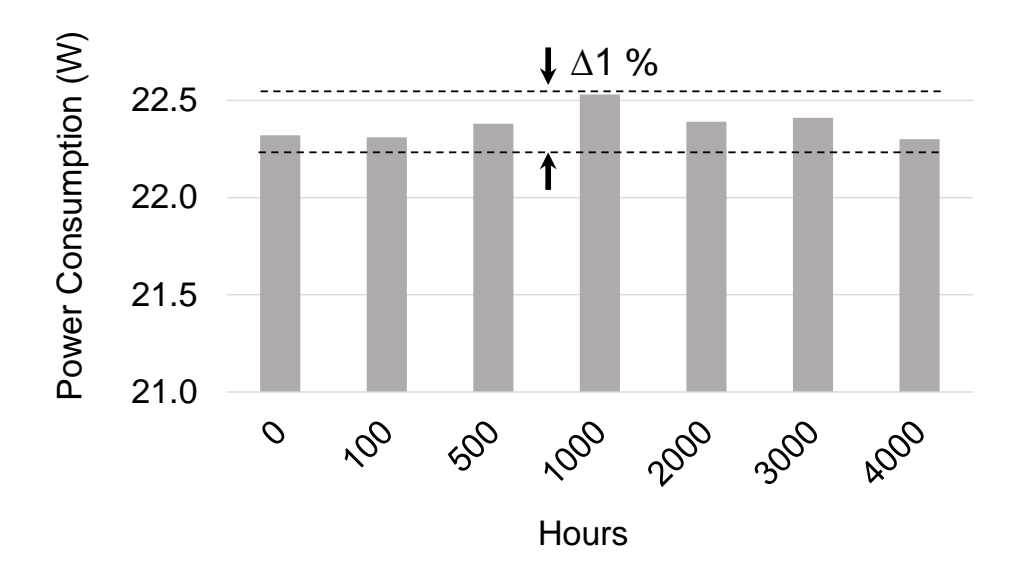


Figure 2.28 Power consumption variation during long-term reliability test

The measurement results of the reliability test run for 4000 hours are shown in Table 2.4. The results indicate no noticeable difference in the overall power consumption, color temperature and the lumen output of the LED luminaire. For power consumption, the maximum deviation between maximum and minimum power observed throughout the test is within 1% of the total power as indicated by the bar chart show in Figure 2.28. Whereas, for light intensity, the variation was within 4% of the total lumen, which is a non-observable change and is well within the acceptable range, as per the lighting manufacturer. The bar chart indicating the light intensity variation is shown in Figure 2.29.

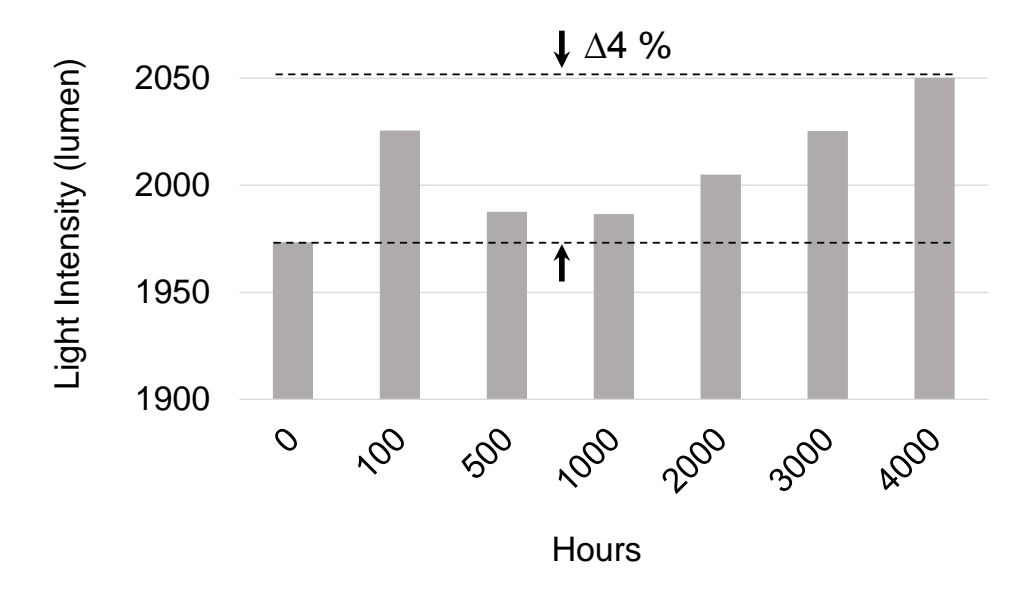


Figure 2.29 Light intensity variation during long-term reliability test

The color temperature variation is measured both in the change in overall color temperature as well as the change in the X and Y coordinates of the CIE (International Commission on Illumination) chromaticity diagram, to verify that the color deviation is acceptable from both perspectives. The color temperature change of less than 1% is measured as shown in Figure 2.30, whereas the chromaticity diagram further verifies that the deviation in X and Y coordinates is within 1%, as shown in Figure 2.31.

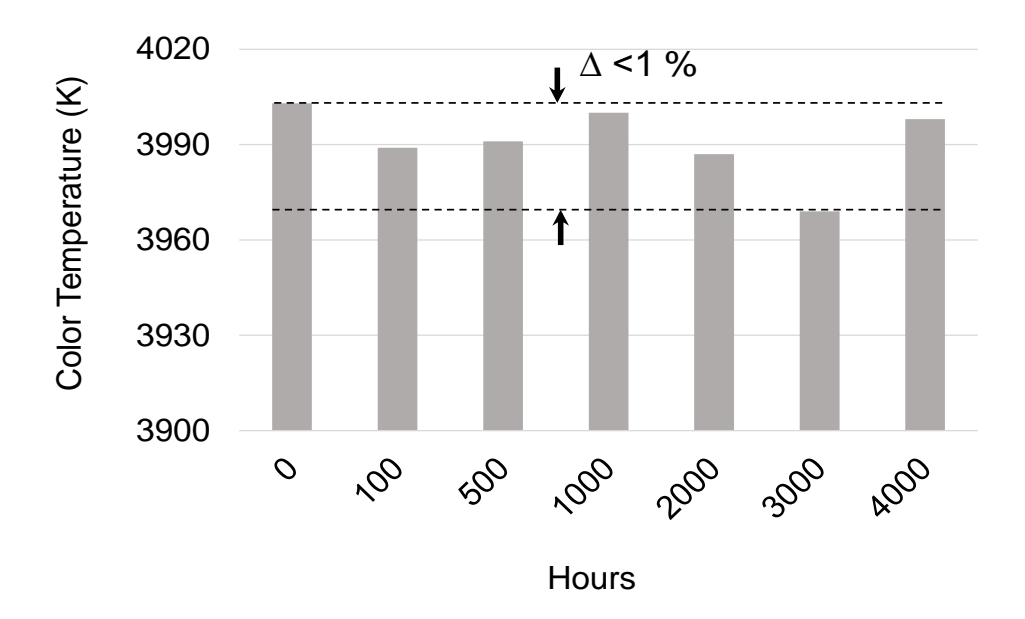


Figure 2.30 Color temperature variation during long-term reliability test

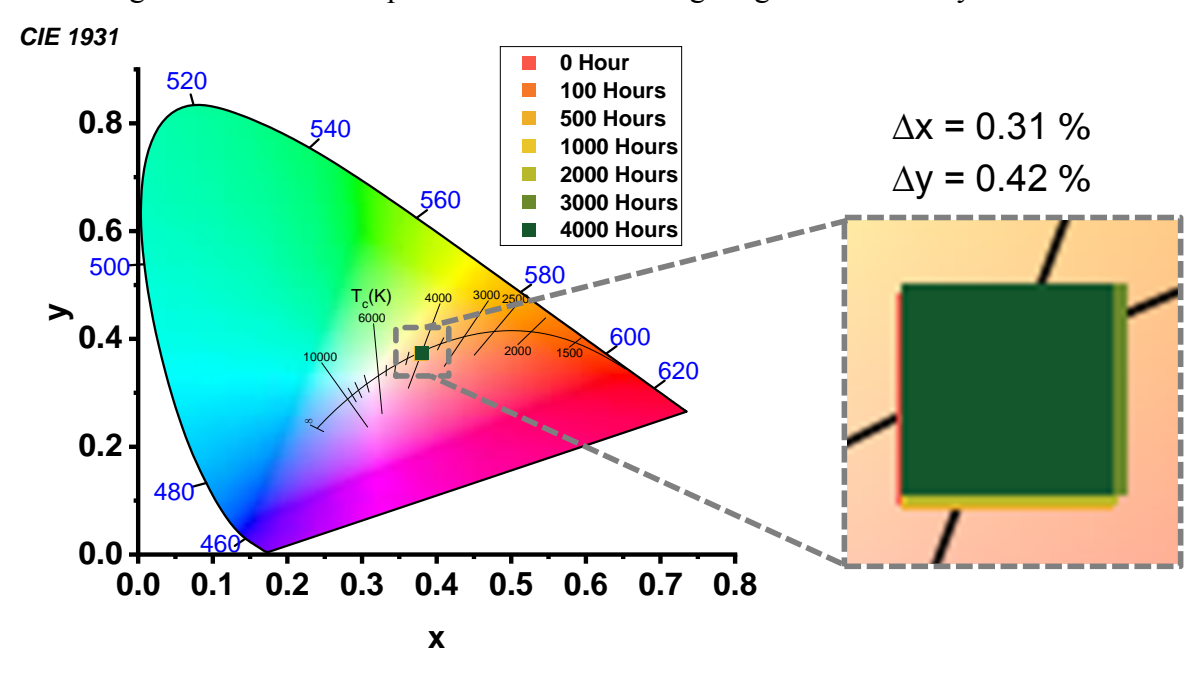


Figure 2.31 Chromaticity diagram indicating the deviation in X and Y coordinates during long-term reliability test

2.12 References

- [1] T. Kishi, H. Tanaka, Y. Umeda and O. Takyu, "A high-speed LED driver that sweeps out the remaining carriers for visible light communications," *Journal of Lightw. Technol.*, vol. 32, no. 2, pp. 239-249, 2013.
- [2] T. Fath, C. Heller and H. Haas, "Optical wireless transmitter employing discrete power level stepping," *J. of Lightw. Technol.*, vol. 31, no. 11, pp. 1734-1743, June 2013.
- [3] I. E. Lee, J. C. Law, K. Y. Chung, et al. "Design and development of a portable visible-light communication transceiver for indoor wireless multimedia broadcasting," in 2nd *IEEE International Conference on Electronic Design (ICED)*, pp. 20-24, 2014.
- [4] S. Zhao, J. Xu, and O. Trescases, "Burst-mode resonant LLC converter for an LED luminaire with integrated visible light communication for smart buildings," *IEEE Trans. Power Electron.*, vol. 29, no. 8, pp. 4392–4402, Aug. 2014.
- [5] F. Che, L. Wu, B. Hussain, et al. "A fully integrated IEEE 802.15. 7 visible light communication transmitter with on-chip 8-W 85% efficiency boost LED driver," *J. Lightw. Technol.*, vol. 34, no.10, pp. 2419-2430, 2016.
- [6] B. Hussain, X. Li, F. Che et al. "Visible light communication system design and link budget analysis," *J. Lightw. Technol.*, vol. 33, no. 24, pp. 5201-5209, 2015.
- [7] Y. Gao, L. Li, P. K. T. Mok. "An AC-input inductorless LED driver for visible-light-communication applications with 8Mb/s data-rate and 6.4% low-frequency flicker," in 2017 IEEE International Solid-State Circuits Conference (ISSCC), pp. 384-385, 2017.
- [8] B. Yu, H. Zhang, L. Wei and J. Song, "Subcarrier grouping OFDM for visible-light communication systems," *IEEE Photon. J.*, vol. 7, no. 5, pp. 1-12, Oct. 2015.
- [9] K. Modepalli and L. Parsa, "Dual-Purpose Offline LED Driver for Illumination and Visible Light Communication," *IEEE Transactions on Industry Applications*, vol. 51, no. 1, pp. 406-419, Jan.-Feb. 2015.
- [10] C.-S. A. Gong, Y.-C. Lee, J.-L. Lai, C.-H. Yu, L. R. Huang, and C.-Y. Yang, "The high-efficiency LED driver for visible light communication applications," *Sci. Rep.*, vol. 6, Aug. 2016, Art. no. 30991.

- [11] W. Pawlikowski, M. Narimani, S. Hranilovic, "A novel method of integrating visible light communications within LED drivers," in *Globecom Workshops (GC Wkshps) 2017 IEEE*, pp. 1-6, 2017.
- [12] W. Pawlikowski, A. Barmaki, M. Narimani and S. Hranilovic, "Light-emitting commutating diodes for optical wireless communications within LED drivers," *IEEE Photonics Journal*, vol. 12, no. 5, pp. 1-11, Oct. 2020.
- [13] V. M. de Albuquerque, G. M. Soares, J. M. Alonso and P. S. Almeida, "A simple resonant switched-capacitor LED driver employed as a fast pulse-based transmitter for VLC applications," *IEEE Journal of Emerging and Selected Topics in Power Electronics*, vol. 9, no. 1, pp. 111-122, Feb. 2021.
- [14] F. Loose, L. Teixeira, R. R. Duarte, M. A. Dalla Costa and C. H. Barriquello, "On the use of the intrinsic ripple of a Buck Converter for Visible Light Communication in LED Drivers," *IEEE Journal of Emerging and Selected Topics in Power Electronics*, vol. 6, no. 3, pp. 1235-1245, Sept. 2018.
- [15] J. Rodríguez, D. G. Lamar, P. F. Miaja, D. G. Aller and J. Sebastián, "Power-efficient VLC transmitter based on pulse-width modulated DC–DC converters and the split of the power," *IEEE Transactions on Power Electronics*, vol. 34, no. 2, pp. 1726-1743, Feb. 2019.
- [16] M. L. G. Salmento, G. M. Soares, J. M. Alonso and H. A. C. Braga, "A dimmable offline LED driver with OOK-M-FSK modulation for VLC applications," *IEEE Transactions* on *Industrial Electronics*, vol. 66, no. 7, pp. 5220-5230, July 2019.
- [17] Mesh networking is blue [Online]. Available:https://www.bluetooth.com/learn-about-bluetooth/recent-enhancements/mesh/
- [18] What is iBeacon? [Online]. Available:http://www.ibeacon.com/what-is-ibeacon-a-guide-to-beacons/
- [19] "CC2540F128, CC2540F256, 2.4-GHz Bluetooth® Low Energy System-on-Chip," Texas Instruments, 2012 [Online]. Available:www.ti.com

- [20] "SmartBondTM DA14580 and DA14583 The most flexible and lowest power Bluetooth® low energy solutions" Dialog Semiconductor. [Online] Available:www.dialog-semiconductor.com
- [21] Getting The Most Out Of LED Lighting [Online]. Available: https://homepages.inf.ed.ac.uk/rbf/CVonline/LOCAL_COPIES/FIRSTSIGHT/LED-lighting.pdf
- [22] N. G. M. Yang, B. Y. R. Shieh, T. F. Y. Zeng and S. W. Ricky Lee, "Analysis of pulse-driven LED junction temperature and its reliability," in 2018 15th China International Forum on Solid State Lighting: International Forum on Wide Bandgap Semiconductors China (SSLChina: IFWS), 2018, pp. 1-3, doi: 10.1109/IFWS.2018.8587392.
- [23] B. J. Huang, M. S. Wu, C. W. Tang, J. W. Chen, "Reliability test of LED driven by PWM technique," *Proceedings of SPIE-The International Society for Optical Engineering*, August 2008.
- [24] SubstiTUBE Advaced DC T8 [Online].
 Available:https://www.ledvance.asia/products/lamps/led-tubes/substitube-advanced-dc-t8/index.jsp

CHAPTER 3 VLC Receiver Design Using CMOS Image Sensor

3.1 CMOS Image Sensor for VLC

Unlike global shutter cameras, CMOS image sensors feature a rolling shutter, which allows the picture to be captured in a sequential manner. Specifically, every time the shutter opens, the sensor selects and captures one row of pixels before the shutter closes and opens again for it to capture the next row, as shown in Figure 3.1 (a). Each row of pixels is first reset before being exposed to the light for a time equal to the exposure time (t_{exp}) followed by a read out time (t_r) . As soon as the pixel row completes read out, the next row is ready to start the read out procedure. This introduces a capture time difference of t_r between adjacent rows, as shown in Figure 3.1 (b). This type of architecture and sequential scanning can help to significantly reduce the size and hardware cost of image sensor.

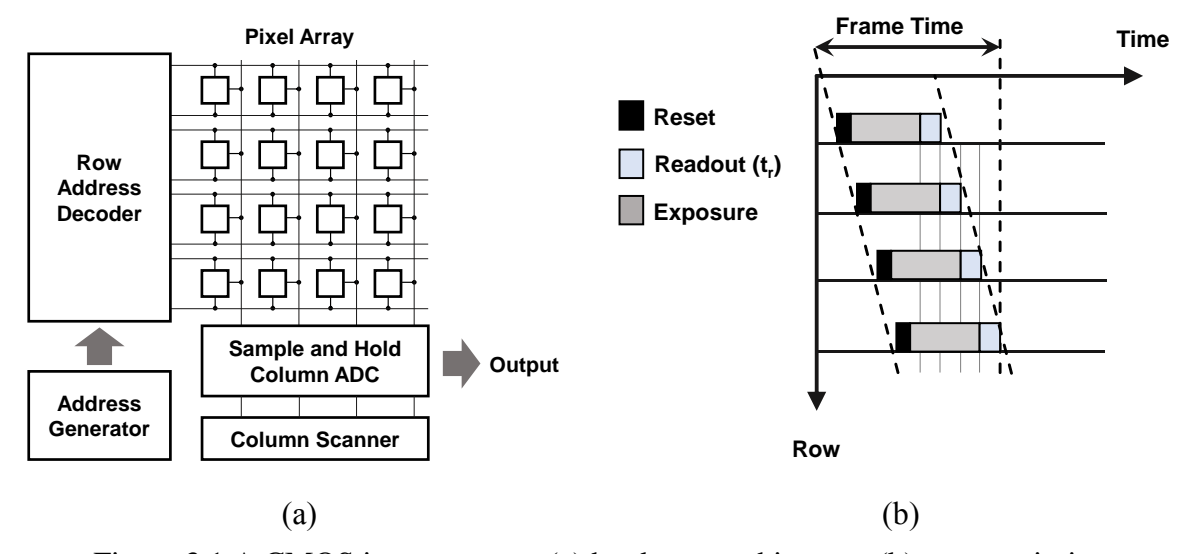


Figure 3.1 A CMOS image sensor: (a) hardware architecture (b) capture timing

If the turn-on and turn-off times of the LEDs are comparable to the speed of the rolling shutter, the image contains a pattern of dark and bright regions, which can be processed to decode a VLC signal [1], [2], as illustrated in Figure 3.2. The width of these dark and bright stripes can be controlled by setting an appropriate frequency. Typically, it is possible to observe a discernable pattern up to a frequency of 20 kHz.

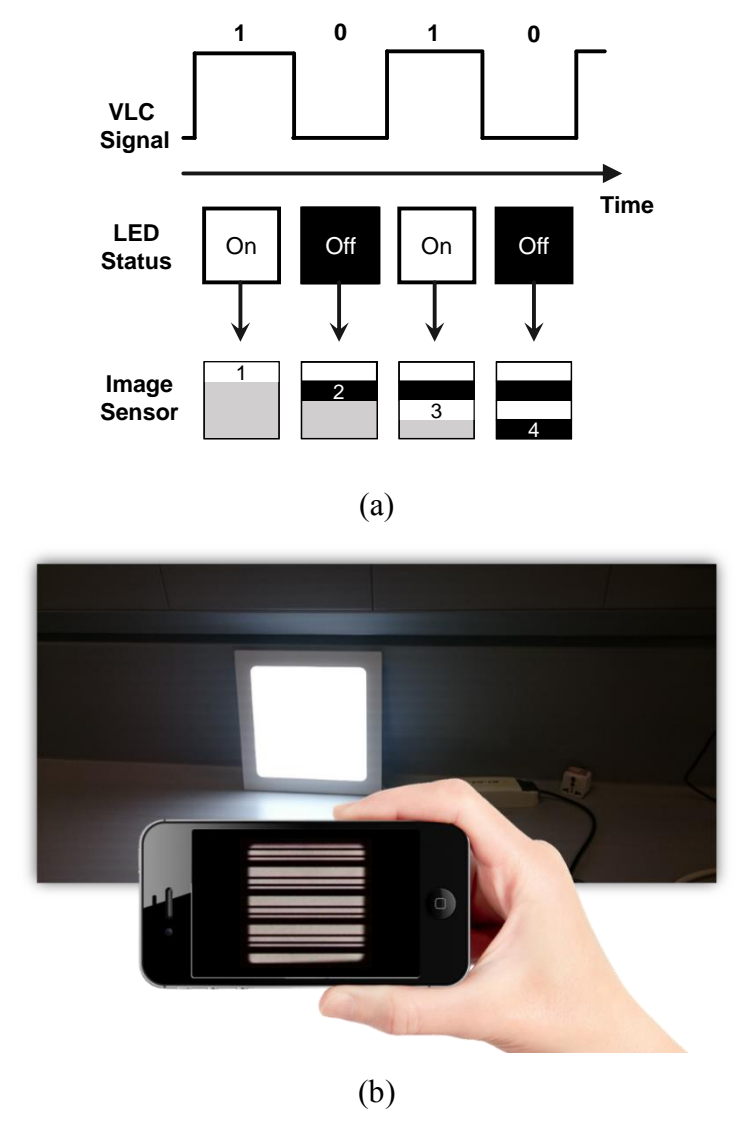


Figure 3.2 (a) Rolling shutter effect on a CMOS image sensor (b) pattern obtained from a modulated LED source using a smartphone

3.2 Related Works

Since the demonstration of VLC using the rolling shutter effect on a CMOS image sensor in [1], several works have been published on VLC using optical cameras [3]. Figure 3.3 is a diagram grouping these related reference works according to their respective areas. Some of these works are based on global shutter cameras [4–7] and can only achieve a very low speed if regular frame rates are used [6], or can achieve higher speeds by using high frame rate cameras with costly hardware [5]. Generally, optical camera communication (OCC) systems using global shutter are targeted at outdoor applications in vehicle-to-vehicle (V2V)

communication for intelligent transportation systems [7]. Other works use rolling shutter-based CMOS cameras for VLC. These are either industrial cameras for industrial and robotic applications [8–10] or smartphone cameras for consumer applications [11–22].

Research on smartphone-based OCC encompasses several directions, including improvement of data rates [11–14], improvement of detection sensitivity via threshold decoding algorithms [15–17], and indoor positioning systems [20–22]. Data rates for a rolling shutter-based communication link can be increased using various techniques, including multilevel intensity modulation [11,12], analog modulation such as orthogonal frequency division multiplexing (OFDM) [13], or using the spatial diversity of transmitters [14].

In [11], a multilevel intensity modulation (m-IM) scheme is proposed. The demonstrated system can achieve a 10 kbps data rate over a range of 2 m. Similarly in [12], a pulse width modulation (PWM)-based multilevel signal is used to achieve a data rate of up to 9 kbps. Further improvement of data rates is demonstrated in [13], where DC-offset based OFDM modulation is used to achieve a data rate of over 22 kbps. However, the modulation schemes presented in these works require complicated and costly transmitter hardware, and are unsuitable for low cost deployment in a practical scenario. Therefore, on-off keying (OOK) is a preferred modulation scheme for smartphone-based OCC systems.

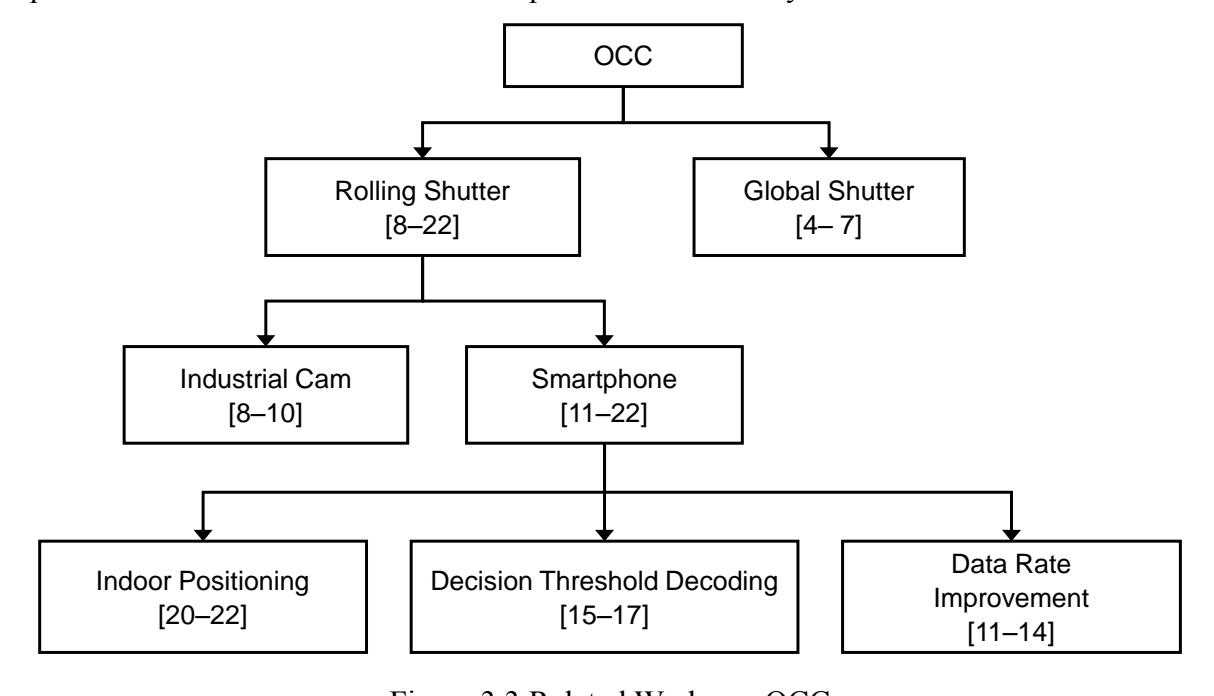


Figure 3.3 Related Works on OCC

The use of spatial diversity to increase the data rate is demonstrated in [14], where multiple LED luminaries are used to simultaneously transmit data that can be combined at the receiver. However, this requires connectivity and data synchronization among the multiple LEDs and puts stringent line-of-sight requirements during practical deployment scenarios. Spatial diversity can also be explored using the non-line-of-sight (NLOS) link to receive the signal from the reflection surface, as demonstrated in [18] and [19].

A number of algorithms for improvement of decision threshold decoding are presented in [15–17]. These algorithms aim to reduce the impact of blooming on the bit error rate (BER) by adaptively decoding the decision threshold. However, the blooming effect is generally observed in relatively higher exposure modes and can be avoided if a high frequency and a high shutter speed are used.

Several works describe the use of an OCC link for positioning [20–22]. These works generally describe the algorithm for calculating the position of the camera based on the geometrical properties of the LED light source without describing the design details of the communication link. More details on the use of OCC for high accuracy indoor positioning are given in Chapter 5.

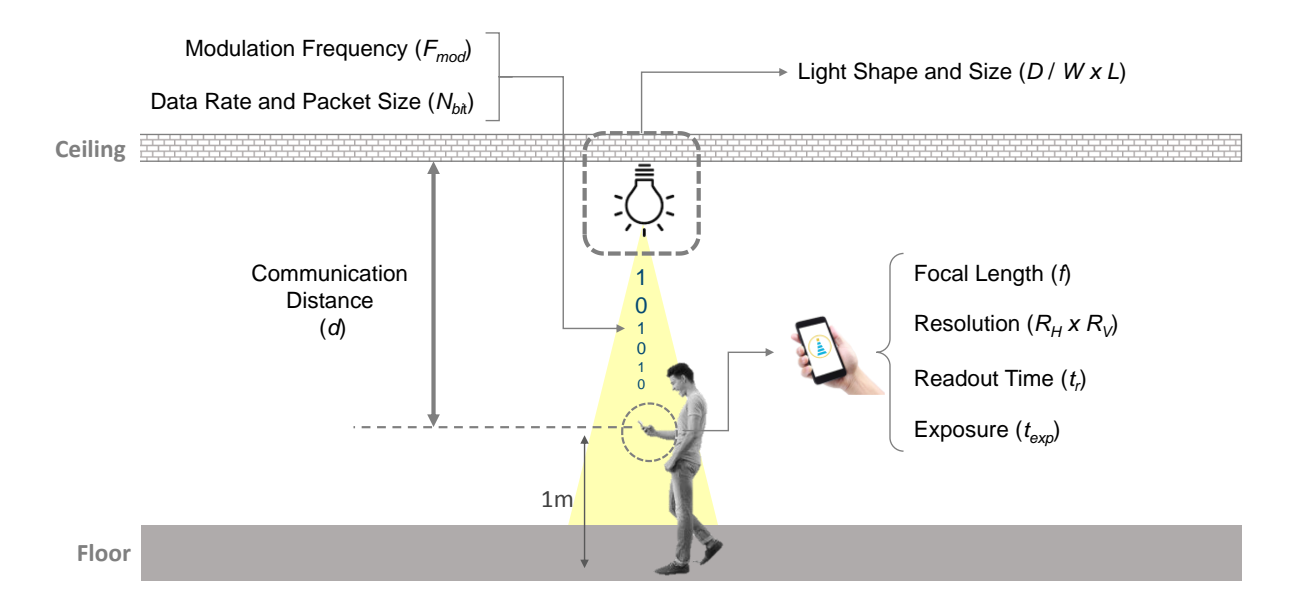


Figure 3.4 Contributions of this chapter include the modeling of key system design parameters for building a practical OCC system for location-based information delivery applications

All the aforementioned works focus on improving the data rate or propose algorithms to improve the sensitivity. However, these works generally rely on a single type of LED light source (predominantly a round-shaped panel light), and one or two types of smartphones as the receiver. Usually smartphones are configured with the highest resolution and the images captured are processed on a computer. Thus far, no work has focused on the practical system design aspects where a number of light shapes and sizes are used as transmitters, nor has a receiver algorithm been designed that can provide a target detection sensitivity for a wide variety of smartphones, each featuring different specifications of the CMOS image sensor. Therefore, in this chapter, an OCC receiver design is presented that takes into account several key aspects of the system design, including the size, shape and color of the LED light source and the types of smartphones used as receivers. A detailed system design model is derived that takes system specifications as input and calculates modulation and coding scheme parameters, including modulation frequency, data rate, packet size, etc. to achieve the target communication distance for location-based information delivery applications, as shown in Figure 3.4.

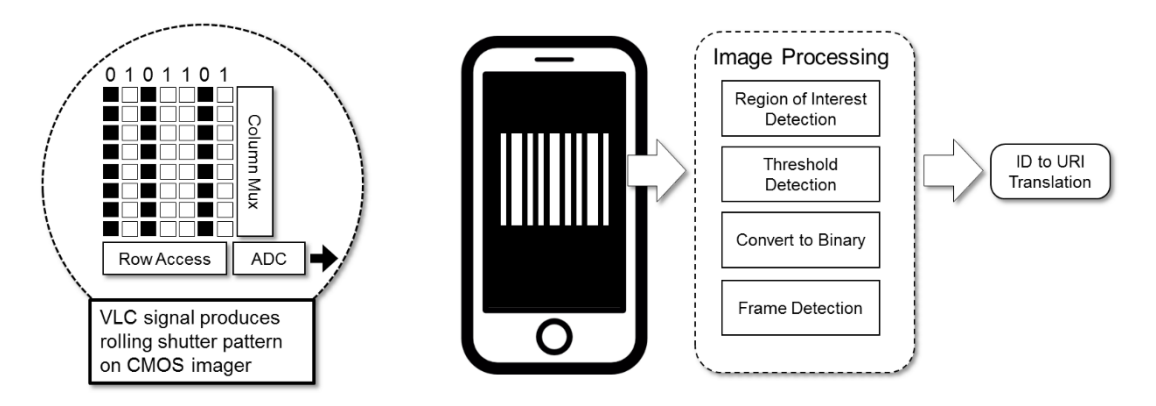


Figure 3.5 Signal processing block diagram of VLC receiver on smartphone

3.3 VLC Receiver Implementation on Smartphone Camera

The processing block diagram of the VLC detection procedure is shown in Figure 3.5. The modulated LED signal is received by the smartphone camera as frames consisting of rolling shutter patterns. To decode the signal, each row of the pattern is translated into a binary stream, which is combined to create a data frame consisting of a unique identifier (ID). The ID is

eventually used by the application software to point to a uniform resource identifier (URI) database.

The detailed image processing steps are shown in Figure 3.6. Since the information in the image is contained as variations of light intensity, the first step in the processing is converting the captured picture to a grayscale intensity image. As shown in Figure 3.6, high intensity areas represent the time interval when the light was on, while low intensity regions represent the periods when the light was turned off.

In the next step, an edge detection algorithm is applied on the image to find the edges/boundary of the area where the rolling pattern of the light exists. This step marks the edges of the area of interest so that it can be cropped out in the next step for further processing. Once the region of interest (ROI) is available, Otsu's filtering method for automatic thresholding is applied to convert the image into a binary image. After the application of Otsu's filtering, each pixel in the image has either an intensity value of 1 or 0.

In the next step, the intensity value of the pixels along each row are summed, as shown in Figure 3.6 (sum of pixels). In the final step, the binary data stream is evaluated from the sum of the pixels by converting each row into either 1 or 0 based on half of the median value of the sum of the pixels. The binary data stream produced in the last step can then be compared with the data frame format in the next step to extract the information payload.

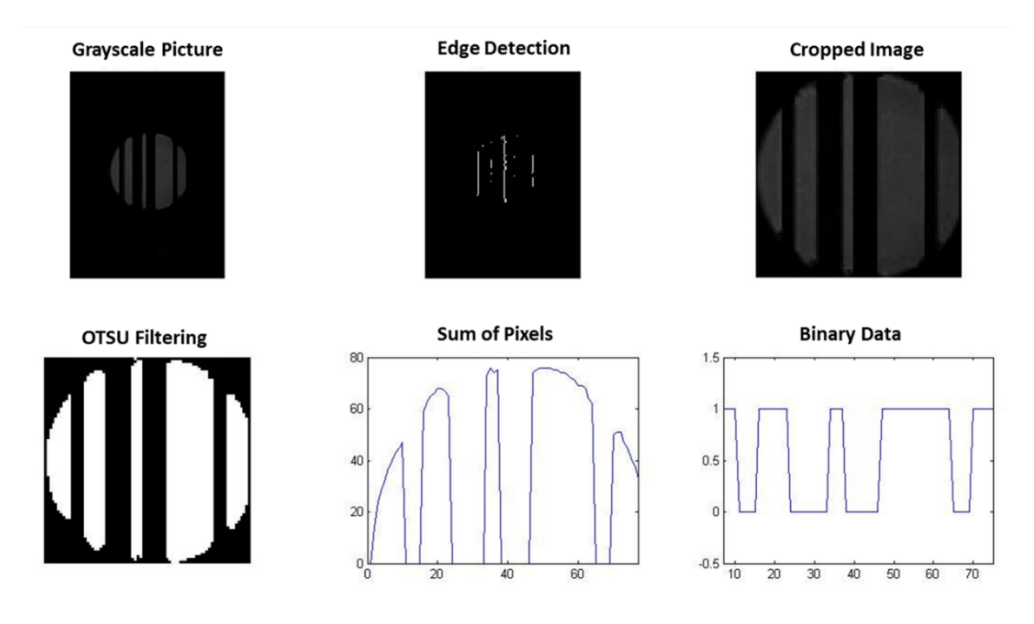


Figure 3.6 Image processing steps to decode VLC signal

Data from a VLC-enabled LED light source is transmitted as continuous frames of a fixed predetermined format. Each frame consists of three parts, preamble, payload, and cyclic redundancy check (CRC), as shown in Figure 3.7. The preamble is a unique pattern that is included in each frame to mark the start of the frame. Since frames are transmitted consecutively and the receiver has no information of when the frame starts, there must be a unique pattern in the data that can be used as an indicator of the frame start. Since this pattern has to be unique, it cannot be included in the actual payload. In addition, the preamble is also used to determine the pixels/bit for decoding the rest of the frame to extract the payload. As the row scanning speed of the image sensor is different for each resolution setting and varies from device to device, it cannot be determined from the scanned image how many rows are scanned during the interval the light transmits one unit of binary information, i.e., 1 bit. In other words, when the light is turned on to transmit 1, how many rows are scanned by the CMOS image sensor during that interval determines the number of unit pixels that constitute 1 bit of information. This pixels/bit information can then be applied on the frame to extract the payload.



Figure 3.7 VLC Data Packet Format

The payload is the portion of the frame that contains the information. This information, contains a unique ID that is mapped to a unique resource. This ID could be a key to enable access to something, a URI to go to a website, or an indicator to perform a function on the receiving device.

Finally, the CRC is an error check sequence that is added at the end of the payload and is used by the receiver to confirm that the received data are correct. In conditions where the light is blocked or light intensity is low, possible errors in the received bits can potentially lead to a false ID that was not intended by the transmitter. Therefore, the CRC or error check sequence ensures the reliability of the received data.

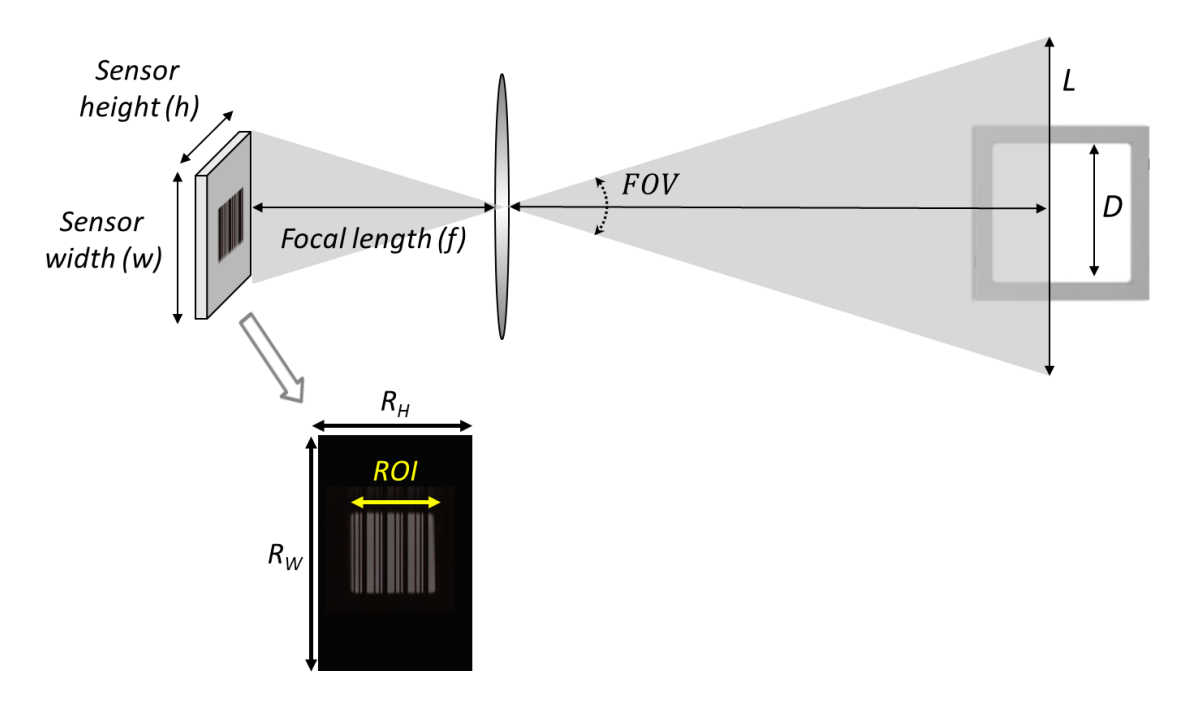


Figure 3.8 Relation between the distance of the object and ROI

3.4 Optical Model of Camera for OCC

Since the image contains information in the form of 2-dimensional rolling shutter pattern, size is a key element for determining the sensitivity of the system as bigger the light size, more number of bits can be fit inside the region of interest (ROI). This is in contrast to the photodetector-based system, where light intensity is a key factor as it directly affects the received signal swing on the receiver side [23]. To understand the relationship between the distance and the captured size of the rolling shutter pattern, the model of pinhole camera is illustrated in Figure 3.8. The size of the object captured at distance depends on the field of view of the camera (FOV) as shown in (3.1).

$$2\tan^{-1}\frac{h/2}{f} = FOV = 2\tan^{-1}\frac{L/2}{d}$$
(3.1)

According to this model, the ratio of light size (D) to the size of the field of view (L), is equal to the ratio of the horizontal image resolution in pixels (R_H) to the size of the lights projection on the image in pixels (ROI), as shown in (3.2).

$$\frac{L}{D} = \frac{R_H}{ROI} \tag{3.2}$$

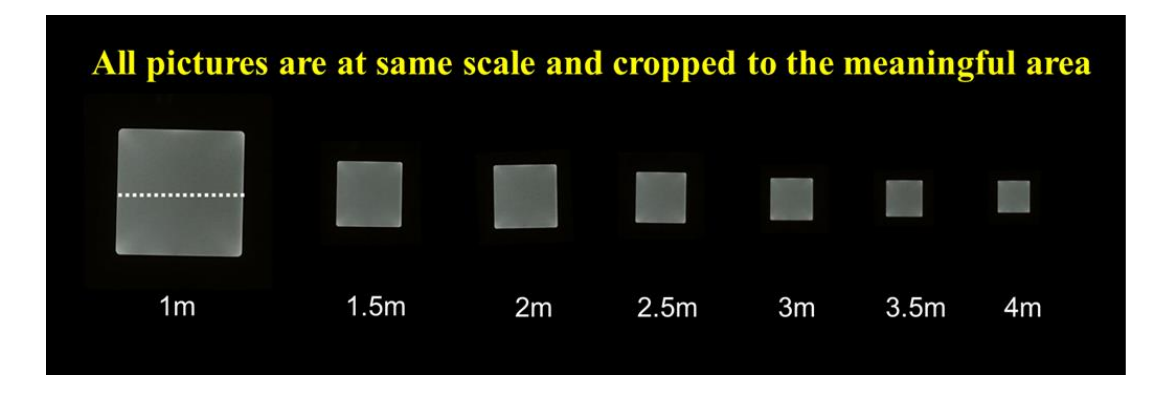
55

Through (1) and (2), ROI can be calculated at a certain distance (d).

$$ROI = \frac{D R_H}{2d \tan(FOV/2)}$$
 (3.3)

,

Measurements are conducted on a square light panel using iPad's front camera to verify the relation derived above. Figure 3.9 shows the measurement results performed on a square light panel which verifies the inverse relation between the number of pixels on ROI against the distance.



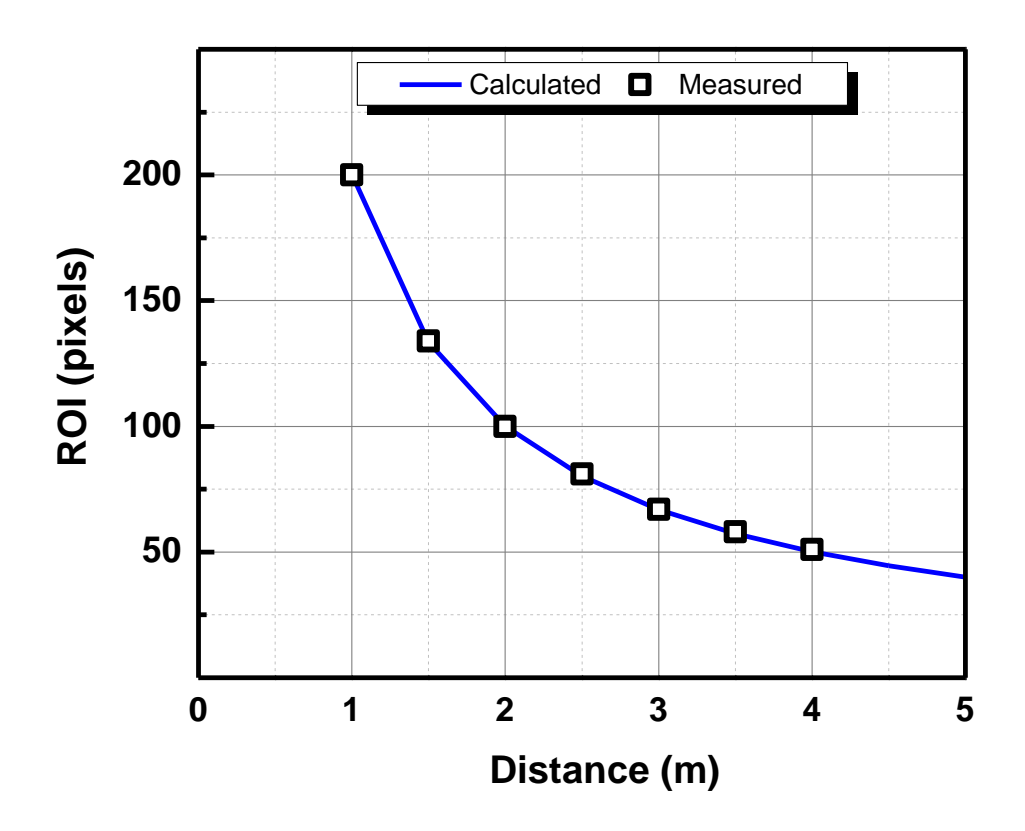


Figure 3.9 Relation between number of pixels on ROI vs distance

3.5 Choosing an Optimum Modulation Frequency

The modulation frequency is a key parameter in building a communication link with optimum performance. Figure 3.10 shows three images of a modulated light source driven at different frequencies. It can be seen that the modulation frequency is directly proportional to the number of received bits. To further illustrate the effect of modulation frequency and distance on the data rate, measurements were taken using an LED light panel of 20 cm x 20 cm and a Lenovo Phab 2 Pro smartphone at three different distances, 0.5 m, 1 m and 1.5 m. Figure 3.11 shows the measurement results and illustrates the relationship between the modulation frequency, communication distance, and amount of data received per frame. The measurement indicates that higher frequency leads to a higher data density in the ROI, whereas increase in distance leads to a smaller ROI and thereby decreases the amount of data per frame. In other words, for a given modulation frequency, the data rate can be increased by reducing the communication distance, or for a given distance, the data rate can be increased by increasing the modulation frequency.

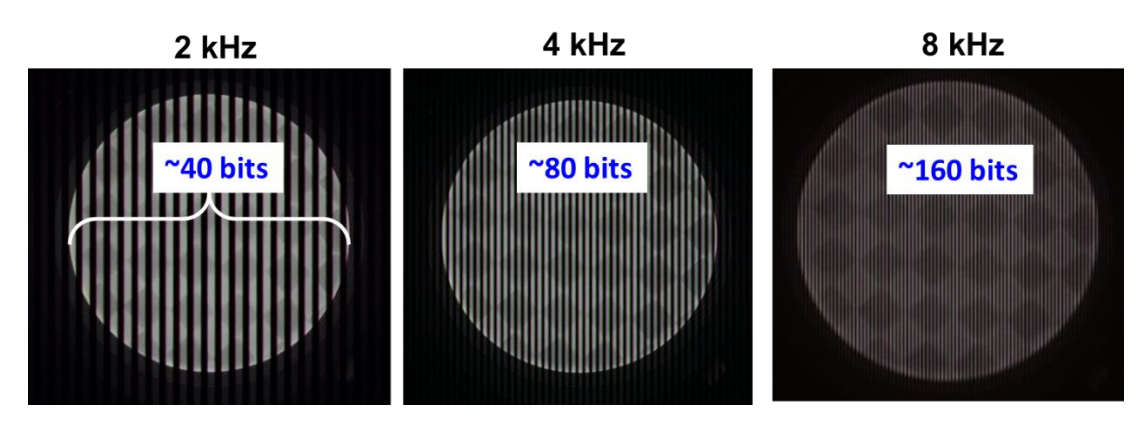


Figure 3.10 Images of a round shaped LED light modulated at various frequencies

Usually in practical applications, for instance indoor positioning, the distance between the camera and the light source is fixed, therefore, it is desirable to increase the modulation frequency to increase the data rate for a given application. However, the maximum modulation frequency is limited by the resolution and the readout time (t_r) of the CMOS sensor. As per the experiments, the modulation frequency should be at least 3 times the readout time of the CMOS sensor (t_r) to ensure the signal waveform does not lose information due to under sampling and

can be successfully decoded. In addition to the consideration of sampling rate, exposure time is also important to be shorter than the time period of the signal such that inter symbol interference does not occur. This relationship between sensor's read-out time (t_r) , minimum exposure time (t_{exp}) and modulation frequency (F_{mod}) is shown in (3.4) and indicated in Figure 3.12. On the other hand, the use of too low frequency is also not desirable, for example <1 kHz, as it may cause light to produce visible flicker in addition to the reduction in data rate.

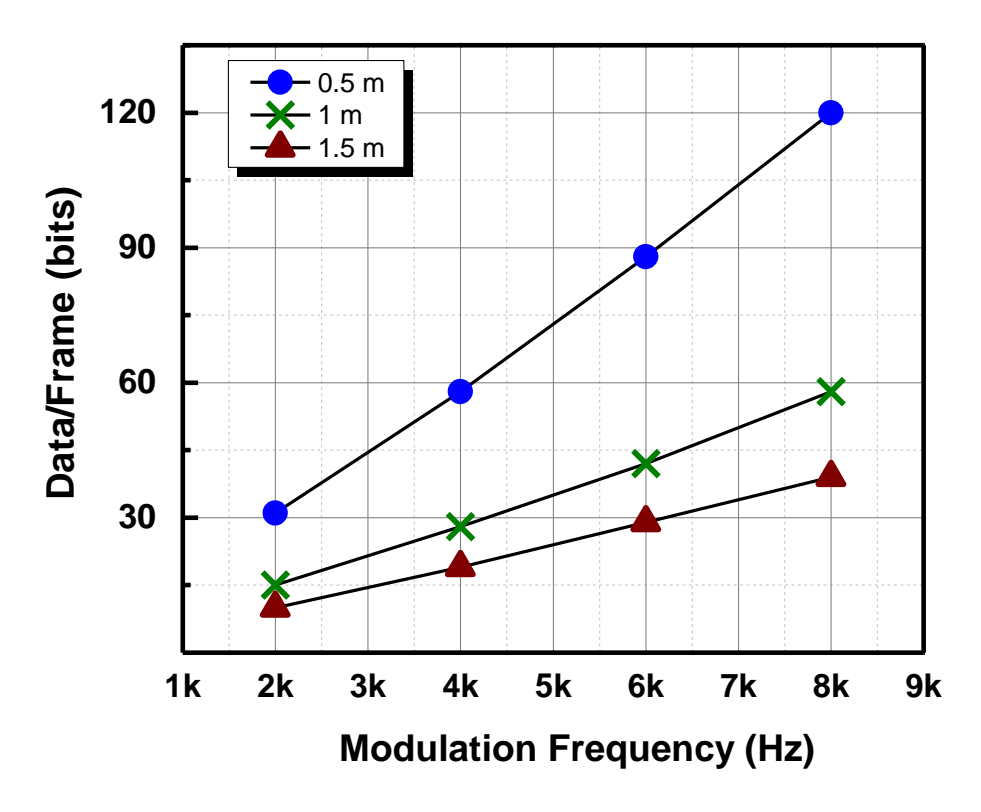


Figure 3.11 Measurement results of frequency and distance dependency on data rate

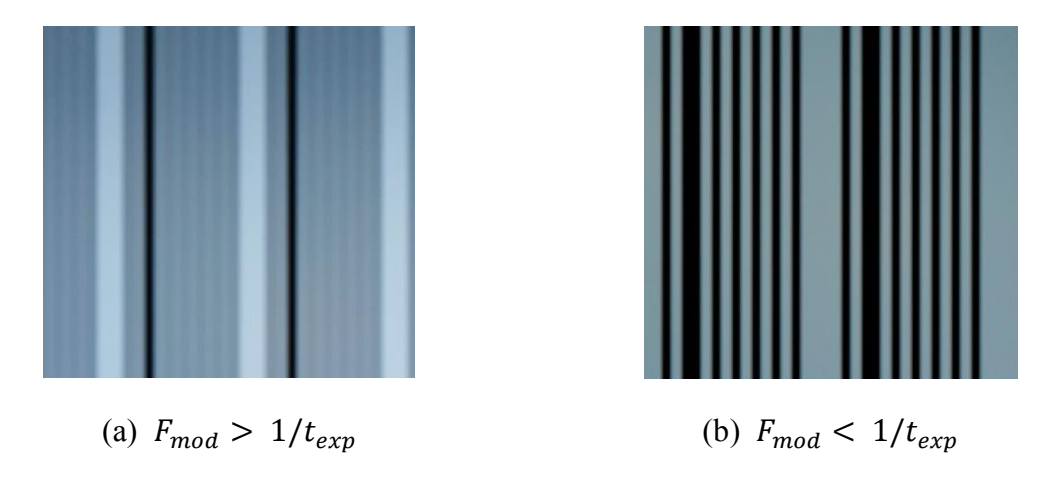


Figure 3.12 The relation between modulation frequency and camera exposure time

$$F_{mod} \le min (1/t_{exp}, 1/3t_{r max})$$
 (3.4)

3.6 Choosing Optimum Capture Resolution

Image capture resolution of the camera is directly proportional to the sensor read-out time (t_r), therefore in OCC, it can be considered equivalent to the sampling rate in a digital oscilloscope. If the resolution is too low, it will lead to under sampling, while too high resolution can lead to a high computation cost. This relationship is illustrated in Figure 3.13 by capturing rolling shutter pattern of an LED with different resolutions. To quantify the impact of resolution on the computation cost of image and signal processing, measurements were conducted using a Huawei P30 Pro smartphone featuring Kirin 980 processor with 8GB ram and running OCC receiver algorithm. The measurement results shown in Figure 3.14, indicate that resolutions of above 1.7 Mega pixels would require a longer processing time than a single frame duration (33ms), with the maximum computation time of 170ms per frame for the highest capture resolution of 8 M pixels. The computation time of longer than frame duration leads to packet loss during data communication and lack of responsivity in indoor positioning applications. Therefore, in order to build practical OCC-based mobile applications, the recommended camera resolution would be below 1.5 Mega pixels to leave enough margins for lower end smartphones and edge devices with relatively less computation power.

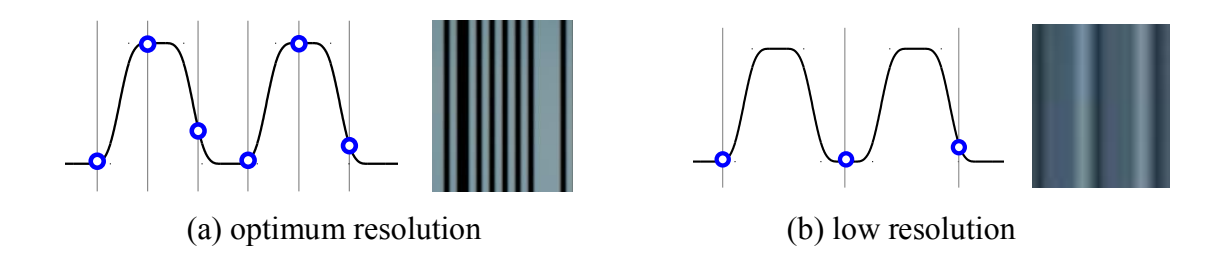


Figure 3.13 The comparison of optimum and low resolution captured images of light

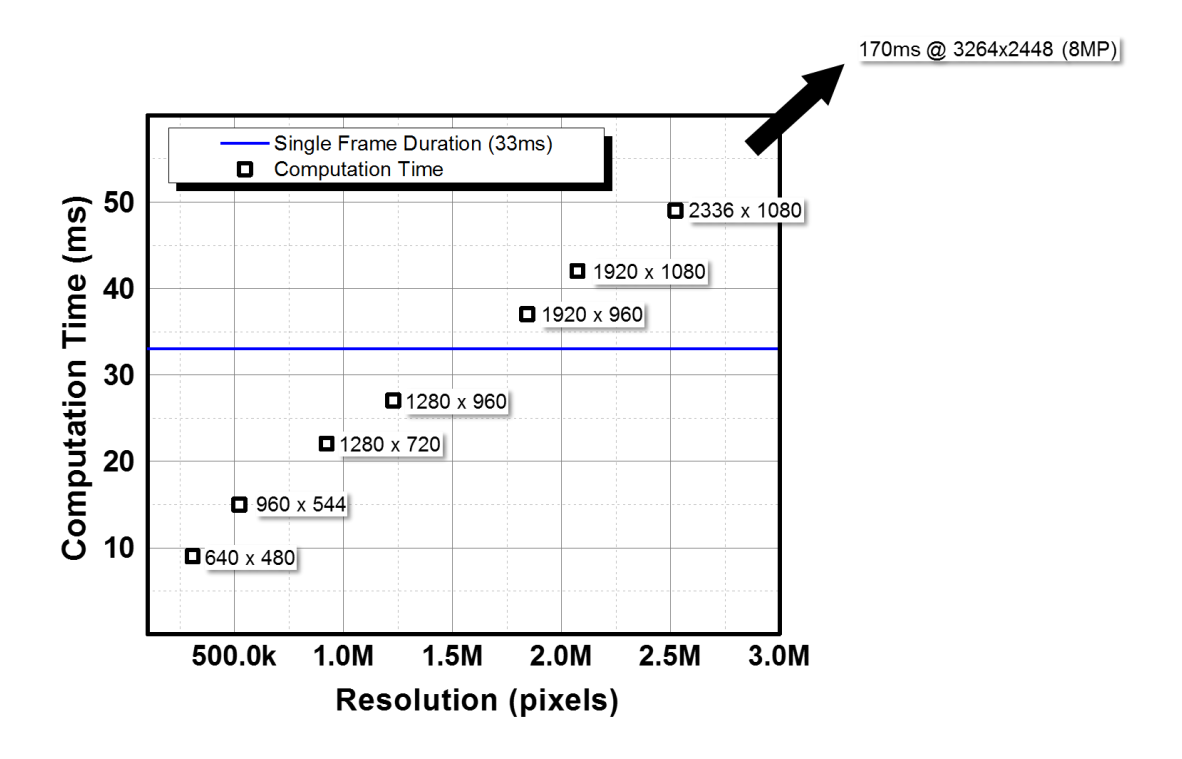


Figure 3.14 Effect of resolution on computation time

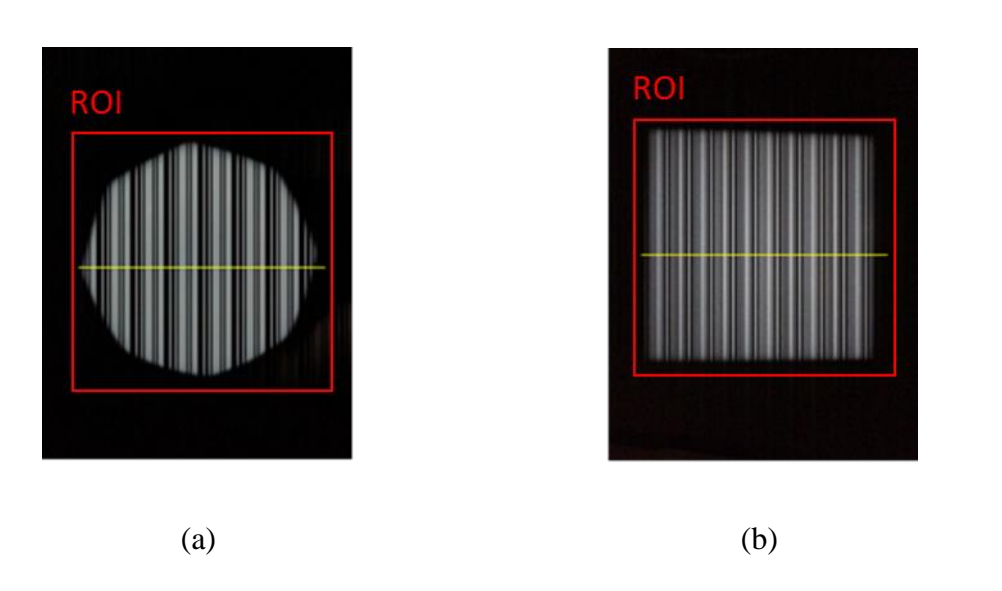


Figure 3.15 Comparison of captured images of two shapes of modulated LED lights: (a) circular (b) rectangular

3.7 Light Shape Dependency on the Detection Performance

LED lighting and signage comes in various shapes and sizes, which can be generally divided in two broad categories of circular and rectangular shaped lighting. Figure 3.15 illustrates the

comparison of images captured of a modulated light source with square and round shapes. The yellow line along the horizontal dimension illustrates that the effective detection range for both of the lights is similar even though they have different areas. Therefore, two luminaries with same horizontal dimension will have similar detection range irrespective of their shape. This can be derived using the relationship between the distance (d) and ROI from (3.3). Given a certain packet size of N_{bit} , and the modulation frequency of F_{mod} , the minimum ROI_{min} required to successfully detect a frame can be calculated as below:

$$ROI_{min} \approx N_{bit} / (F_{mod} \times t_r)$$
 (3.5)

By inputting the relationship between ROI and distance (d) from (3.3),

$$d_{max} \approx \frac{D \times R_H}{2 \times ROI_{min} \times tan(FOV/_2)}$$
 (3.6)

$$d_{max} \approx \frac{D \times R_H}{2 \times N_{bit} / (F_{mod} \times t_r) \times tan(FOV/2)}$$
(3.7)

Where d_{max} denotes the maximum detection distance given a certain diameter of light (D).

Measurements were conducted on several luminaries of different sizes and shapes to verify the above relationship, as depicted in the Figure 3.16. Each luminaire was used as a transmitter and its sensitivity was characterized in terms of the maximum detection distance i.e., the farthest possible distance from smartphone where the data could be successfully decoded by the smartphone. The experimental results are shown in the Figure 3.17 below. The results validate the direct relation between light size and the maximum communication distance. In addition, it can be observed that lights with similar diameter have same detection distance irrespective of their shape. Therefore, it can be concluded that light shape does not matter as long as the diameter (D) is long enough to fit required number of bits in one frame.

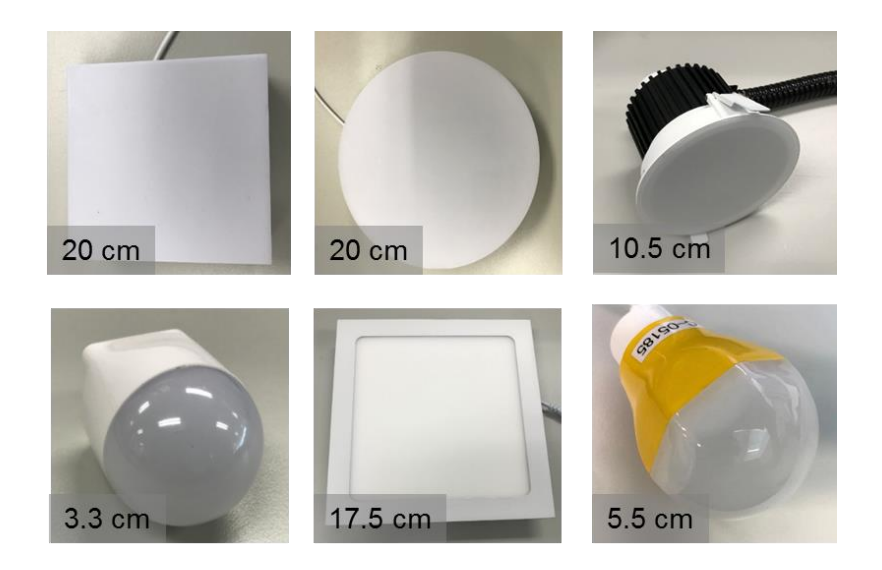


Figure 3.16 Various shapes and sizes of lights used in the experiment

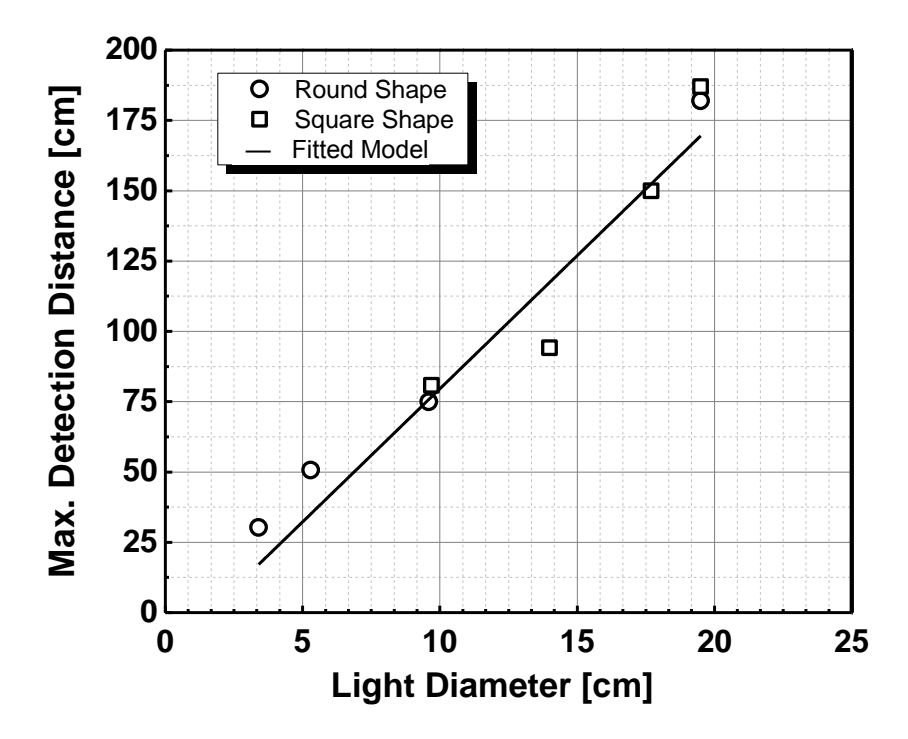


Figure 3.17 Measurement results of comparison of light shape and size dependency on detection performance

3.8 Light Color Dependency on the Detection Performance

Characterization of detection dependency on light color is important as LED signage and Light boxes usually come in various colors. Use of color temperature lighting is also becoming popular in general lighting where the user can set the color of luminaire on a wider range of color temperatures from as warm as reddish white to as cool as bluish white as illustrated in Figure 3.18.

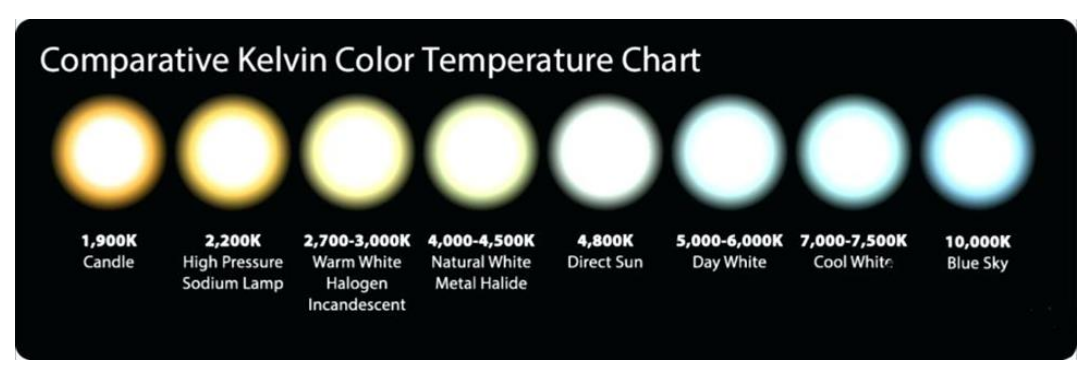


Figure 3.18 Color temperatures of white LED used for general illumination [24]

The colored image is generally stored as RGB image, which is essentially three planes of red, green and blue base colors. The conversion of equivalent grayscale image for signal processing is performed by taking a weighted aggregate of these colors for each pixels according to the following equation.

$$Grayscale\ Equivalent = 0.30\ \times Red + 0.59 \times Green + 0.11\ \times Blue$$
 (3.8)

Given the above equation, the relative grayscale intensity of each color filter can be easily calculated which is directly proportional to the maximum possible detection range of the communication link.

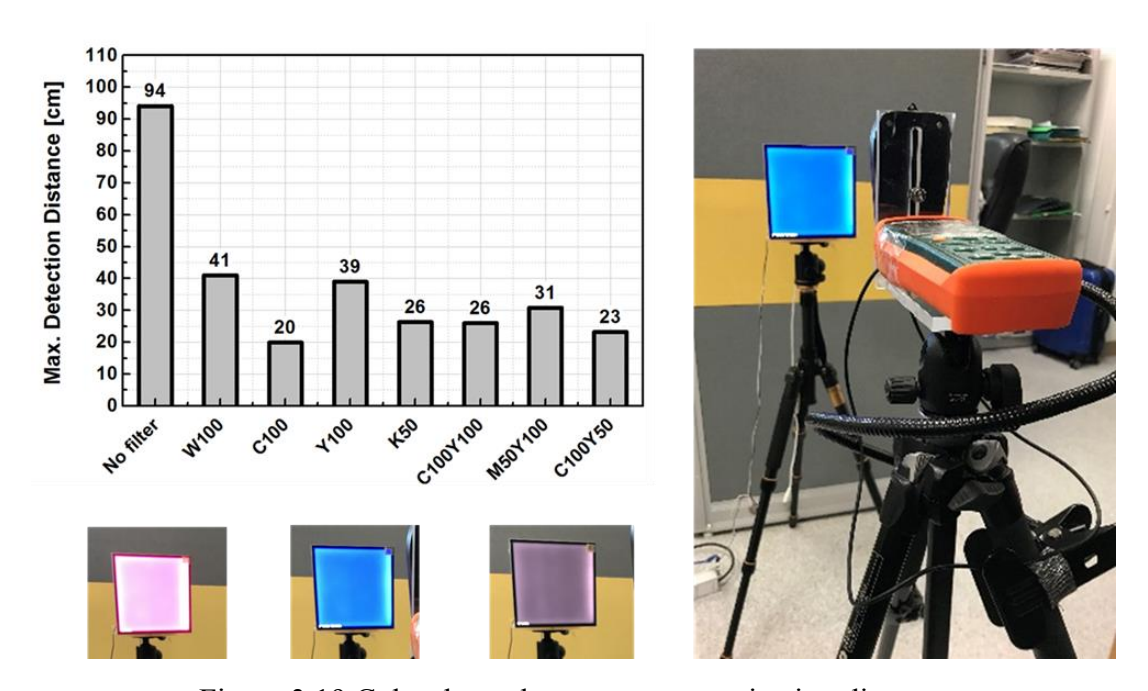


Figure 3.19 Color dependency on communication distance

To determine the dependence of the communication distance on color, measurements were conducted on a light panel with different color filters while the intensity of the base luminaire was kept constant. The measurement setup and the results are shown in Figure 3.19. It can be seen that for brighter color filters for example white (W100) and yellow (Y100) the communication distance is long while the range is comparatively smaller for darker filters.

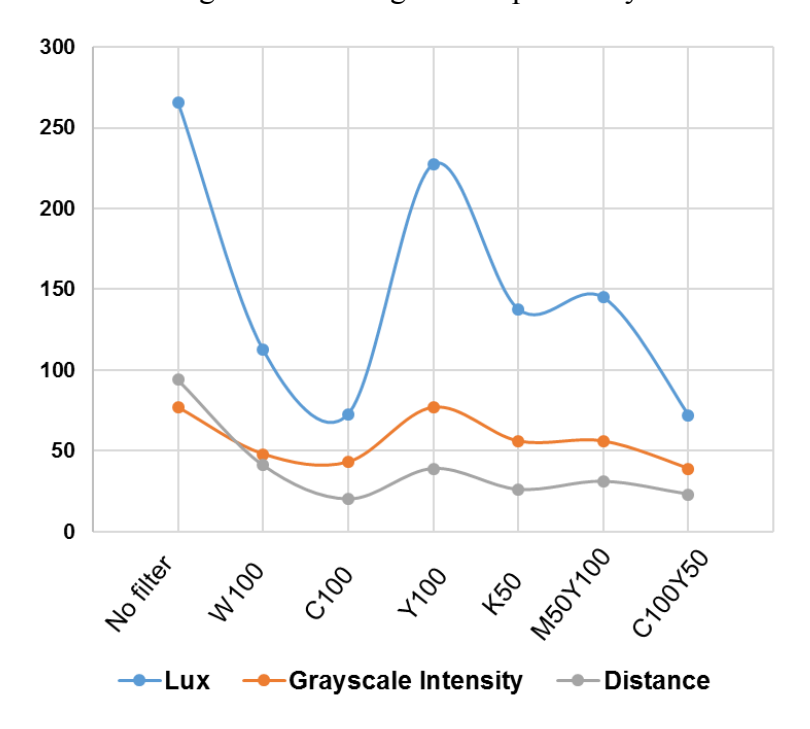


Figure 3.20 Comparison of received lux, grayscale intensity and maximum detection distance for various color filters

A more detailed graph is shown in the Figure 3.20. It shows the relation between the received light intensity from a light meter (lux), the received maximum grayscale pixel intensity for the received data and the detection distance for various color filters.

3.9 Dependency on Smartphone Models

Different smartphone devices feature image sensors that are different in their image acquisition characteristics. It is expected that various models of smartphones will have different performance for OCC. Figure 3.21 shows detection performance comparison for different devices using the same transmitter. Even though the same values for modulation frequency, light size, and resolution are set, the detection distance is different for each device.

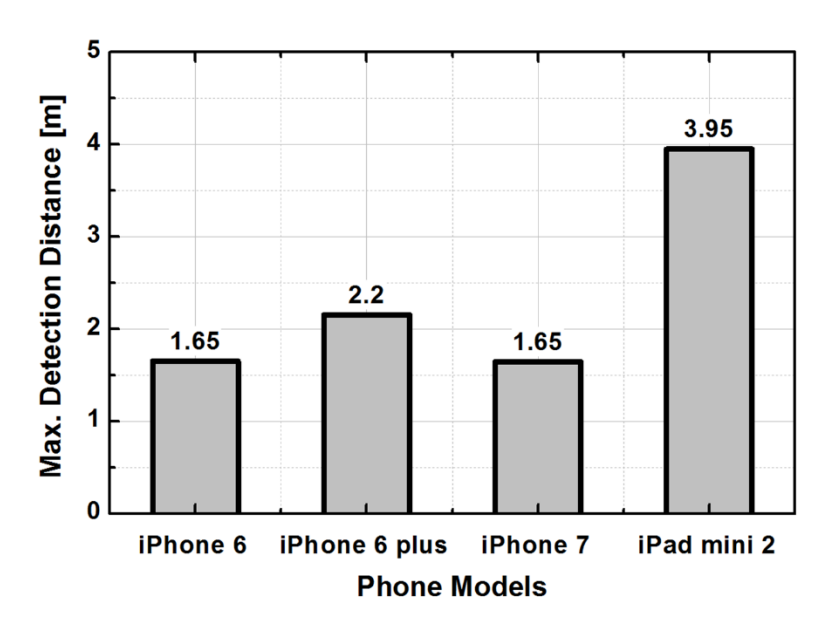


Figure 3.21 Detection performance comparison for various models

This is because these phones differ in their sensor read-out times (t_r), focal lengths (f) and FOVs. In addition, it is not straightforward to set the exposure value of each phone to be exact similar, therefore, even though the values of ISOs are kept similar, image captured from one phone will be different as compared to the other in terms of the pixel grayscale intensity and the amount of noise. The difference in the camera hardware of various smartphones is further illustrated in Figure 3.22. Smartphones including iPhone 7, Lenovo Phab2, Samsung S7 Edge, and XZ Premium are all set at an exposure of 1/10,000 seconds, and an ISO of 100, with a capture resolution of 1280×720 pixels. It can be observed that the readout time (t_r), and thereby, image-scanning rate of XZ premium is the fastest at 13 pixels/bit, whereas the Lenovo Phab2 has the slowest scanning rate of 3 pixels/bit, and hence the slowest readout time. This leads to the conclusion that XZ with the fastest scanning rate and read-out time will determine the maximum communication distance that can be achieved for a given frequency, whereas the Lenovo Phab2 smartphone will determine the fastest modulation frequency that we can use before under-sampling occurs.

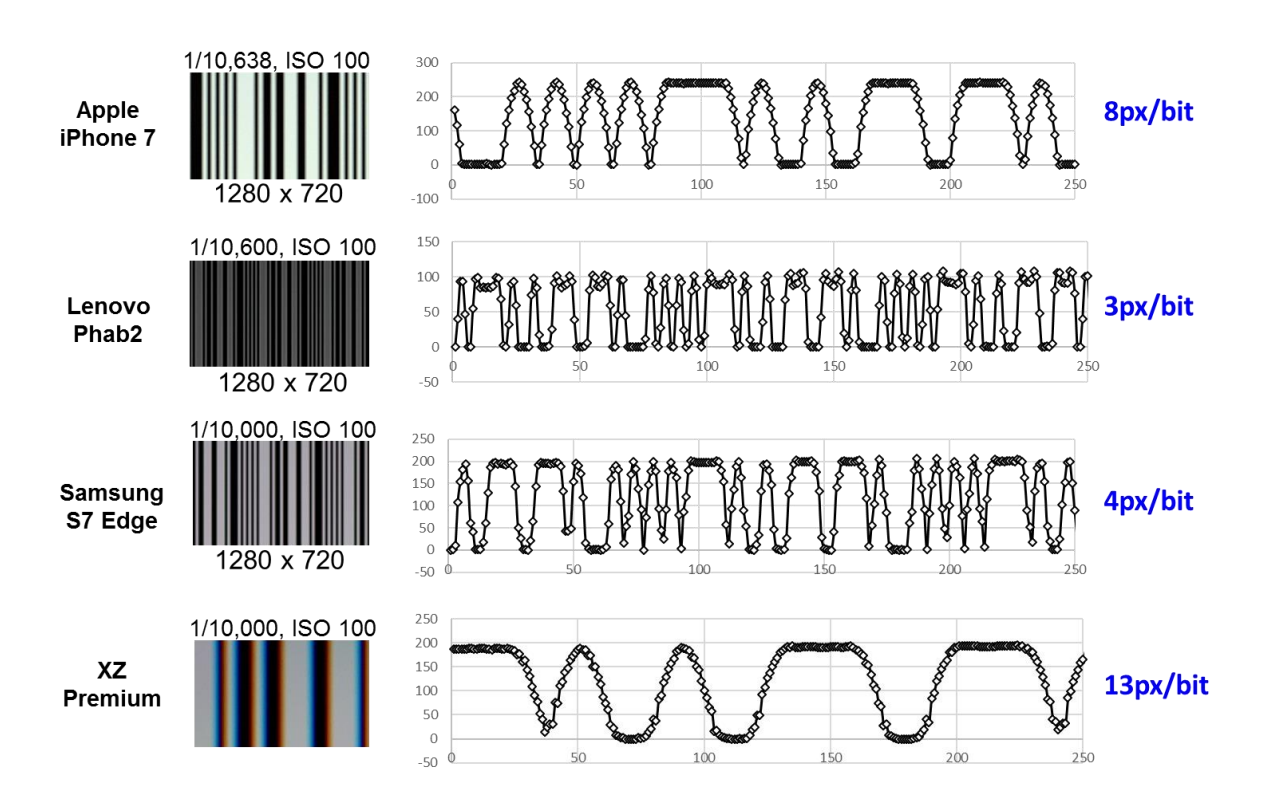


Figure 3.22 Comparison of image-scanning rate of various smartphones

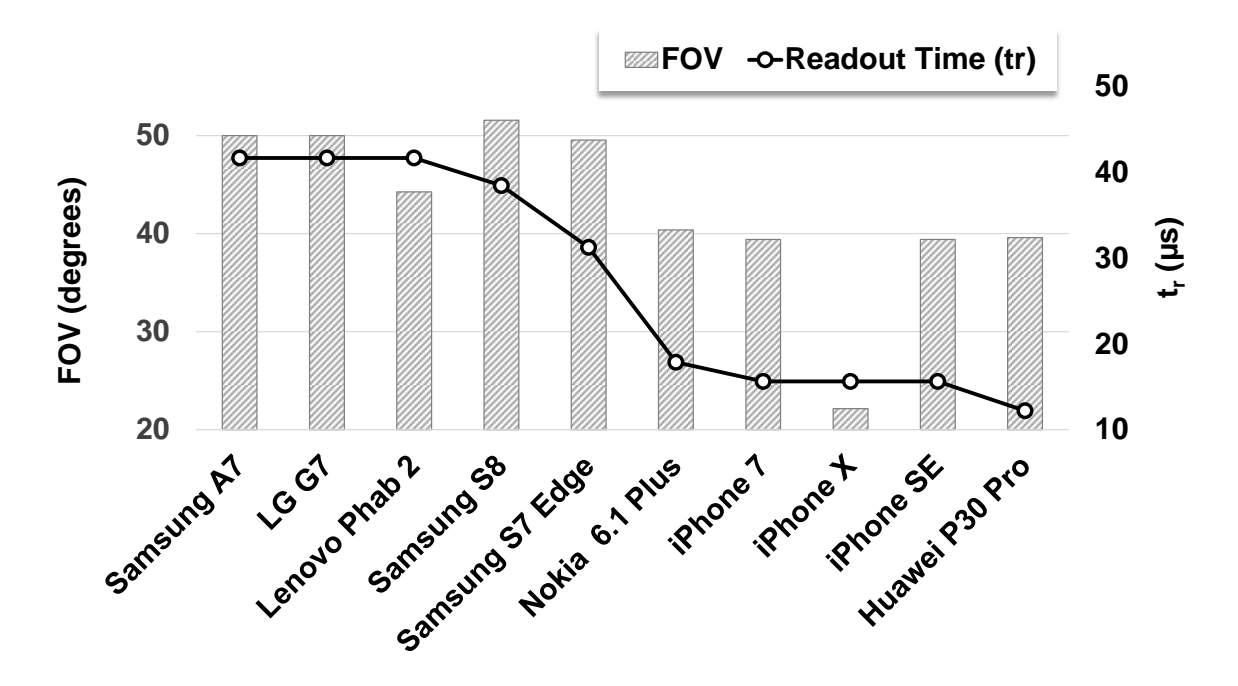


Figure 3.23 Comparison of FOV and readout time (t_r) of ten different smartphone models

In addition to the difference in readout time, the smartphone camera hardware also differs in their focal length and, therefore, features a varying range of FOVs. A comparison of FOVs and readout times of 10 different smartphones is shown in Figure 3.23, indicating a broad range

of FOVs from 22 to 50 degrees, and readout times of 12 to 42 us. This variation in hardware parameters presents a challenge of designing an OCC system for meeting a target set of specifications for a practical deployment. Following section describes the detailed guidelines for building such practical systems.

3.10 OCC System Design Guidelines

Given the dependency of OCC performance on light size, communication distance, camera parameters, and variation among different CMOS image sensors hardware, it is challenging to consider all the design trade-offs and bottlenecks to meet a set of target specifications. Therefore, this section presents a design flow for calculating key parameters for an OCC system.

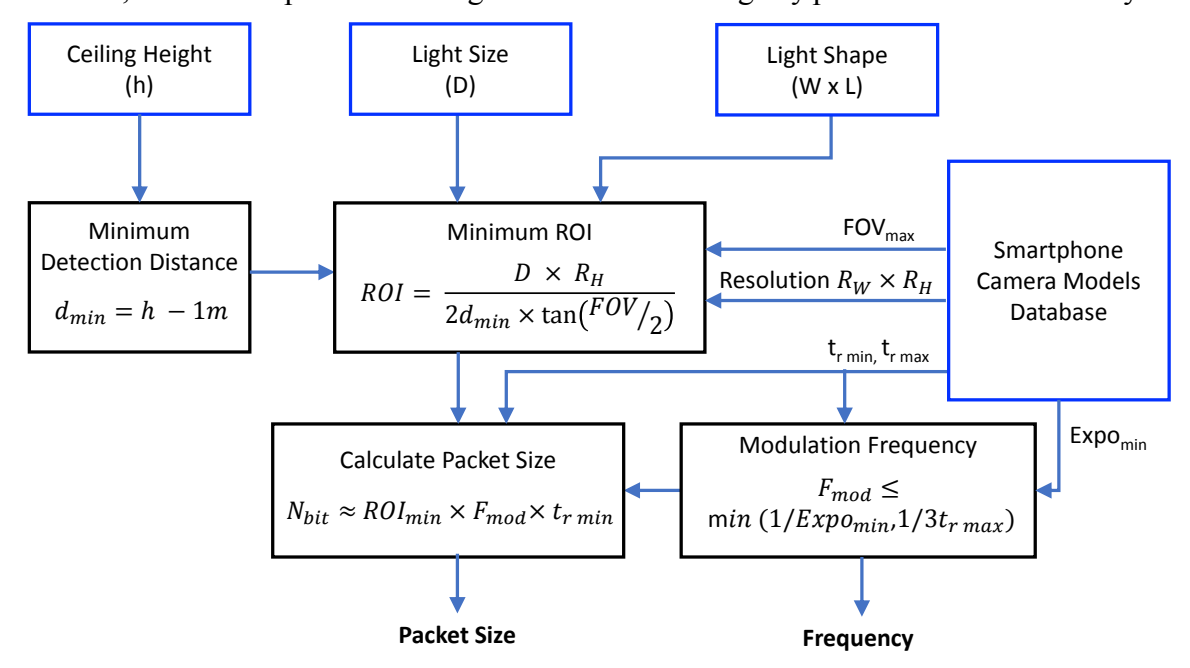


Figure 3.24 OCC system design flow

Figure 3.24 shows the OCC system design flow chart. In a practical application scenario where ceiling lighting-based indoor positioning is required, systems parameters including, the ceiling height, light size, and shape are fixed, while the modulation frequency and data rates need to be optimized to achieve the target navigation capability. In addition, it is important to have the database of smartphone CMOS camera parameters, including focal lengths, available capture resolutions, and sensor readout times, as these will determine the design bottlenecks.

As illustrated in the flowchart, the height determines the minimum required communication distance, which is combined with light size and shape information, as well as cameras FoV and resolution to determine the minimum ROI. On the other hand, the exposure and the readout times of the sensors are used to calculate the modulation frequency, which is combined with the required ROI to determine the packet size, which leads to the required data rate. In the following, an exemplary system is implemented to achieve a target set of specifications to verify the validity of the system design approach.

Table 3.1 OCC system design sepecifications

Target Distance	1.5 m
Light Size	40 cm x 40 cm
Light Power	10 Watt
Modulation Scheme	NRZ-OOK
Modulation Frequency	8000 Hz
Data Packet Size	32 bits

In order to verify the aforementioned OCC system design approach, an OCC system for a target application was designed to achieve a set of target specifications for 10 different models of smartphones, as listed in the Table 3.1. The chosen light is a 40 cm x 40 cm light panel that is targeted to achieve a communication distance of 1.5 meters for all smartphones. The parameters of the smartphones, including the exposure time, focal length, resolution, and sensor read-out time are put into the system design flow along with the required communication distance and the light size, leading to the calculation of two of the key system design parameters i.e. modulation frequency and the frame packet size. The calculated modulation frequency is ~8000 Hz while the packet size is determined to be 32 bits.

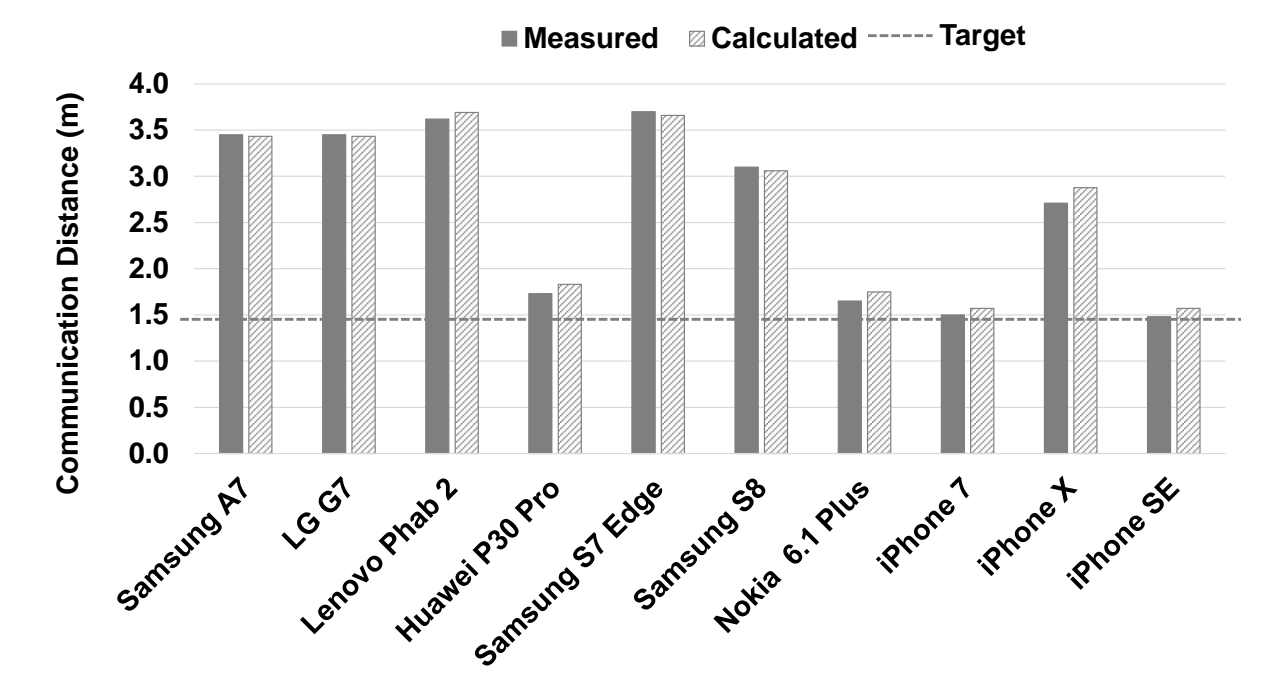


Figure 3.25 Comparison of various smartphone models based on calculated design parameters and measured performance values

Figure 3.25 shows the measurement results indicating that all the models have met the target specifications with iPhone 7 and iPhone SE setting the bottleneck for the design parameters. In addition, the measurements match well with the calculated results with maximum error of < 0.17 m and the mean error of less than 0.07 m.

3.11 References

- [1] C. Danakis et al., "Using a CMOS camera sensor for visible light communication", Proc. IEEE Globecom Workshops, 2012.
- [2] M. Liu, K. J. Qiu, S. Li, F. Che, B. Hussain, L. Wu, and C. P. Yue, "Towards indoor localization using visible light communication for consumer electronic devices," in *Intelligent Robots and Systems (IROS), 2014 IEEE/RSJ International Conference on*, 2014.
- [3] T. Nguyen, A. Islam, T. Hossan and Y. M. Jang, "Current status and performance analysis of optical camera communication technologies for 5G networks," IEEE Access, vol. 5, pp. 4574-4594, 2017.

- [4] N. Bani Hassan et al., "Non-line-of-sight MIMO space-time division multiplexing visible light optical camera communications," *Journal of Lightwave Technology*, vol. 37, no. 10, pp. 2409-2417, 15 May15, 2019.
- [5] S. -J. Kim, J. -W. Lee, D. -H. Kwon and S. -K. Han, "Gamma function based signal compensation for transmission distance tolerant multilevel modulation in optical camera communication," *IEEE Photonics Journal*, vol. 10, no. 5, pp. 1-7, Oct. 2018.
- [6] M. A. Atta, B. Hussain and A. Bermak, "Channel length modeling and experimental demonstration ofadaptive threshold under-sampled CamCom for low-SNR transmitters," *IEEE Photonics Journal*, vol. 10, no. 6, pp. 1-12, Dec. 2018.
- [7] T. Nguyen, A. Islam and Y. M. Jang, "Region-of-interest signaling vehicular system using optical camera communications," *IEEE Photonics Journal*, vol. 9, no. 1, pp. 1-20, Feb. 2017.
- [8] H. Nguyen, M. D. Thieu, T. Nguyen and Y. M. Jang, "Rolling OFDM for image sensor based optical wireless communication," *IEEE Photonics Journal*, vol. 11, no. 4, pp. 1-17, Aug. 2019.
- [9] Q. Liang and M. Liu, "A tightly coupled VLC-inertial localization system by EKF," *IEEE Robotics and Automation Letters*, vol. 5, no. 2, pp. 3129-3136, April 2020.
- [10] H. Chen et al., "Color-shift keying for optical camera communication using a rolling shutter mode," *IEEE Photonics Journal*, vol. 11, no. 2, pp. 1-8, April 2019.
- [11] V. P. Rachim and W. Chung, "Multilevel intensity-modulation for rolling shutter-based optical camera communication," *IEEE Photonics Technology Letters*, vol. 30, no. 10, pp. 903-906, 15 May15, 2018.
- [12] J. Lee, S. Yang and S. Han, "Optical pulse width modulated multilevel transmission in CIS-Based VLC," *IEEE Photonics Technology Letters*, vol. 29, no. 15, pp. 1257-1260, 1 Aug.1, 2017.
- [13] J. Lain, Z. Yang and T. Xu, "Experimental DCO-OFDM optical camera communication systems with a commercial smartphone camera," *IEEE Photonics Journal*, vol. 11, no. 6, pp. 1-13, Dec. 2019.

- [14] Y. Yang, J. Hao and J. Luo, "CeilingTalk: Lightweight indoor broadcast through LED-camera communication," *IEEE Transactions on Mobile Computing*, vol. 16, no. 12, pp. 3308-3319, 1 Dec. 2017.
- [15] Z. Zhang, T. Zhang, J. Zhou, Y. Lu and Y. Qiao, "Thresholding scheme based on boundary pixels of stripes for visible light communication with mobile-phone camera," *IEEE Access*, vol. 6, pp. 53053-53061, 2018.
- [16] Z. Zhang, Y. Qiao, T. Zhang and Y. Lu, "Fractional weight moving average based thresholding scheme for VLC with mobile-phone camera," *IEEE Photonics Journal*, vol. 11, no. 1, pp. 1-8, Feb. 2019.
- [17] Z. Zhang, T. Zhang, X. Tang, Y. Lu and Y. Qiao, "Reducing grayscale value fluctuation for mobile-phone camera based VLC system," *IEEE Photonics Journal*, vol. 10, no. 6, pp. 1-10, Dec. 2018.
- [18] Y. Yang, J. Nie, and J. Luo, "ReflexCode: Coding with superposed reflection light for LED-camera communication," in *Proc. 23rd Annu. Int. Conf. Mobile Comput. Netw. MobiCom*, 2017, pp. 193–205.
- [19] F. Yang, S. Li, Z. Yang, C. Qian, and T. Gu, "Spatial multiplexing for non-line-of-sight light-to-camera communications," *IEEE Trans. Mobile Comput.*, vol. 18, no. 11, pp. 2660–2671, Nov. 2019.
- [20] X. Liu, X. Wei and L. Guo, "DIMLOC: Enabling high-precision visible light localization under dimmable LEDs in smart buildings," *IEEE Internet of Things Journal*, vol. 6, no. 2, pp. 3912-3924, April 2019.
- [21] Y. Li, Z. Ghassemlooy, X. Tang, B. Lin and Y. Zhang, "A VLC smartphone camera based indoor positioning system," *IEEE Photonics Technology Letters*, vol. 30, no. 13, pp. 1171-1174, 1 July, 2018.
- [22] R. Zhang, W. Zhong, Q. Kemao and S. Zhang, "A single LED positioning system based on circle projection," *IEEE Photonics Journal*, vol. 9, no. 4, pp. 1-9, Aug. 2017.

- [23] B. Hussain, X. Li, F. Che, C. P. Yue, and L. Wu, "Visible light communication system design and link budget analysis," *IEEE/OSA Journal of Lightwave Technology*, vol. 33, no. 24, pp. 5201–5209, Dec. 2015.
- [24] "Color Temperature and LED: Understanding How to Choose LED Lamps for Warm and Cool Applications" [Online] Available: https://solutions.borderstates.com/color-temperature-and-led-understanding-how-to-choose-led-lamps-for-warm-and-cool-applications/

CHAPTER 4 Smart Lighting and Displays

The ubiquity of LED lighting and display devices makes VLC an indispensable technology for building a smart society. In addition, the line-of-sight property of visible light proves advantageous for a wide range of location-based services. This chapter covers the design and implementation of VLC integrated smart lighting and display systems to provide ambient intelligence in smart venues.

4.1 Smart Lighting

4.1.1 Existing Solutions on Smart Lighting Control

Being a ubiquitous device with a significant impact on energy, lighting is considered a very important part of IoT and smart home infrastructure. Therefore, a lot of effort has been made recently in turning ordinary LED lightings into smart lighting. Most residential smart lighting is compatible with three popular smart home systems, i.e., Amazon Echo, Apple Home Kit and Google Home, to allow lighting control via voice commands through their smart speakers [1–3]. Figure 4.1 illustrates the type of technologies that are featured in smart lighting systems nowadays.

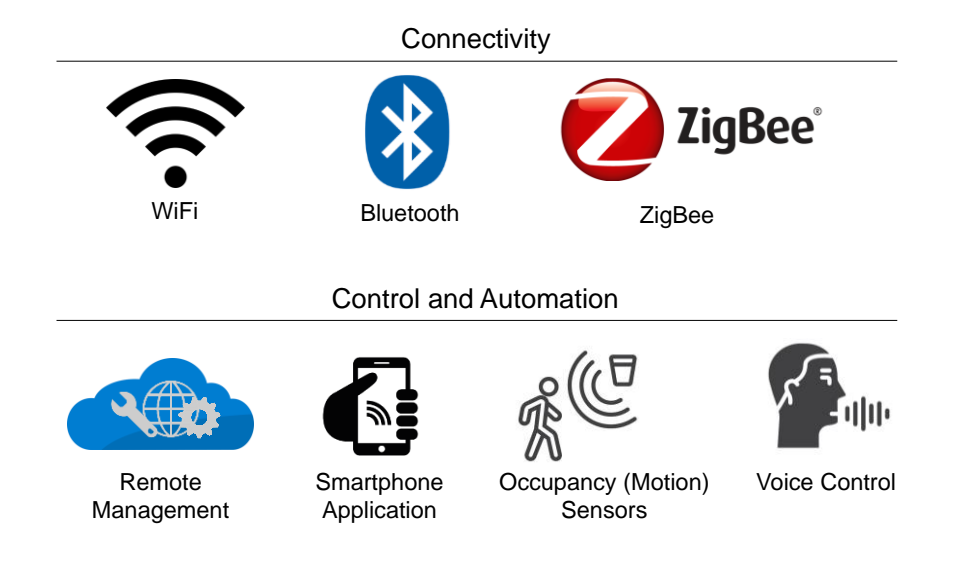


Figure 4.1 State-of-the-art technologies for smart lighting systems.

The most important feature of a smart lighting system is the wireless connectivity, which is primarily achieved using one or a combination of three technologies: WiFi, ZigBee and Bluetooth.

- (1) WiFi allows the lighting device to become a part of the smart home ecosystem where it can be connected to a central hub in addition to the other lighting or smart home devices. These devices can then be controlled and monitored simultaneously from a remote location as they are connected to the Internet backbone through WiFi.
- (2) ZigBee was primarily introduced for providing low-power connectivity over a long reach in a number of devices for enabling control and automation. It relies on mesh networking protocol where each device on the network can communicate with other devices. Thereby, it allows the communication of hundreds of devices on the network eliminating the need of having a control gateway near every device. It requires a central control hub for pushing the control commands onto the lighting network. Many of the popular lighting systems for a smart home support ZigBee, such as Philips Hue [4]. However, ZigBee must be combined with Wi-Fi or a Bluetooth gateway to connect to the user devices such as smartphones, tablets and wearables. In contrast, Bluetooth and WiFi can be directly accessed on those devices.
- (3) Bluetooth has become popular recently following the release of its new protocol standard called Bluetooth Low Energy (BLE), which offers low-power burst communication mode for conserving energy in battery-powered IoT devices. Since Bluetooth is supported by many operating systems that run on consumer devices including smartphones, it is quite suitable for lighting connectivity and control via smartphone applications. With the recent announcement of mesh networking support in Bluetooth, it is expected that Bluetooth will be a preferred choice over ZigBee and other wireless technologies for future smart lighting [5]. In addition, Bluetooth in smart lighting can be used to create proximity beacons and provide location-based services such as route planning, advertisement, event promotion, etc. [6]. When interacting with consumers' smartphones and wearables, these beacons can generate an extensive amount of useful behavioral data that can be studied to improve services and user experiences.

In addition to the wireless connectivity, another fundamental function provided by smart lighting is on/off and dimming control, which is considered vital for energy savings in industrial and outdoor lighting such as street lighting. In addition, modern indoor lighting for smart homes feature color temperature tuning for optimizing the light colors according to the time of the day or personalizing the room environment according to the mood of the user.

4.1.2 VLC-enabled Smart Lighting and Control

Even though lighting control via a smartphone app (and RF wireless) makes it very convenient for a user to manipulate various lighting devices without having to access a switchboard as in the case of traditional lighting. However, when there are a number of lights inside a room and the user wants to selectively control one of the lights (for example, on/off control, dimming or color temperature tuning), it becomes difficult to identify on the phone which light needs to be selected from a list of lighting devices. By leveraging the line-of-sight property of visible light and the point-and-grab gesture of OCC to capture information from the light using the camera, VLC is ideally suited to solve the light identification problem.

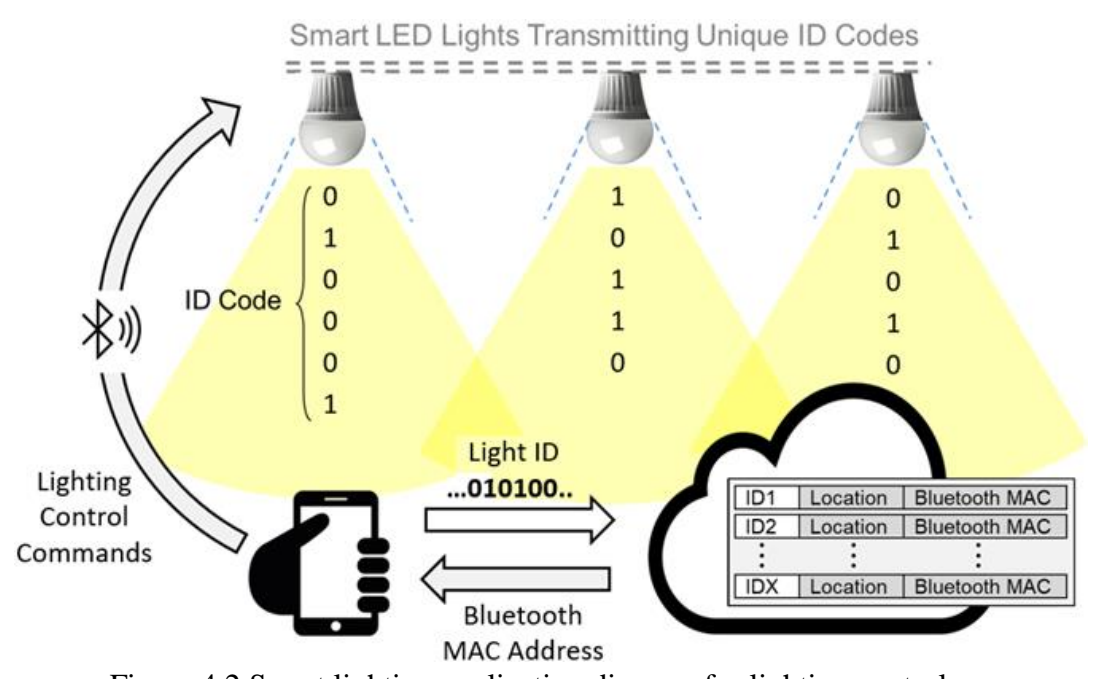


Figure 4.2 Smart lighting application diagram for lighting control.

As shown in Figure 4.2, each light transmits a unique VLC identifier (ID) code which is mapped to the Bluetooth media access control (MAC) address of that light. The user of a smart

lighting system can point the camera of his personal device to the targeted light to receive the ID code. The received light ID is then translated to a corresponding MAC address that is stored either locally on the personal device or on a remote server. With the help of the acquired MAC address, the user's device can be wirelessly connected to the lighting device to change the settings.

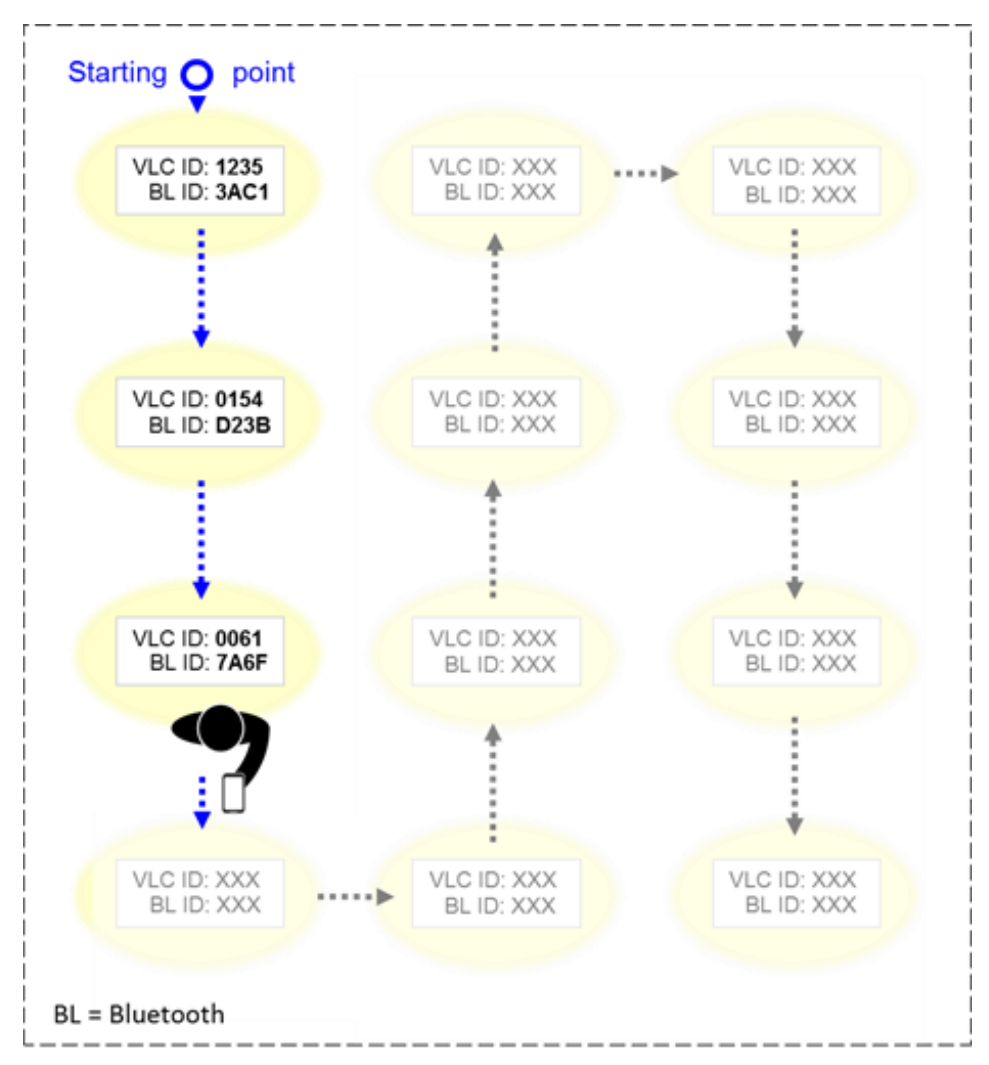


Figure 4.3 Smart lighting installation and mapping procedure

4.1.3 Smart Lighting Installation and Mapping

One of the biggest challenges for smart lighting is the installation and first-time setup as the location of each light must be mapped to its corresponding Bluetooth ID along with its location coordinates on the blueprints of the building. However, the light installation is always performed in bulk and it requires a large amount of engineering work and has high cost to have

the light installation coordinates marked on each light packaging and then have the lights carefully installed at the specified location. Instead, it is more practical to map the lights' locations after the light fitting is completed.

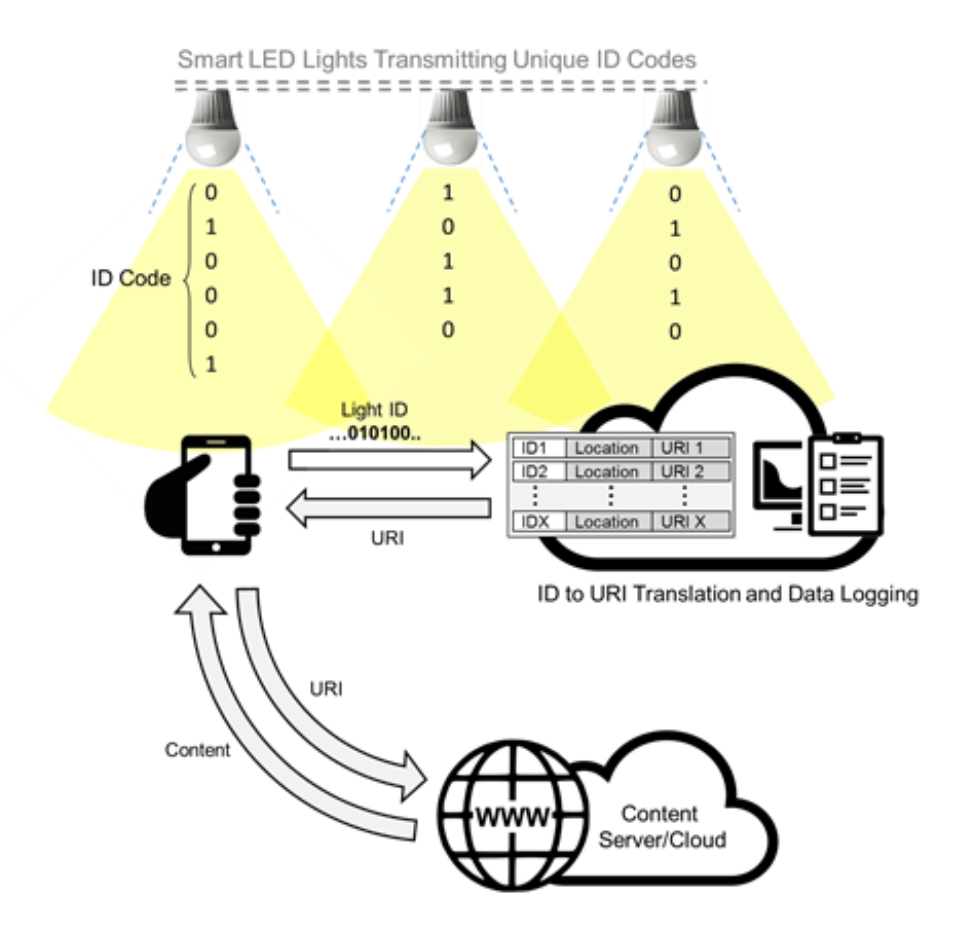


Figure 4.4 Location-based information delivery system using VLC in smart lighting

The smart installation and mapping procedure are illustrated in Figure 4.3. The person in charge of mapping carries a handled device, a smartphone or a tablet running the mapping application. The application shows the map of the building, and the person mapping can choose the starting point and orientation based on his current location. Once the starting point is determined, the movement of the person can be tracked on the application via the accelerometer and gyroscope sensors available on the handheld device. As the person walks under a light, the front camera of the handheld device receives the VLC ID signal, which is then mapped on the location shown on the screen. Since each VLC ID is paired with a Bluetooth MAC address, the application automatically knows the Bluetooth MAC address of the light as soon as it recognizes its VLC ID. Since the lights are installed at a fixed location on the map and the

person follows a fixed path on the map, the location tracking accuracy required by the accelerometer and gyroscope does not need to be very high. Once the person has walked across the whole building, the VLC IDs and Bluetooth MAC addresses of all the lights along, with their location coordinates, are collected and can be uploaded to the server to be later used for maintenance purposes and providing location-based services.

4.1.4 Smart Lighting with VLC for Location-based Services

With iBeacon being used for proximity and geo-fencing-based applications, VLC can be used to provide precise location-based information. Figure 4.4 shows the architecture of the location-based information delivery system using VLC in smart lighting. An end user can receive the ID code from the lights in his proximity using his personal device, which is then translated to the corresponding URI. The user can be wirelessly linked to the content server or cloud with the acquired URI to access the desired location-based service or content. Since each interaction between the user and light ID goes through the cloud, it can be used to collect the behavioral data of each user. The accumulated data for all the users in a venue can be analyzed to study behaviors and walking patterns of users and produce location heat maps in large public and commercial venues such as shopping malls, airports and train stations.

4.2 Smart Displays

Displays have a key role in the infrastructure of AI driven smart homes and smart cities as they are not only an essential element of IoT network for providing intelligence ambience but at the same time they provide a direct contact for human machine interaction. Therefore, modern smart displays feature technologies for both interaction and connectivity. State of the art technologies for interaction include smart speakers for voice commands, for example Amazon Alexa and Google Assistant, in addition to more traditional methods of touch and gesture recognition. On the other hand, connectivity primarily relies on Bluetooth, WiFi or a combination of both to enable communication with personal devices such as smartphone, tablets or wearables.

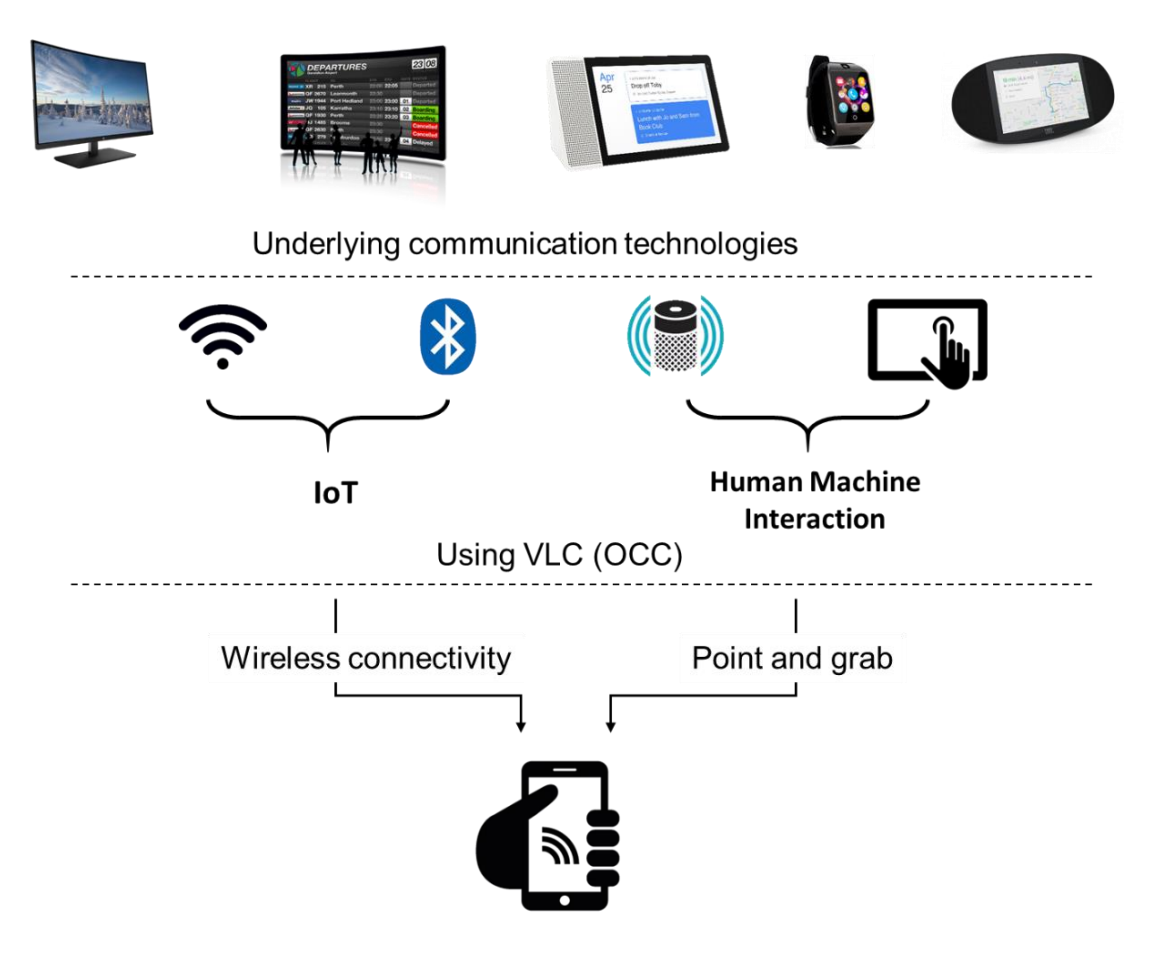


Figure 4.5 How VLC can be used to complement state-of-the-art in smart displays

However, in large public venues and exhibitions where there are a number of smart displays within eyesight and multiple users want to interact simultaneously, for example information display board at an airport, It is not possible to use any direct interaction methods such as voice, touch or gesture recognition. Therefore, users rely on Bluetooth and WiFi to pull information from smart displays on their personal devices. However, in such scenario, location and direction accuracy is extremely important as the information must be collected from the intended display. Unfortunately, both WiFi and Bluetooth suffer from limited accuracy due to lack of directionality and RF interference and hence do not provide a user friendly method of interaction. On the other hand, VLC or LiFi being highly directional can be used as an extension of human machine interaction and a bridge for IoT to provide a location and direction accurate interaction method, as shown in Figure 4.5. In other words if VLC can be enabled in a display, a user can point his phone camera in the direction of his intended display and can pull

information on his personal device using optical camera communication with minimum interference from nearby devices.

4.2.1 Enabling VLC in LCD Displays

An LCD uses an LED backlight to enlighten the pixels on screen, which are essentially color filters selectively illuminated via liquid crystals. Modern LCD displays use LEDs as the backlight for higher energy efficiency, better contrast ratio and improved picture quality. These ordinary displays can turn into smart displays by modulating the LED backlight to establish a OCC link. Since the information is transmitted simultaneously while displaying content, it can be time synchronized with the display to make it content and location specific, for example, a TV can provide information about the program being displayed). Similarly, an advertisement about a product or event can broadcast a URL about the advertised product or give directions to the venue respectively.

Seen by human eye



Exposure 1/140 s ISO-267 (a)

Seen by CMOS camera



Exposure 1/9615 s ISO-267 (b)

Figure 4.6 Image of a VLC modulated LCD display captured using a CMOS camera under different exposures

The LCD backlight can be modulated to transmit information irrespective of the content that is being displayed on the screen. Figure 4.6 shows the images of a VLC modulated LCD display that are captured using a CMOS camera of a smartphone under different exposure settings. Figure 4.6(a) is captured using higher exposure such that the amount of light captured is like

the perception of human eyes. On the other hand, the image in Figure 4.6(b) is captured employing a low exposure setting at fast shutter speed, which makes the rolling shutter pattern visible on the captured image. The rolling shutter pattern cannot be perceived by human eyes as it is far beyond the flicker threshold of the eye. Hence the VLC signal does not interfere with the display content. Furthermore, ordinary QR code shown on the LCD could potentially be used to provide the same function as our OCC link, however it has limited range as most of the display area must be devoted to the advertisement image and only a small fraction of the display area can be used for showing the QR code. In addition, in case of our proposed VLC link, since the LED backlight is modulated to transmit information (Figure 4.6(b)), the entire display is used to broadcast the OCC based VLC signal and hence can provide a larger detection size and thus a longer communication range by a smartphone camera compared to scanning ordinary QR codes.

4.2.2 Design of LCD Display-based VLC System

The overall transmitter system that broadcasts VLC signal using an LCD display is shown in Figure 4.7. Transmitter side mainly consists of an LCD display module with a VLC controller. The VLC controller features an MCU based ID controller to generate binary sequences for unique identifiers (ID). The VLC modulator is interfaced to the backlight driver to modulate the backlight of the LCD with on-off keying (OOK) modulation according to the binary stream generated by the ID controller

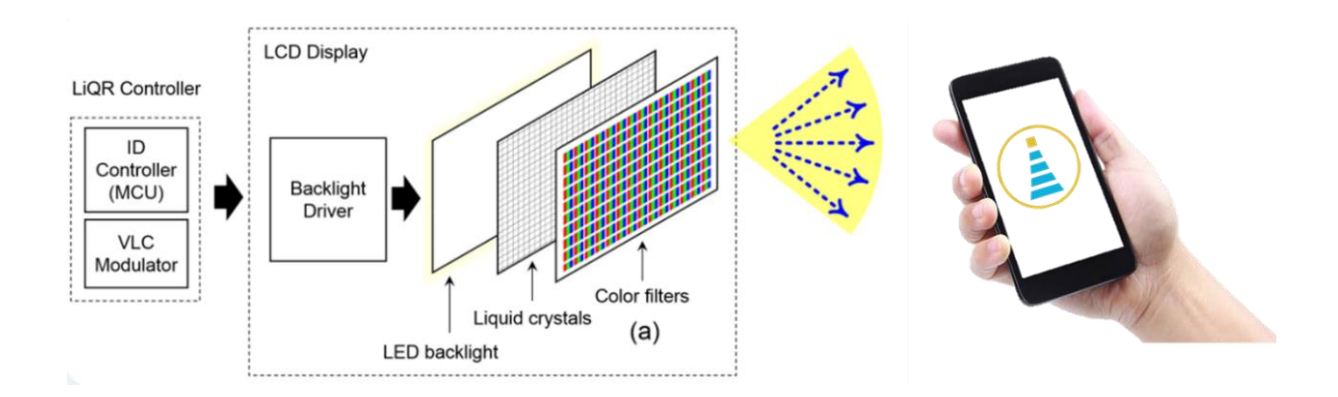


Figure 4.7 VLC broadcast system using LCD

4.2.3 OCC-based Receiver Design for Display

On the receiver side, a smartphone with CMOS camera captures the image of LCD display as shown in Figure 4.8. The captured image contains transmitted ID in the form of rolling shutter pattern that can be decoded using image processing. The image is processed by first detecting the area of interest and then determining the threshold between dark and white stripes to translate the image into binary streams of 1s and 0s. The binary stream is then compared with data frame structure to identify preamble, payload and error check sequence. The payload is finally mapped to the unique resource identifier (URI) and passed to the application layer which loads the relevant content associated with the URI.

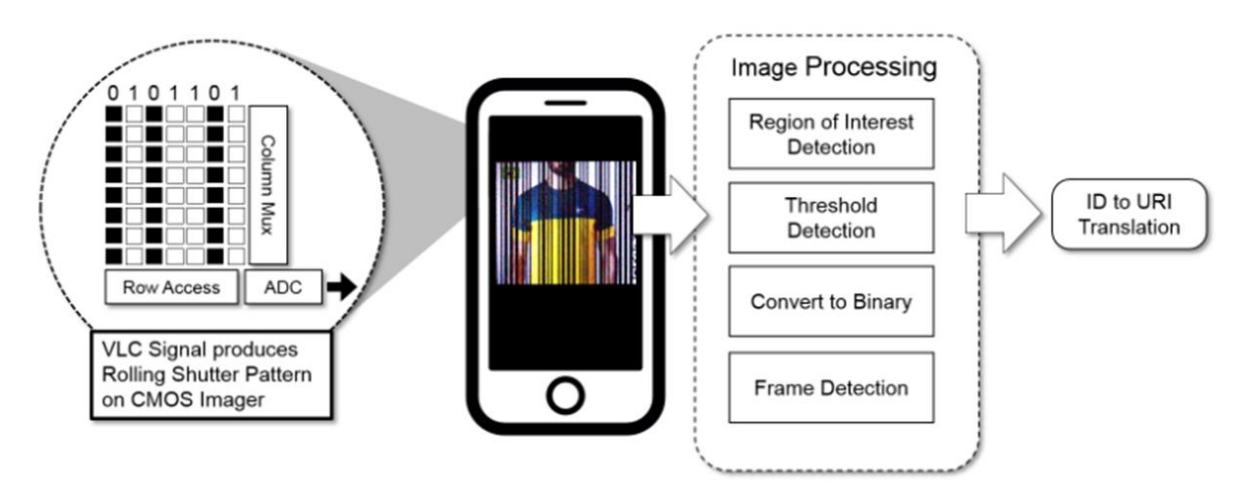


Figure 4.8 VLC signal detection using CMOS camera on mobile device

4.2.4 Retrofitting an LCD Display Module

Generally every LED backlight driver features a dimming control to adjust the screen brightness according to the ambient lighting conditions. This dimming is achieved using a PWM control signal that is provided externally either from an ambient light sense circuit or the on-board LCD display control MCU. In order to modulated the backlight, this PWM input can be directly driven by the OOK modulation signal that is generated by the VLC/LiFi controller as shown in the Figure 4.9.

In addition, one of the key challenge while modulating LCD displays is to maintain the screen brightness which can theoretically reduce to 50% when the backlight is modulated using

OOK broadcast signal. Therefore, in order to compensate for the reduction in brightness due to modulation, the backlight LED current must be doubled. This can be achieved by modifying the value of current sense resistor of the backlight LED driver as shown in the Figure 4.9.

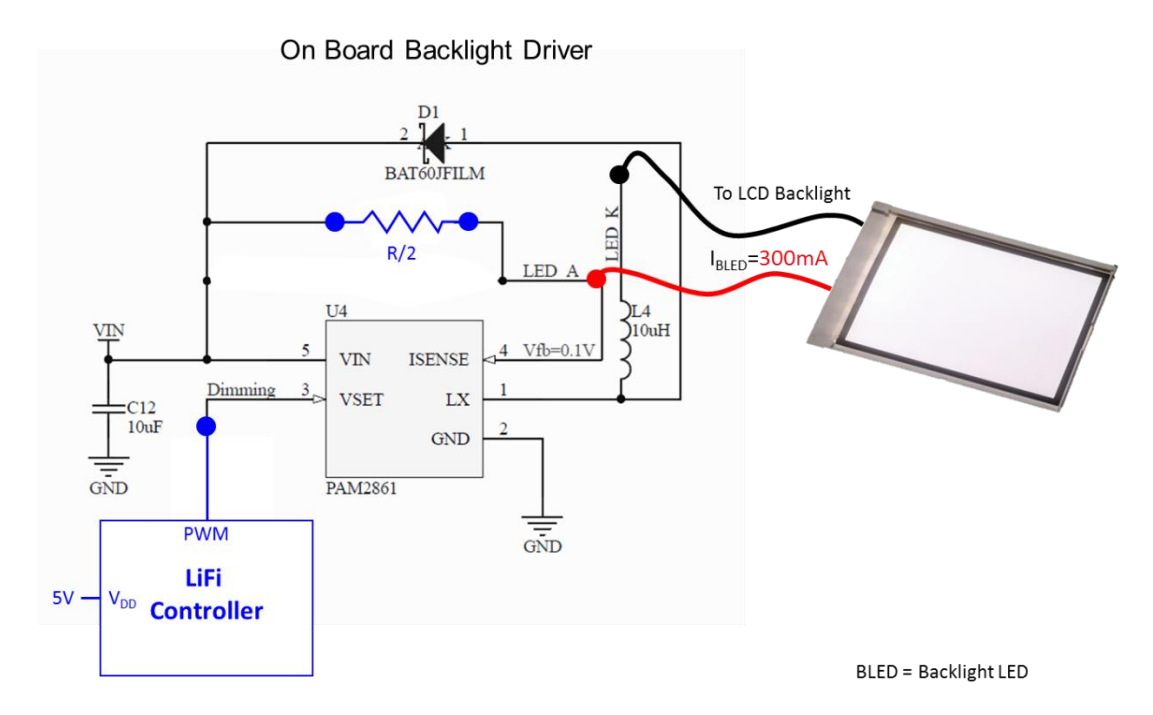


Figure 4.9 Retrofitting VLC in LCD module

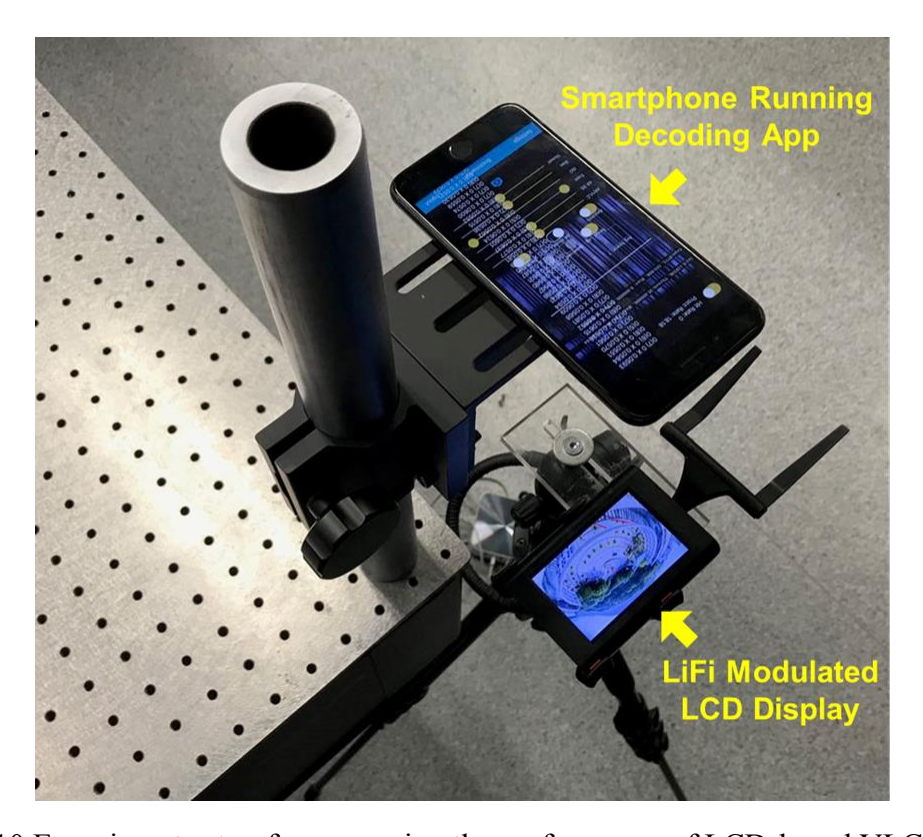


Figure 4.10 Experiment setup for measuring the performance of LCD-based VLC system

4.2.5 Experimental Results

The measurement setup is shown in Figure 4.10 with VLC modulated LCD display mounted to a fixed stand. The display is powered by a 5V battery. A VLC controller programmed with the broadcast ID is driving the PWM input of the backlight controller of LCD display module. The receiver is an iPhone 7 plus mounted to a movable fixture to change the distance between display screen and phones back camera. The phone is running the decoding application.

4.2.6 Sensitivity comparison between LCD display and LED light

Displays are generally much less brighter in comparison to the lights as they are meant to be directly viewed by human eyes. Therefore, image sensors sensitivity must be kept really high in order to receive a detectable signal intensity. This requires the ISO of the camera to be pushed really high in order to achieve a high contrast between dark and bright stripes of the rolling shutter pattern. However, the increase in ISO comes with a lot of noise that affects the quality of the received signal and reduces the detection range. In the Figure 4.11, two images captured of an LCD display and an LED spot light with their respective signal amplitude data are shown for comparison. The image from LCD appears very noisy as compared with a smooth image captured from the light. Similarly, the added noise in the signal amplitude data of LCD can also be observed very clearly which leads to lower detection range due to poor signal to noise ratio.

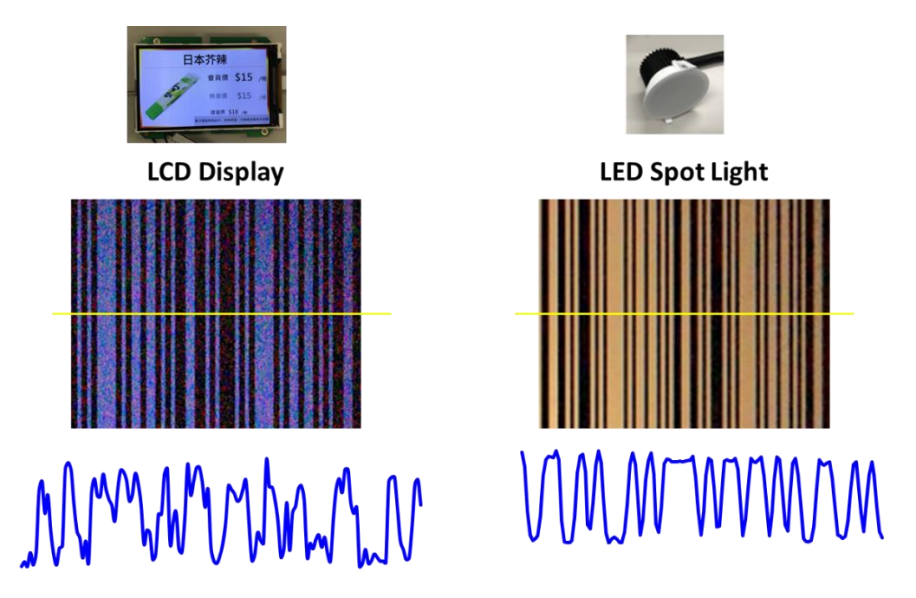


Figure 4.11 Comparison of received signal from an LCD display and LED light

4.2.7 Dependency of Detection Performance on Display Content and Communication Distance

These measurement results shown in Figure 4.12 illustrate how detection sensitivity is affected when a graphic image is being displayed on the screen in comparison to a flat white image. This is due to the fact that the received signal data of the rolling shutter pattern does not only depend on the intensity of the backlight but it is also directly affected by the intensity of the color of each pixel. In other words, pixels inside a dark region of an image will have relatively lower intensity values in comparison to the brighter region. This imbalance in the intensity values for high dynamic range images poses a challenge for determining detection threshold values. Conventional method of calculating threshold by averaging the pixel values leads to a poor detection performance as seen in the measurement results. If a hit rate of 70% (being able to successfully decode 7 frames out of 10) is set as benchmark, a 30cm distance achieved using a white flat image is reduced to 10cm when an image of relatively higher dynamic range is used.

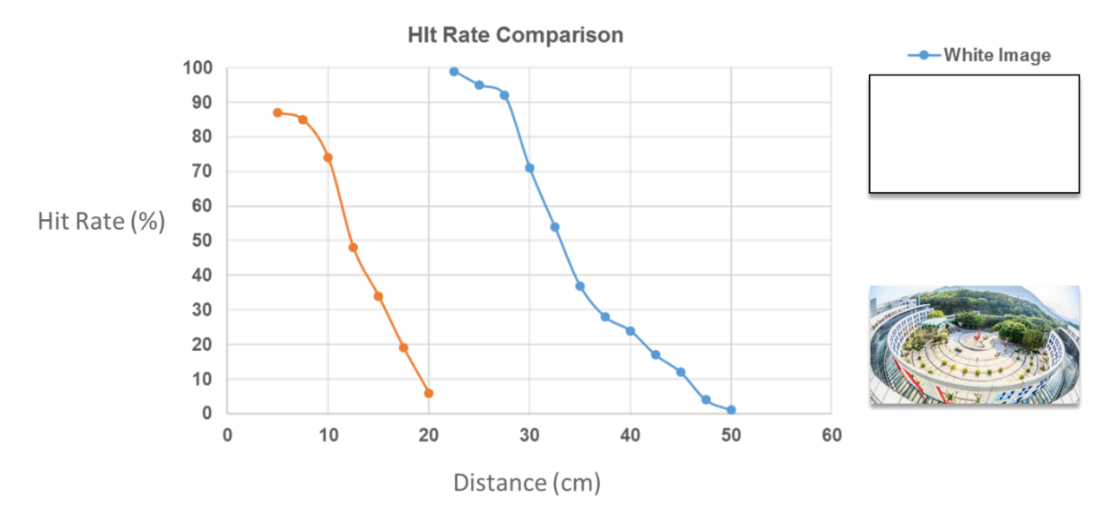


Figure 4.12 Effect of distance and display content on detection performance

4.3 References

- [1] Amazon Alex [Online]. Available: https://www.amazon.com/all-new-amazon-echo-speaker-with-wifi-alexa-dark-charcoal/dp/B06XCM9LJ4
- [2] Google Home [Online]. Available:

 https://store.google.com/au/product/google_home
- [3] Apple Home Kit [Online]. Available:

 https://www.apple.com/hk/shop/accessories/all-accessories/homekit
- [4] Philips Hue [Online]. Available: https://www2.meethue.com/en-us
- [5] Introducing Bluetooth Mesh Networking [Online]. Available: http://blog.bluetooth.com/introducing-bluetooth-mesh-networking
- [6] What is a Beacon? [Online]. Available: https://www.beaconstac.com/what-is-a-bluetooth-beacon

CHAPTER 5 VLC and PDR-based High Accuracy Indoor Navigation

5.1 Introduction

High-accuracy indoor navigation is important for a wide range of futuristic internet of things (IoT) applications for consumers and industry [1]. For instance, indoor positioning systems (IPSs) are the principal component of intelligent location-based services (LBSs) in smart cities, for deployment in locations such as airports, train stations, shopping malls, and hospitals, and with target applications that include navigation, asset tracking, workforce management, location-based emergency response and automation. However, with the global positioning system (GPS) only useable outdoors, there is no single positioning technology that can work indoors with acceptable accuracy, pervasiveness, and affordable implementation cost.

Pedestrian dead reckoning (PDR), which relies on the built-in sensors of smartphones, is a key component of nearly every indoor positioning technology, as it does not require any infrastructure other than a smartphone [2,3]. However, since PDR relies on estimating positions based on step count, its accuracy relies on the correct estimation of pedestrian step size and heading direction, which are both challenging to estimate correctly. Step size estimation suffers due to variation in pedestrians' step sizes and walking patterns. Meanwhile, the heading direction is usually estimated via the built-in smartphone compass that relies on a magnetometer and accelerometer and suffers from errors due to its sensitivity to buildings' metallic structure and nearby metallic objects and electrical appliances. Therefore, PDR positioning accumulates error with every step and must be calibrated using other IPS technologies such as WiFi [4–7], Bluetooth [8,9], geomagnetics [10,11], acoustics [12], or sensor-based landmark detection [13].

The problem is that these other IPS technologies and landmarks themselves lack accuracy and precision. For instance, RF-based solutions suffer from multipath effects and shadowing in indoor environments, which lead to poor accuracy and stability [14,15]. In addition, these systems are not suitable for deployment in sensitive environments due to severe electromagnetic interference and health concerns [16]. Meanwhile, WiFi-, geomagnetic-, and

landmark-based solutions are sensitive to the changing indoor environment and hence require regular site surveying for fingerprint and landmark updating in order to maintain acceptable accuracy. Hence, when PDR is combined with these IPSs, the position can only be corrected up to the baseline accuracy of the employed IPS, while key issues related to step length, heading angle, and pedestrian and device heterogeneity are either left unresolved or are solved using other computationally complex methods [17], [13], [18], [19]. Therefore, in order to realize cm-level accuracy for pervasive indoor applications, a cm-level baseline IPS technology must be employed.

Visible light communication (VLC), which uses ordinary LED lighting to broadcast information is a promising technology for providing data communication and indoor positioning for IoT applications [20, 21]. Thanks to their low-cost, energy efficiency, and reliability, LEDs continue to be widely used in applications including lighting, display and signage [22], creating opportunities for VLC deployment in a wide range of IoT applications [23–25]. Furthermore, thanks to the rolling shutter effect of CMOS image sensors, VLC can be made ubiquitously available in consumer smartphones using optical camera communication (OCC) [26, 27]. The accuracy of OCC-based visible light positioning (VLP) systems can be as high as a few cm [28–31]. Therefore, if combined with PDR, high-accuracy VLP-based IPSs could be ideal for resolving the challenges associated with PDR accuracy.

A few prior works have proposed to combine VLP with PDR to extend the coverage of IPSs [21], [32–34]. However, these works employ VLP in a conventional way, for accumulated PDR error correction, without fully utilizing the high-accuracy VLP location estimate to solve key problems of PDR relating to pedestrian step length diversity and device heterogeneity. In this work, we propose to use high-accuracy VLP to not only correct the PDR accumulated error, but also to calibrate the step size and heading direction of pedestrians to address the sensor inaccuracy, user diversity and device dependency issues, without using any map constraints or sensor-based landmarks as proposed in previous works. We implement our algorithm as a complete indoor navigation application with a digital map to measure the real-time performance of our proposed solution.

Our contributions are summarized as follows.

- 1) We design LiDR, a PDR-based IPS that uses VLP for pedestrian stride length estimation and heading angle calibration for individual users to address the device heterogeneity and user diversity challenges of PDR.
- 2) We propose to use high-accuracy VLP positioning signals to estimate pedestrian step length by measuring the walking speed of the pedestrian while passing under the LED light.
- 3) We propose an algorithm to correct the heading angle error of PDR by utilizing the geometrical features of the LED lighting shape.
- 4) We implement our proposed system on an Android-based indoor navigation application with a digital map and backend cloud server containing user, device, and light- specific parameters. The real-time positioning performance of the application is verified in a 40x40 m experimental lab to demonstrate <1 m precision.

The rest of the chapter is organized as follows. Section 5.2 presents the relevant literature review. The design methodology and implementation details are discussed in Section 5.3, and experimental results and discussions are presented in Section 5.4. Finally, a conclusion is drawn in Section 5.5.

5.2 Related Work

5.2.1 VLP with PDR

VLP systems have an inherent drawback due to the line-of-sight (LOS) property of VLC, which requires that the light must be received by the smartphone camera at all times, but this is not possible in practical scenarios for several reasons. Firstly, the spacing between adjacent lights is usually larger than the smartphone camera's field of view (FoV), leading to occasional blind spots in the camera view during walking. Secondly, areas such as hallways and corridors usually have much thinner light density, leaving a distance of several footsteps between adjacent lighting fixtures. Lastly, at some venues, it may not be feasible to enable VLC in all

lighting fixtures due to cost and modification requirements, leaving fewer lights for VLP coverage.

Therefore, the proposed use of PDR with VLP in the literature has been primarily aimed at eliminating the LOS blockage and extending the coverage. In [32], an RSS-based VLP system was fused with a foot-mounted PDR device. However, the system was tested in an impractically small area of less than 3 m x 3 m with a high density of seven VLC lights. A smartphone-based high- accuracy VLP system with PDR was proposed in [33]. However, the scope of the experiment was limited to a straight corridor with large heading errors in PDR on the return path. In [34], OCC- based light ID detection was used to correct PDR error within a predefined radius of the LED coverage area without realizing high-precision VLP. Similarly, [21] proposed a simulation model for VLC RSSI-based positioning combined with PDR for locating photodiode (PD)-based receiving devices. Although their simulation results claimed a high accuracy of 4.3 cm, the lack of experimental verification and requirement of a PD-based receiver makes it unsuitable for practical consumer smartphone-based IPS deployment.

In addition to the lack of practical deployment considerations and limited experimental verification, the aforementioned works use VLP as a PDR calibration tool without addressing the practical limitations of PDR. On the other hand, our focus is on using VLP to resolve limitations including step length differences, heading angle error, device heterogeneity and user diversity.

5.2.2 Stride-Length Estimation

Step length can be estimated either using direct acceleration integration or through indirect methods such as biomechanical models or statistical methods [17]. Direct methods require double integration of acceleration to find displacement, which results in sensor error being integrated and causing large deviation in measurements [17,35].

Biomechanical methods rely on modeling the direct relationship between acceleration and stride length. For instance, [36] proposed to use the mean of the acceleration in each step to calculate stride length. Similarly, [37] determined the step length based on the cyclic nature of

walking by measuring the arms' swing. Weinberg's model [38] is popular for hand-held smartphones, estimating step length based on the maximum and minimum peaks of vertical acceleration, and it has been shown to perform well in smartphone-based PDR [2].

Context-based methods [39,40] and regression-based methods [41] rely on probabilistic estimation of walking patterns and smartphone carrying state, based on feature extraction from sensor data. However, a wrong estimation of context or carrying state could lead to large errors in step length estimation, as it is not possible to accurately model the diversity of walking patterns and smartphone carrying states of pedestrians.

The use of neural network-based methods for step length estimation has also been proposed in the literature [42,43]. However, these methods are expensive in both implementation complexity and hardware requirements.

The use of optical flow for estimating the step length of pedestrians using the backside camera of a smartphone was proposed in [18]. However, this method involves complex image processing and is not suitable for VLP systems that utilize the frontside camera and ceiling-mounted lights.

The aforementioned methods focus only on solving a generic model to be applied to pedestrians, without taking into consideration the device heterogeneity or the diversity in human walking patterns. Recently, a neural network-based personalized stride length estimation method [44] that addresses the heterogeneity of pedestrian step length via online learning was proposed. However, this method requires magnetic fingerprint-based map matching, which makes the computation heavy on the edge device. In addition, neural network-based online methods require additional computation power on the cloud side, making the whole system very complex and costly to implement. In contrast, our proposed system can instantaneously estimate the step length of a pedestrian walking under VLC-modulated lights without relying on any computationally complex trajectory mapping or neural networks.

5.2.3 Heading Angle Estimation

In addition to the wrong step size, the other major source of error in PDR navigation systems is heading angle, which is primarily due to the sensitivity of the smartphone compass to

magnetic distortions caused by building structures and nearby metallic objects in indoor environments. The proposed solutions in the literature generally aim at solving this problem by either using only the smartphone's built-in sensors to mitigate the effects of magnetic distortions or using map- and trajectory-based heading correction methods.

Several methods rely only on using sensor data to find the heading direction. For instance, [2] proposed to alternatively use a magnetometer or gyroscope to avoid magnetic disturbances at the corners while turning 90°. WalkCompass [19] combines data from the smartphone's inertial sensors to minimize the magnetic interference and corrects the heading direction error by up to 8° of accuracy. Similarly, [45] used a normalized gravity vector from a smartphone rotation vector sensor within one-step to obtain heading direction during various smartphone carrying modes.

Map-aided heading correction relies on identifying paths on corridors, matching pedestrian trajectories with navigation paths and avoiding wall crossovers [13], [46]. In [13], the authors proposed to correct the heading by constraining the user's location between two landmarks in a straight corridor for calibration, followed by gyroscope-only heading estimation. Similarly, [47] proposed to correct the heading error in PDR using a position estimate acquired through WiFi RSSI using linear regression while the user is walking in a straight line. In [48], an indoor-outdoor positioning system using crowd sensing data was proposed, where heading error is corrected by matching the PDR traces during the indoor-outdoor transition based on detecting landmarks at the gate.

The limitation of all of the above methods is that they rely either on using sensor fusion to identify the heading direction or pedestrian trajectory matching on a map, which makes the methods computationally complex and only applicable in certain locations. On the other hand, our proposed method uses light geometry to instantaneously calibrate the heading while the pedestrian is walking under VLC-modulated lights, at a comparatively lower computational cost.

5.3 Methodology

5.3.1 System Overview

The system architecture of LiDR is shown in Figure 5.1, where a person is shown walking with a smartphone under VLC- modulated smart LED lights transmitting unique identifiers (IDs). As the person passes under an LED light, his position, orientation and walking stride length are calibrated via a high- accuracy angle of arrival (AoA)-based visible light positioning (VLP) signal, but when the person is walking in between the lights, such that there is no light seen by the smartphone camera, PDR is used to estimate his location. The light configuration information including, light ID, location in the building, and orientation, is stored in the cloud along with the building's digital map database. The PDR- and VLP-related device specific parameters are also stored and continuously updated in the cloud for later access and sharing among users and devices.

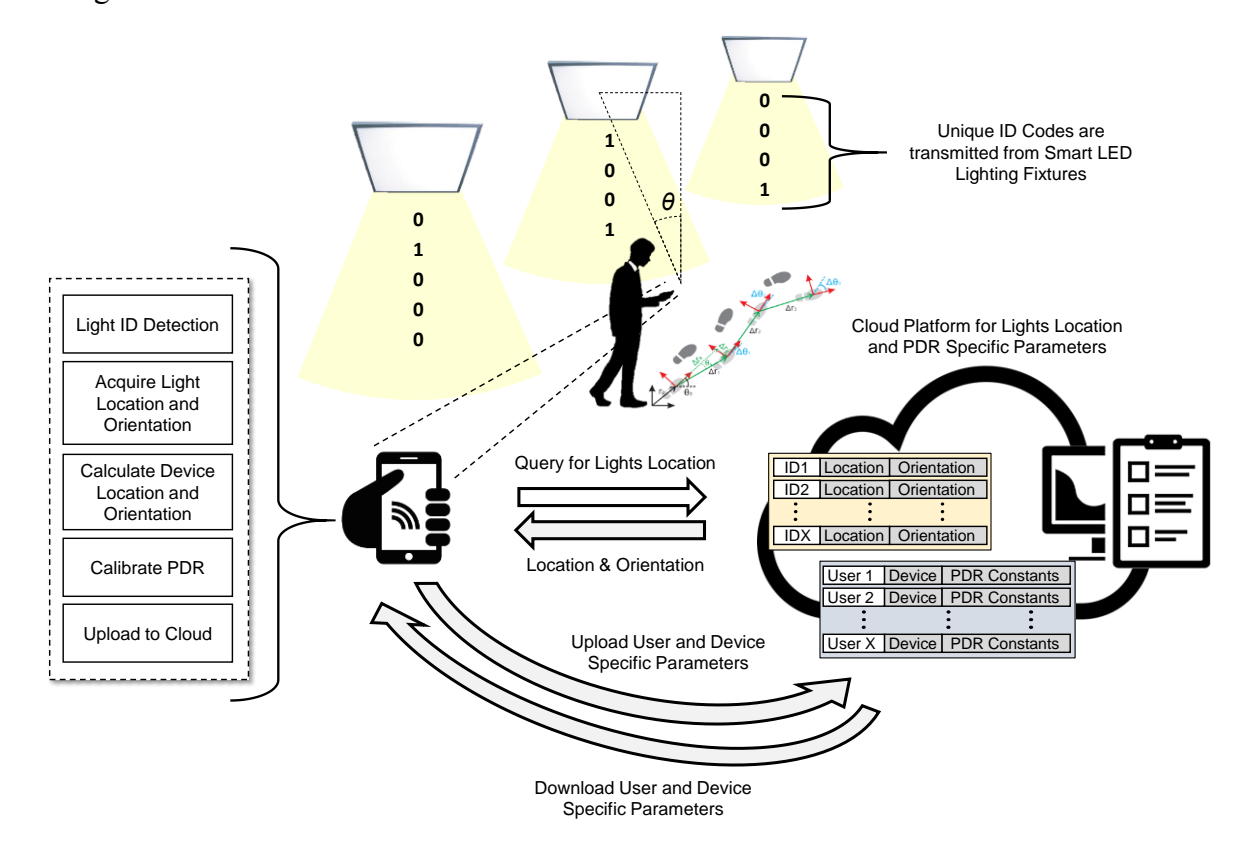


Figure 5.1 System Overview: Combined usage of VLC AoA-based positioning and pedestrian dead reckoning with cloud-controlled backend database to provide high-accuracy indoor localization.

5.3.2 Dead Reckoning

There are several ways of tracking smartphone acceleration to detect pedestrian steps, which involve detecting the smartphone holding state and pedestrians' walking mode [49]. In this work, we will primarily focus on the case where the user is actively navigating while holding the phone in hand, and looking at the screen. Therefore, we choose to use the vertical acceleration for step detection [2]. Since the smartphone is likely to be held at a slightly tilted angle in this case, as illustrated in Figure 5.2, the smartphone's pitch angle needs to be considered to effectively extract the vertical acceleration component from the y- and z-axis of acceleration. The smartphone's 3D acceleration w.r.t the world frame acc_w is given as

$$acc_W = R_{x,y,z} * acc_{x,y,z}$$

$$(5.1)$$

where Rx,y,z is the 3D rotation matrix of the smartphone w.r.t to the world reference frame and $acc_{x,y,z}$ is the 3D acceleration w.r.t the smartphone's reference frame. The vertical acceleration component acc_v can be extracted as

$$\begin{bmatrix} acc_x \\ acc_y \\ acc_v \end{bmatrix} = R_z R_y R_x * \begin{bmatrix} acc_x \\ acc_y \\ acc_z \end{bmatrix}$$
 (5.2)

However, if we only consider the smartphone's tilt angle around the x-axis, i.e. pitch angle, we can simplify it as follows:

$$\begin{bmatrix} acc_x \\ acc_y \\ acc_y \end{bmatrix} = R_x * \begin{bmatrix} acc_x \\ acc_y \\ acc_z \end{bmatrix}$$
 (5.3)

$$\begin{bmatrix} acc_x \\ acc_y \\ acc_v \end{bmatrix} = \begin{bmatrix} 1 & 0 & 0 \\ 0 & -\cos\theta_x & \sin\theta_x \\ 0 & \sin\theta_x & \cos\theta_x \end{bmatrix} * \begin{bmatrix} acc_x \\ acc_y \\ acc_z \end{bmatrix}$$
(5.4)

which leads to the following expression:

$$acc_v = acc_y \sin \theta_x + acc_z \cos \theta_x \tag{5.5}$$

However, the accelerometer data can have both noise and multiple spikes due to differences in the walking patterns of the pedestrians. Therefore, in order to suppress the spikes, we must apply a low pass filter on the accelerometer data with a cut off frequency of 2.5 Hz, which is assumed to be the maximum walking step rate of a pedestrian in normal circumstances. The employed filter is a moving average-based attenuator with the output expression given below:

$$y_{t} = \begin{cases} x_{t}, & t = 1\\ x_{t}\alpha_{t} + (\alpha_{t} - 1)y_{t-1}, & t > 1 \end{cases}$$
 (5.6)

The attenuation factor α is calculated as follows:

$$\alpha_t = \frac{(\tau_t - \tau_{t-1})}{[T + (\tau_t - \tau_{t-1})]}$$
(5.7)

where τ_t and τ_{t-1} represent the system clock at instance t and t-1 respectively and T is the time constant of the filter. The filtered vertical acceleration waveform is shown in Figure 5.2.

The step detection is performed by tracking the positive and negative peaks of vertically filtered accelerations, hereafter referred to as peaks and valleys. In order to ensure the peaks and valleys belong to a valid step, we ensure that the difference between the peak and valley is greater than a threshold and the time difference between the last and current step is no more than the period of the maximum walking step frequency (WF_{max}). The step condition is shown in the following equation:

$$t_{k}^{step} = \begin{cases} t \middle| (a_{t=t^{peak}} - a_{t=t^{valley}}) > \epsilon_{step} \\ t \middle| (t - t_{k-1}^{step}) > 1 \middle|_{WF_{max}} \end{cases}, \tag{5.8}$$

where t_k^{step} is the time of the kth step, ϵ_{step} is the peak to valley threshold, $a_{t=t^{peak}}$ and $a_{t=t^{valley}}$ represent the peak and valley accelerations respectively and are defined in the following equations:

$$t^{peak} = \{t \mid a_t > a_{t+1}, a_t > a_{t-i}, 1 \le i \le n_p \}$$
(5.9)

$$t^{valley} = \{t \mid a_t < a_{t+1} , a_t < a_{t-i}, \ 1 \le i \le n_v \}$$
(5.10)

We set $n_p = 2$ and $n_v = 1$ respectively. The walking frequency WF is calculated as follows:

$$WF = {}^{N} / \sum_{k=2}^{N} (t_{k}^{step} - t_{k-1}^{step})$$
 (5.11)

where N = 5 to consider only the five most recent steps to continuously adapt to the changing walking speed of the pedestrian.

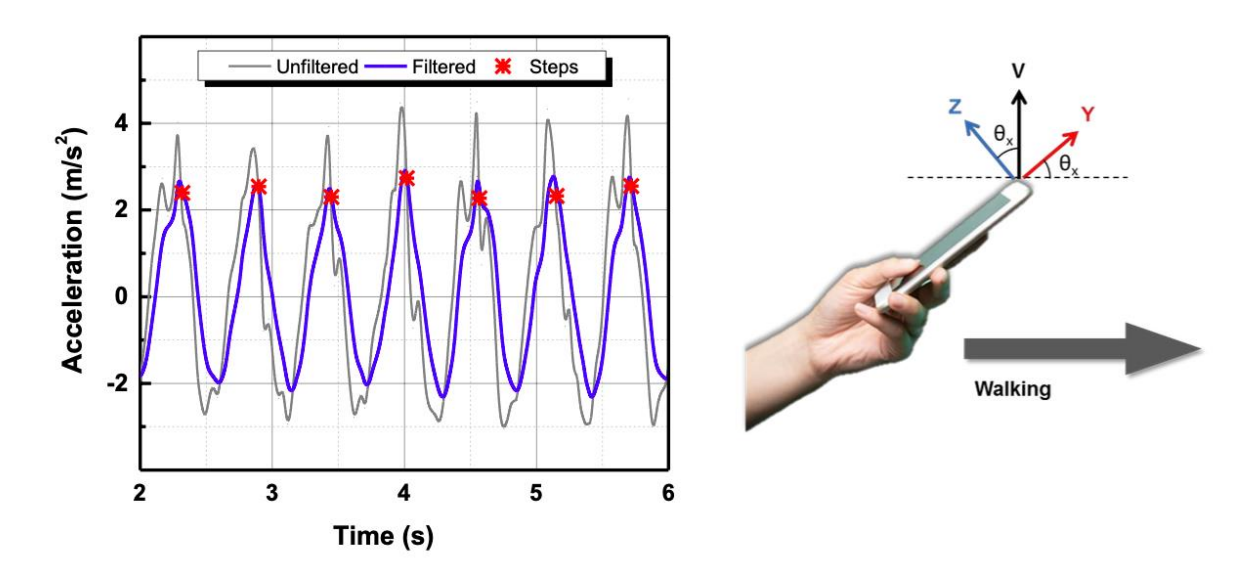


Figure 5.2 Vertical acceleration waveform and smartphone holding state while walking.

In order to consider the impact of device diversity on step detection, we conducted an experiment to compare accelerometer waveforms on four different models and brands of

smartphones. The data were collected while simultaneously holding all the smartphones in the hand to ensure every device would experience the same acceleration, as shown in Figure 5.3. The comparison shows that the waveforms of all the devices are nearly identical, except minor differences in amplitude, with the Samsung smartphone recording the largest amplitude while the Oppo device had the smallest amplitude among the four devices. These results indicate that the PDR detection algorithm can perform identically on these smartphones if the step detection thresholds are tuned according to the relative acceleration amplitude of each device. Therefore, in order to address these variations, we use a variable step detection threshold ϵ_{step} defined as follows:

$$\epsilon_{step} = \frac{\sum_{k}^{k-N} (a_{t=t_{k}^{peak}} - a_{t=t_{k}^{valley}})}{2N}.$$
 (5.12)

Here, N = 5 is kept the same as in (5.11).

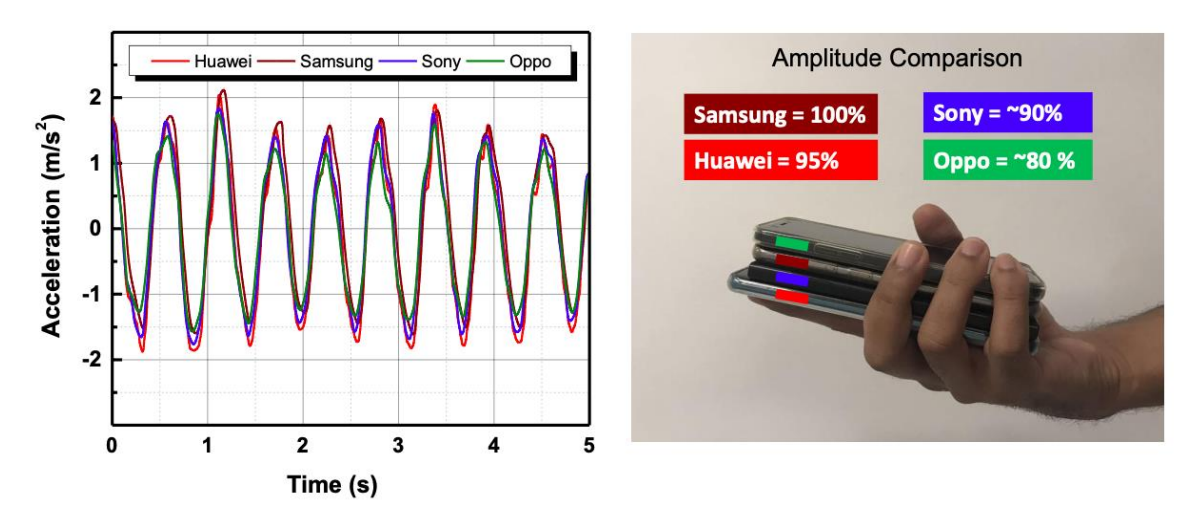


Figure 5.3 Comparison of accelerometer waveform recorded from various Android devices.

5.3.3 Visible Light Positioning

Very high-accuracy VLP can be realized using optical camera communication. With the light ID being detected via OCC, the relative position between the smartphone and the LED light can be calculated via the AoA based on the camera's projective geometry. Figure 5.4 shows the basic principle for VLP via the camera's projection, which is given as

$$p_c = C [R|T] P_w (5.13)$$

where, p_c is a point's coordinates on an image, with its real- world coordinates being P_w , C is the camera intrinsic matrix and is found through camera calibration, and R and T are the rotation and translation matrices of the smartphone respectively. R is calculated by the smartphone gyroscope and is available through the Android sensor API. T determines the real-world location of the smartphone w.r.t to the point P_w . The equation can be rewritten as

$$s \begin{bmatrix} u \\ v \\ 1 \end{bmatrix} = \begin{bmatrix} fx & 0 & c_x \\ 0 & fy & c_y \\ 0 & 0 & 1 \end{bmatrix} [R|T] \begin{bmatrix} X \\ Y \\ Z \\ 1 \end{bmatrix}$$
 (5.14)

Here, s is the scaling factor of image point's homogenous coordinates. For VLP, the real-world position of the center of the LED is known. Therefore, if we know the center coordinates of the LED's projection on the image (u,v), we can solve (5.14) for T to find the relative position of the smartphone w.r.t the LED's center.

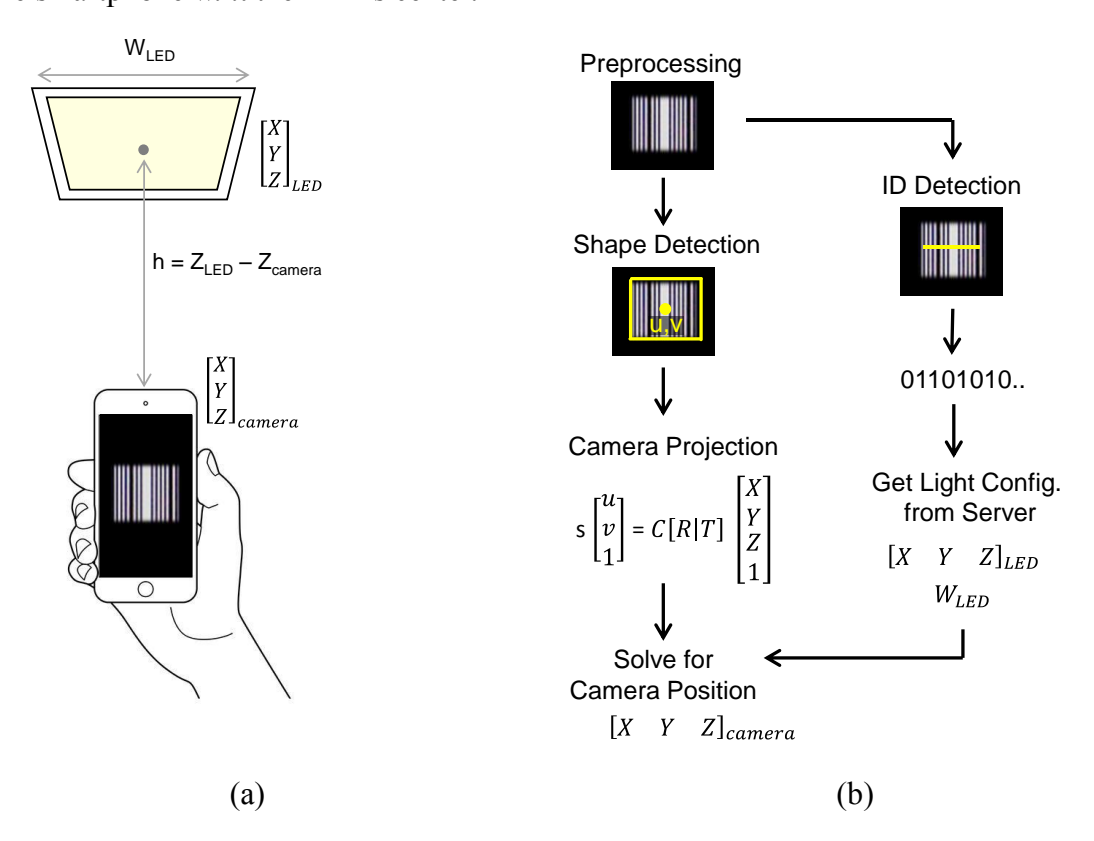


Figure 5.4 Visible light positioning using optical camera communication: (a) image capture, (b) processing steps.

5.3.4 Stride-Length Estimation

Step-length estimation via VLP requires the smartphone camera to see the LED light continuously for a period of at least twice the step rate, such that the position at the start and end of the step can be detected to measure the step length accurately. Therefore, the wider the FoV of the smartphone camera, the more reliable the step length estimate will be. The available FoV of the camera is dependent on the height of the ceiling, which is fixed for a particular indoor venue. For instance, in a venue with a ceiling height of 2.7 m, an average-height pedestrian holds the smartphone at about 1.5 m from the ceiling, which will give a coverage range of 2m for a typical front camera FoV of 67°, as shown in Figure 5.7(b). However, as shown in Figure 5.6, while the person is holding the phone in front of his body, half of the FoV is blocked by the person's own head, which can reduce the effective FoV. In addition, the natural holding position of the smartphone is slightly tilted to allow the person to see the full face of the screen while walking, which results in a pitch angle, which can be up to 30° or higher. This leads to an even smaller FoV and thus can reduce the range over which the step length can be estimated.

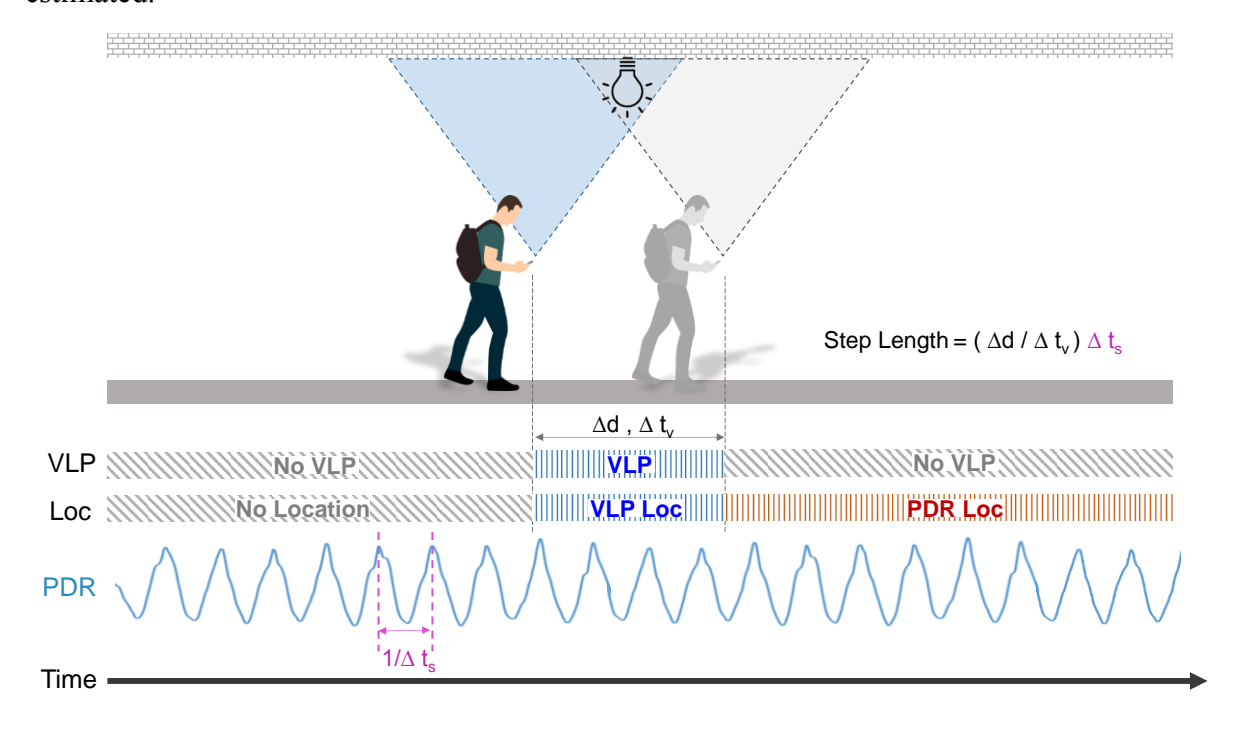


Figure 5.5 Using visible light positioning for measuring step size of a pedestrian.

We conducted an experiment by having a pedestrian carry an Android smartphone (Huawei P30 pro) with a FoV of 67° and walk under a 2.7 m-high ceiling light, and recorded the results, as shown in Figure 5.7(a). The measurements show that the effective area of 2 m FoV is reduced to 0.8 m with only 1 step recorded during that interval. This leads to an important conclusion that it is not feasible to directly estimate the step size by measuring the VLP distance traveled during the two consecutive step detection peaks. Instead, a more reliable approach is to measure the walking speed of the person and use the step rate to determine the step length.

The concept of using VLP to measure the step length of the pedestrian is presented in Figure 5.5. When a pedestrian passes under the light while holding the smartphone, his position can be tracked using VLP with high accuracy (\sim 10 cm) and a fast update rate of up to 30 frames/second for a period of time Δt_v , while the smartphone camera can see the light. The distance traveled during this period (Δd) can then be used to calculate the walking speed of the pedestrian. With the information of the step interval available, the step length of the pedestrian can be estimated by the product of the walking speed and step interval. The location tracked by the VLP at time t is given as

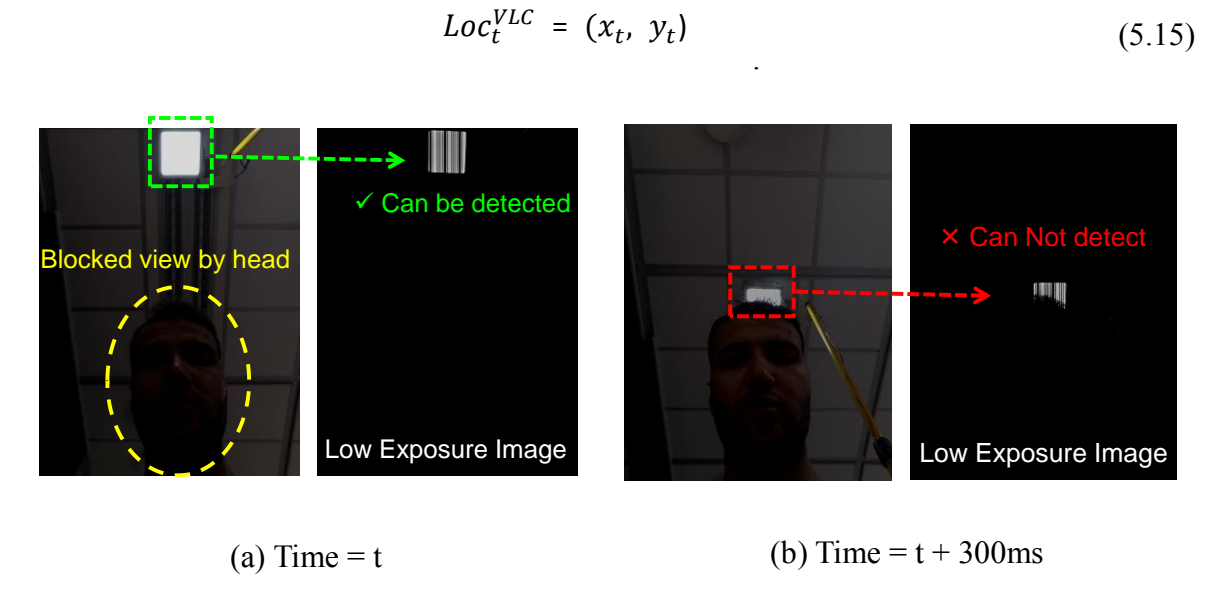


Figure 5.6 Front camera view with its corresponding low-exposure image captured while the pedestrian is walking under the light and holding the phone in front, at two instances.

The walking speed WS_t of the pedestrian can be measured using the first and last VLP location of the recent consecutive VLP location outputs, which is given as

$$WS_{t} = \frac{d\left(Loc_{1}^{VLC}, Loc_{N}^{VLC}\right)}{t_{k=N} - t_{k=1}} \mid t > (t_{k=N} + 2\Delta t_{VLC}), \tag{5.16}$$

where Δt_{VLC} is the VLP location output rate and Loc_N^{VLC} is the last VLP location captured by the smartphone camera. The step length can then be found as

$$Step Size = \frac{WS_t}{WF_t}$$
 (5.17)

The walking speed and step size of a pedestrian can vary as they walk out of the VLP coverage area and before they arrive under the next light for recalibration. Therefore, we can employ Weingberg's [38] acceleration amplitude-based step size estimation equation to extract the subject-dependent constant from the measured step size in (5.17). Weingberg's step size estimation equation is given as

$$Step Size = k\sqrt[4]{(a_{t=t^{peak}} - a_{t=t^{valley}})}$$
(5.18)

With our predetermined step size, we can find k as follows:

$$k = \frac{\sqrt{(x_N - x_1)^2 + (y_N - y_1)^2}}{t_{k=N} - t_{k=1}}$$

$$\sqrt[4]{(a_{t=t}^{peak} - a_{t=t}^{valley})}$$
(5.19)

According to the experimentation performed in [50], the distance measurement accuracy of Weinberg's model is less than 1 m for a distance of up to 10 m. Therefore, if a VLC light is available every 10 m, the target accuracy of <1m can be achieved.

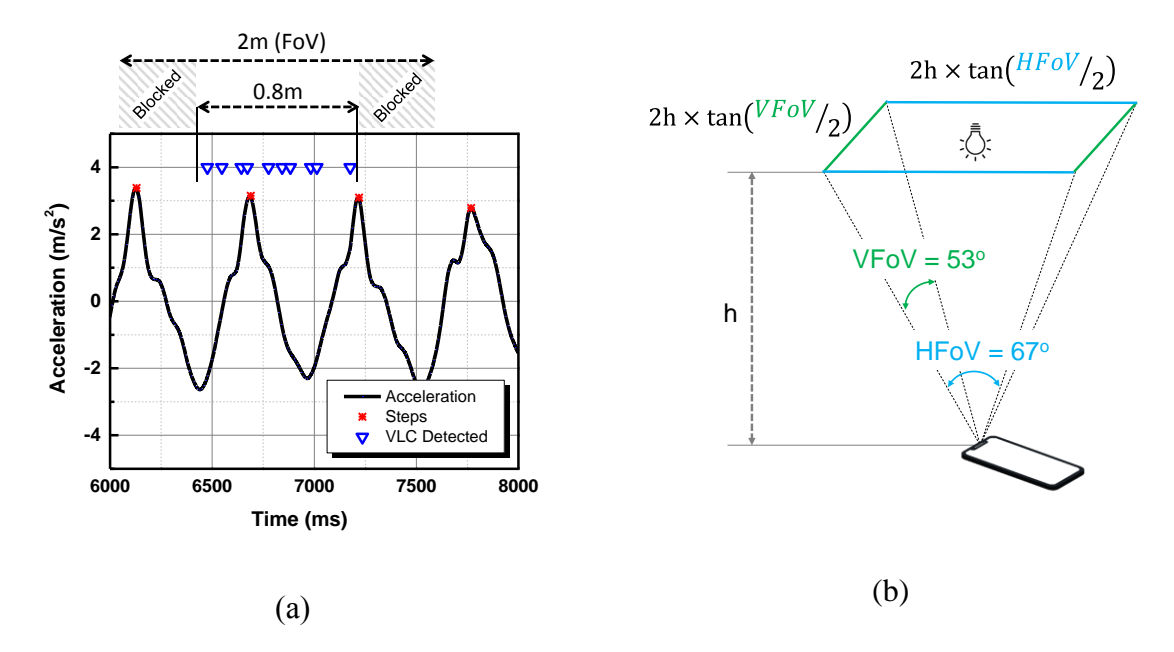


Figure 5.7 Step size estimation via partially blocked FoV during pedestrian walking: (a) position tracking during effective FoV, (b) FoV and height of ceiling.

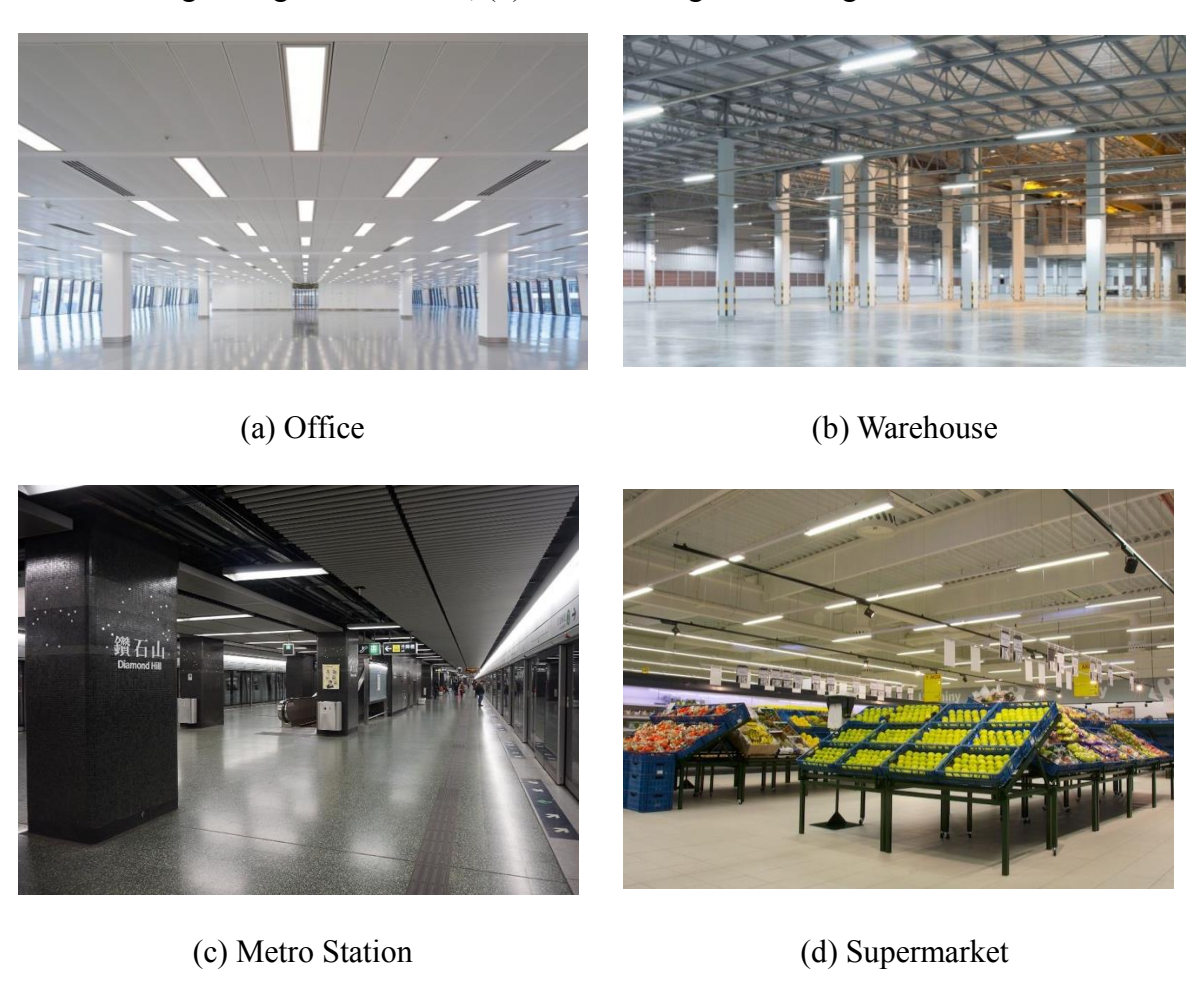


Figure 5.8 Rectangular lighting at commercial and industrial venues.

5.3.5 Heading Angle Correction

Heading angle correction is a very challenging problem to solve for accurate PDR as the smartphone's compass can be easily influenced by the building's structure and nearby metal. However, with VLC AoA being used for accurate positioning, the heading angle calibration can also be performed simultaneously using the geometry of the LED light.

Since the majority of the lighting used at commercial and industrial venues is in a rectangular shape, as shown in Figure 5.8, it makes intuitive sense that light shape can be utilized for precise estimation of the heading of pedestrians while they are passing under the light. In addition, since the image processing and signal decoding is already being performed for the location estimate of the pedestrian, the heading angle correction can be incorporated into the algorithm at a relatively low additional computational cost.

The algorithm relies on the lights' geometry and installation orientation information, which can be stored in the building's map database and can be made available through the cloud. The width (W) and length (L) determine the shape of the rectangle, whereas the angle θ_L specifies the compass orientation along the longer dimension of the rectangle. It is important to note that both square-shaped light panels and tube-lights are a special case of a rectangular shape, with W = L and $W \ll L$ respectively. Since the order of the corners from the detected image cannot be determined absolutely, the algorithm is only used to correct the heading angle to the true orientation of the nearest corner, as explained below. The steps involved in angle correction are described as follows:

A) Setting up Light Configuration Database

Geometry-based angle correction requires the light's shape and orientation information to be preloaded in the database. As in Figure 5.9 (a), for each light, the database must hold its light ID, width (W), length (L) and installation orientation (θ_L) along the longer dimension i.e., L given in degrees from the north.

B) Orientation of Corners

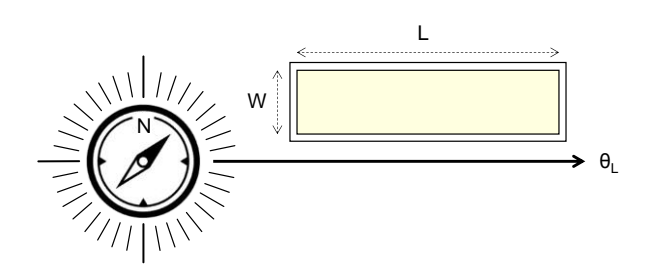
Based on a light's orientation θ_L , we can find the orientation of each corner from the center, as shown in Figure 5.9 (b). If the orientation angle for the light's ith corner is denoted as θ_i^C , then the four corner angles of a rectangular light can be calculated as

$$\theta_{i}^{C} = \begin{cases} \theta_{L} + \arctan\frac{W}{L}, & i = 1\\ \theta_{L} + \arctan\frac{W}{L} + 2\arctan\frac{L}{W}, & i = 2\\ \theta_{L} - \arctan\frac{W}{L} - 2\arctan\frac{L}{W}, & i = 3\\ \theta_{L} - \arctan\frac{W}{L}, & i = 4 \end{cases}$$

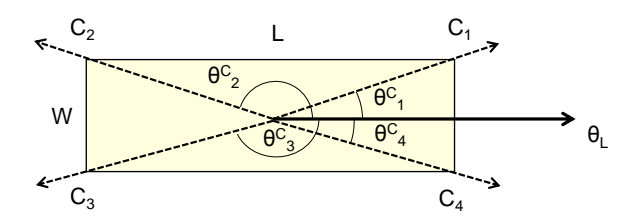
$$(5.20)$$

These corner angles' expressions can be simplified for a square light, where W = L, as

$$\theta_{i}^{C} = \begin{cases} \theta_{L} + \pi/4, & i = 1\\ \theta_{L} + 3\pi/4, & i = 2\\ \theta_{L} - \pi/4, & i = 3\\ \theta_{L} - 3\pi/4, & i = 4 \end{cases}$$
(5.21)



(a) Measuring the real-world orientation and size of light



(b) Calculating the corner angles of light

Figure 5.9 Heading angle estimation from rectangular light shape.

For a tube-light, where W << L, we can further simplify the expression to approximate the rectangular shape as a line with two corners, as

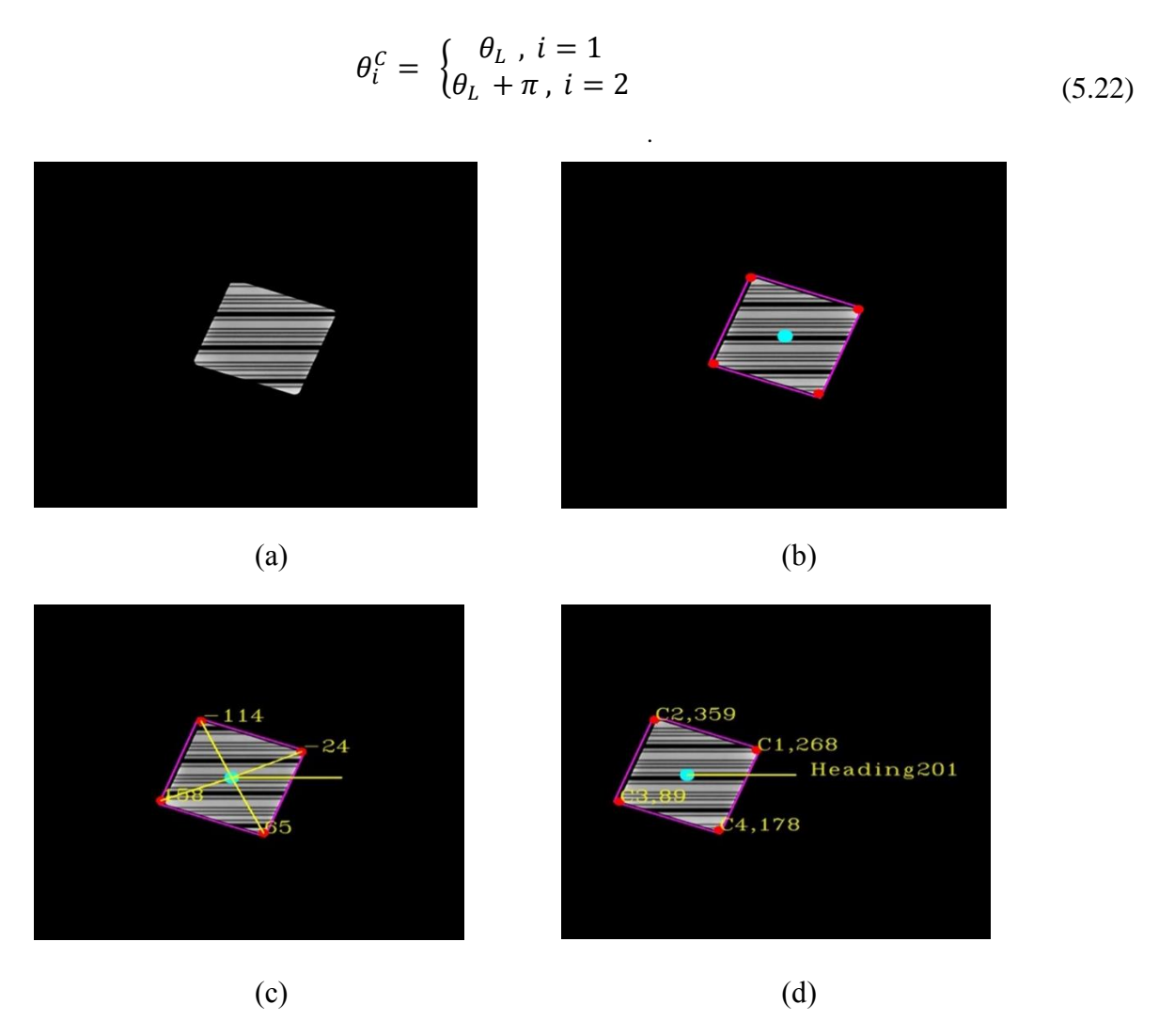


Figure 5.10 Image processing steps for heading angle correction: (a) grayscale converted image of a square downlight LED panel, (b) corner and median detection (c) corner angles w.r.t to smartphone axis, (d) estimated world orientation of corners and smartphone heading.

C) Angle Correction

During the image processing for VLP, the light shape and corner information is already available, as shown in Figure 5.10(b). The angle correction can be applied by finding the estimated orientation of each corner based on the smartphone's compass and minimizing the difference between the estimated orientation and the real-world orientation calculated in the previous step. We find the angle between the positive y-axis of the smartphone and each corner,

denoted as Ci , add it to the smartphone compass reading and find the estimated orientation of each corner $\varphi_i^{\it C}$, as follows:

$$\varphi_i^C = \theta_{compass} + \angle C_i, i = a, b, c, d$$
 (5.23)

Here a,b,c,d denote the subscripts for the corners of the light's projection in an image, as opposed to 1,2,3,4, which denote the corners in the real world. However, the order of correspondence between the image corners and real-world corners is not known, but can be found by minimizing the difference, shown as

$$i = k \mid \min(\theta_k^c - \varphi_i^c) \ i = a, b, c, d, \ 1 \le k \le 4$$
 (5.24)

Hence, we can find the correction offset to add to the smartphone compass to correct the heading error as

$$\theta_{offset} = \min(\theta_k^C - \varphi_i^C) \tag{5.25}$$

The maximum tolerable compass error that can be corrected by the proposed method depends on the number of possible orientations of the smartphone that could lead to identical images of the light. For instance, a square-shaped light could have an identical projection when viewed from four different orientation angles of the smartphone with a difference of 90°. Hence, the maximum tolerable compass error for a square light is 45°. Similarly, for a rectangular-shaped light, with L > W, there are only two possible orientations of the smartphone, with a difference of 180°, and hence, the maximum tolerable compass error is 90°. This correction capability is in good agreement with the measured data of various smartphones published in [51], which reported an 80% compass error of less than 45°.

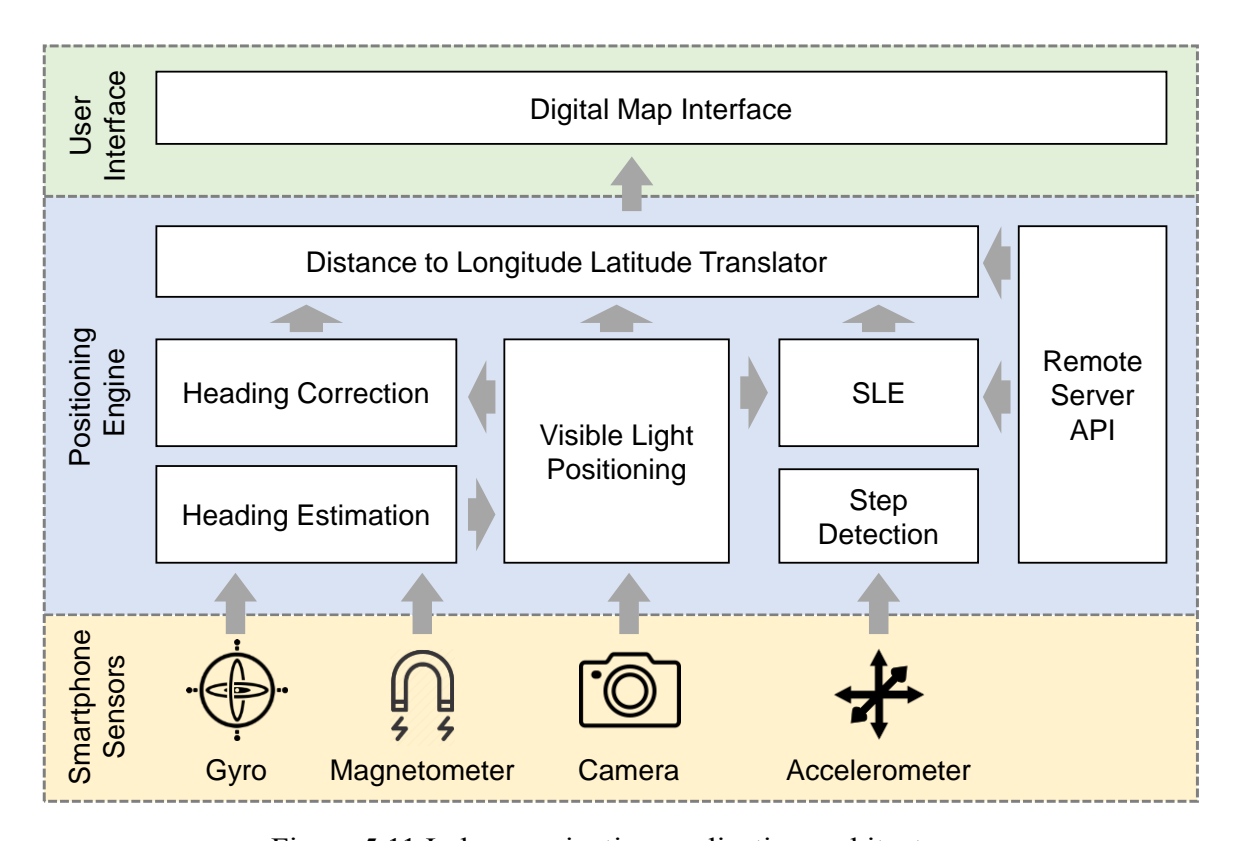


Figure 5.11 Indoor navigation application architecture.

5.3.6 Software Integration

The complete indoor positioning function is realized in an Android-based indoor navigation application, which shows the real-time location of the user on a digital map. The application architecture is shown in Figure 5.11, which highlights the software integration of various sensors, positioning engine and application front end user interface. The data from the sensors is collected through their respective APIs and used by the positioning engine for absolute position and orientation calculation. Meanwhile, the remote server API provides lighting configuration information to the positioning engine which includes lights' GPS coordinates, dimensions and installation orientation. This configuration information is used for heading estimation and relative position calculation by the distance to longitude and latitude translation block, which provides the location coordinates for the digital map to update the user's location cursor.

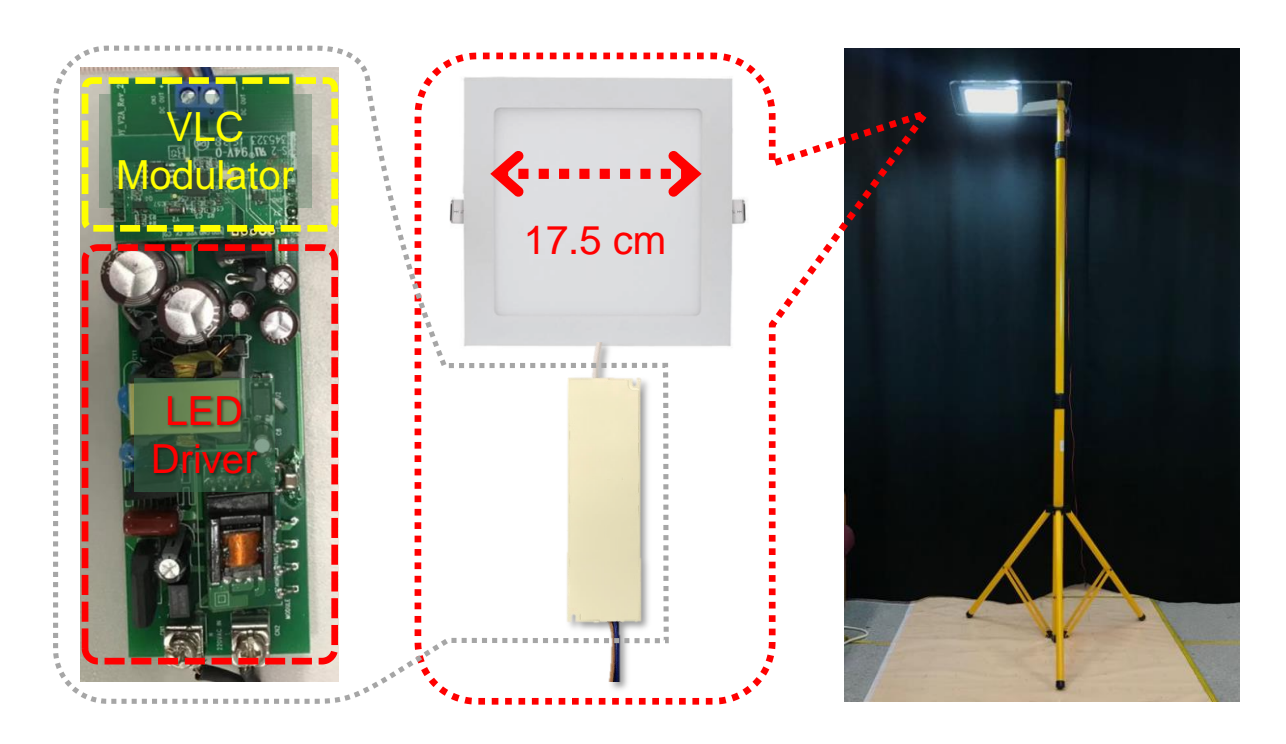


Figure 5.12 Square-shaped smart LED light mounted on an adjustable light pole.

5.4 Experiment and Evaluation

For testing and evaluation, we ran our LiDR indoor navigation application on an Android smartphone (Huawei P30 Pro). The experiments were carried out in our laboratory with an area of ~100 m2. LED square-shaped light panels mounted on a pole with adjustable height and embedded with a VLC modulator were used as smart LED lights in our experiment. The smart LED hardware consists of a power supply unit and a down-light square panel with an area of 17.5 x 17.5 cm, as shown in Figure 5.12. The LED power supply comprises a standard 18 Watt constant-current LED driver with an MCU-based VLC modulator module integrated on a single PCB. The VLC modulator for each LED is programmed to a unique ID to identify its installation location with building and floor information, its orientation and its size in the cloud database.

We first evaluated the performance of each algorithm individually, starting with VLP, then combining VLP and dead reckoning for step-length estimation, followed by the heading angle correction algorithm. Finally, we evaluated the LiDR indoor navigation application to characterize the positioning accuracy performance of our whole system.

5.4.1 Visible Light Positioning

The accuracy of VLP directly impacts the accuracy of the PDR step size estimation and calibration. Therefore, it is the most critical factor in determining the overall performance and reliability of our proposed LiDR system. Figure 5.13(b) shows the measurement setup, consisting of a 1.5 m tall light pole with a square LED light panel mounted at the top and a Cartesian coordinates chart pasted on the floor with the LED's center positioned at the origin. For an average ceiling height of 2.7 m, an average-height pedestrian usually holds the smartphone at about 1.5 m distance from the ceiling. Therefore, the height of the LED is set to be 1.5 m in the experiment. During the recording of positioning data, the smartphone is placed at points on the grids each 20 cm apart while tilting the phone at various random tilt angles. The pitch and roll angles are varied up to 30° and 20° respectively, which cover the natural smartphone holding state of pedestrians while walking during navigation. The magnitude of the positioning error at each point is calculated by measuring the difference between the ground truth and the measured position. The cumulative density function (CDF) of the positioning error, shown in Figure 5.13(a), indicates that the mean positioning error is about 8 cm with maximum-recorded error of less than 20 cm.

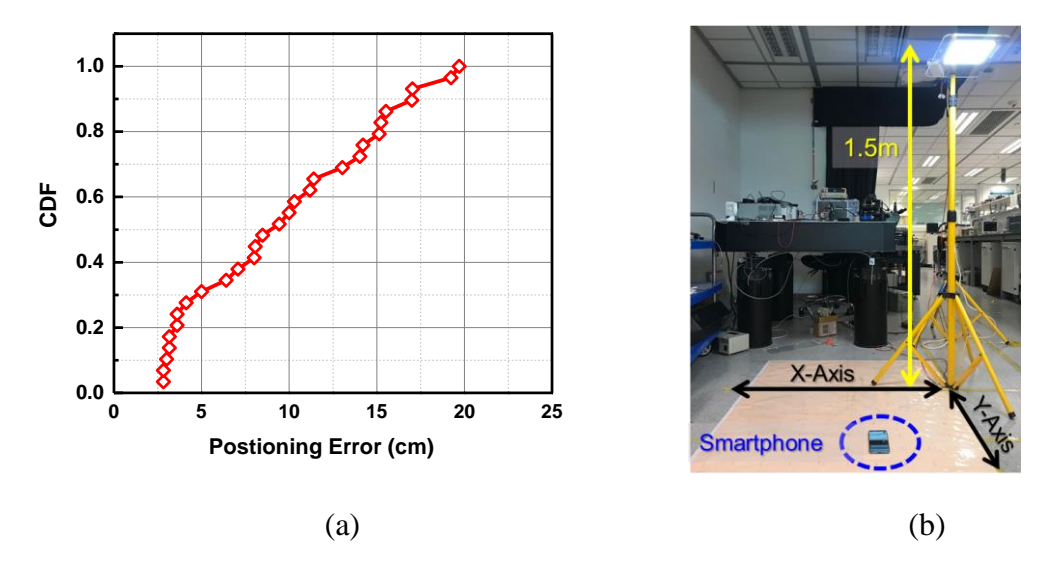


Figure 5.13 VLC AoA positioning accuracy measurement: (a) measurement setup, (b) cumulative density function of positioning error.

5.4.2 Step-Length Estimation

To verify the accuracy of the step length estimation, we conducted an experiment by placing the LED in a corridor of about 9 meters' length at a height of 2.7 m from the floor, as shown in Figure 5.15(b). The pedestrian held the smartphone in hand and walked under the light at three different speeds 50 times to have his step length measured by the Android application running the proposed algorithm. To provide a reference for actual step size during the walk, we calculated the average step length of the person based on the number of steps taken during the 9 m distance. Figure 5.15(a) shows the x-y Cartesian graph of the measured positions of the pedestrian at three different walking speeds in an area of 1.6 m x 1.6 m with the LED at the origin. The graph shows that, on average, an area of 80 cm is covered by the high accuracy VLP estimate and can cover less than 2 steps of the pedestrian during the walk.

The CDF of the step length estimation error for the aforementioned experiment is shown in Figure 5.14. The mean step length error is 3.8 cm with a maximum-recorded error of less than 9 cm. This leads to an inference that in order to keep the average positioning error < 1 m, a VLC light must be deployed every 26 steps, which leads to an average 13 meter walking distance between each light, assuming an average pedestrian step length of 50 cm.

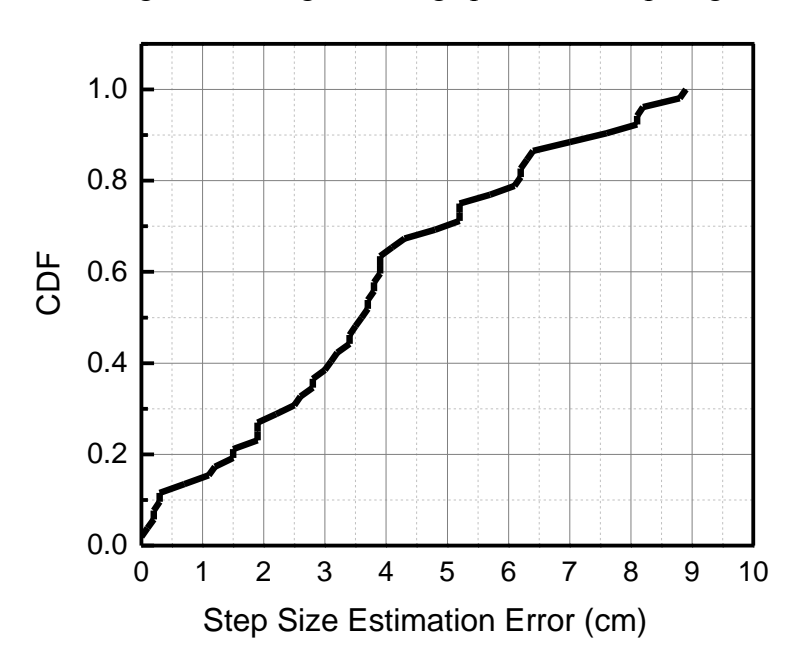


Figure 5.14 Cumulative density function (CDF) of step size measurement error.

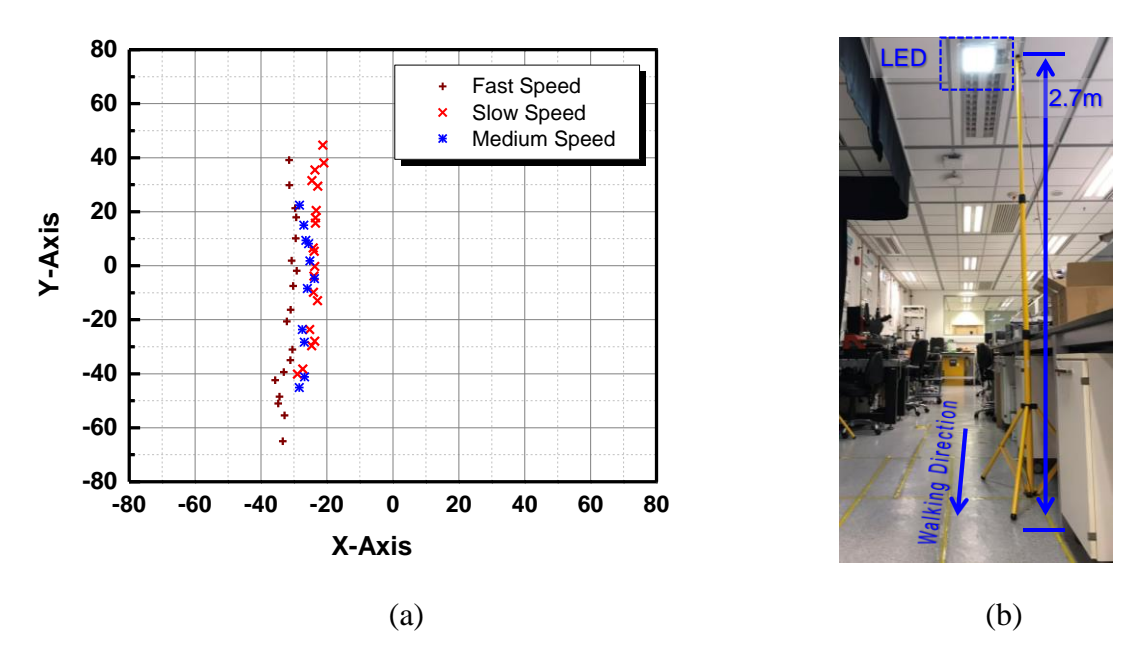


Figure 5.15 Step length estimation experiment: (a) VLP tracking results at three different walking speeds, (b) setup.

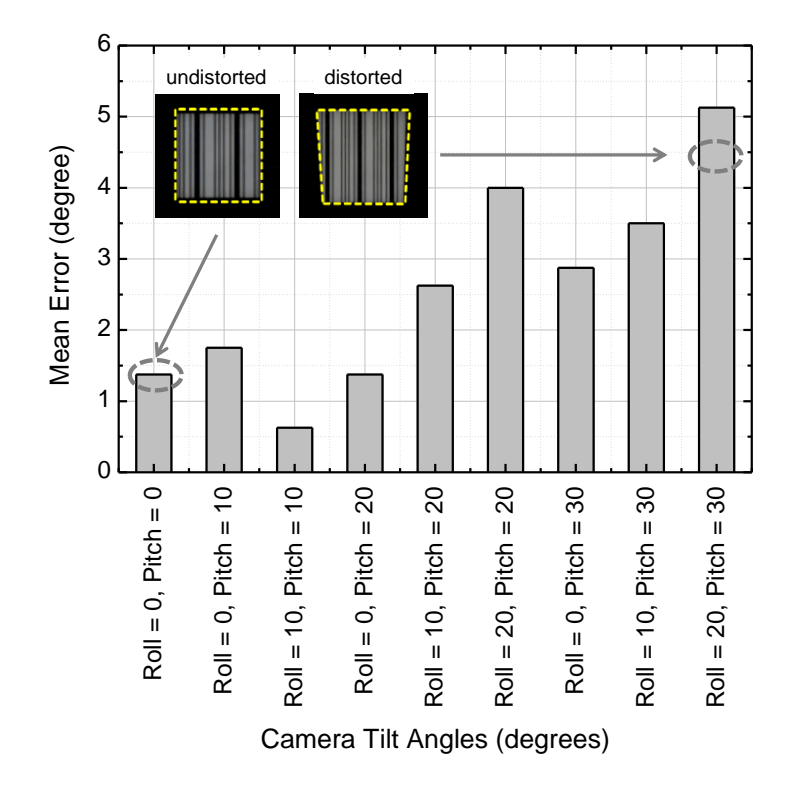


Figure 5.16 Heading angle estimation error due to camera tilt.

5.4.3 Heading Angle Correction

The effect of tilt on the average estimated heading error is shown in Figure 5.16. When the smartphone is tilted, the square shape of the light gets distorted and results in error in the

heading angle estimation. In the experiment, we measured the heading angle estimation error for various smartphone tilt angles by varying the roll and pitch angles from 0° to 30° and 20° respectively. The average heading angle estimation error is directly proportional to the amount of tilt, with maximum recorded error being 5° for the maximum tilt.

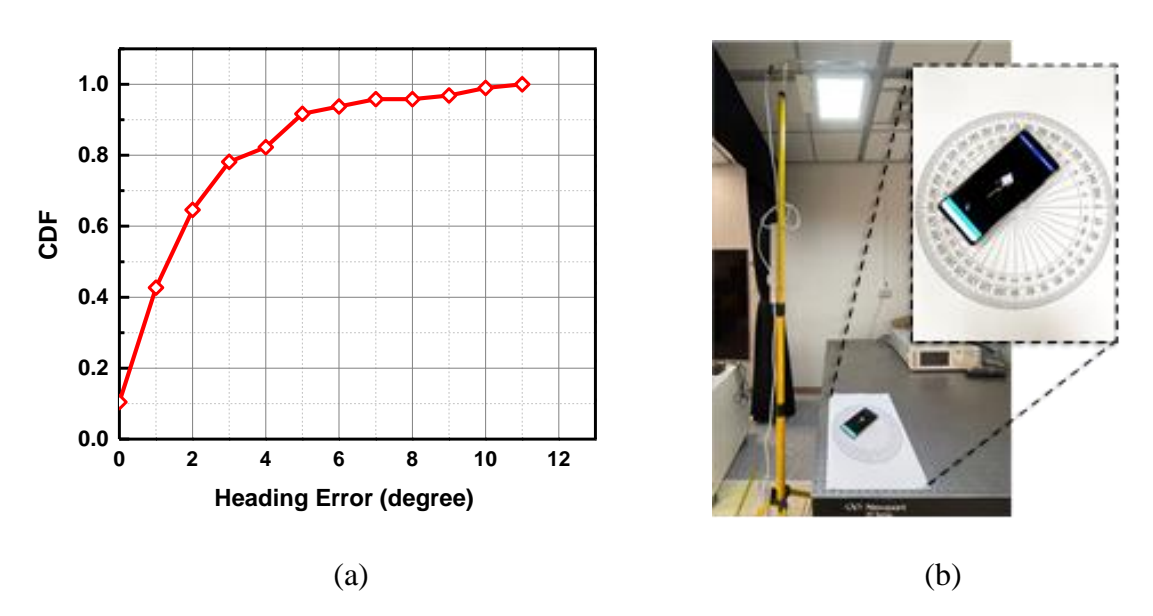


Figure 5.17 VLC heading angle estimation: (a) cumulative density function of heading estimation error (b) measurement setup

Figure 5.17 shows the heading angle estimation measurement setup and the CDF plot of heading angle estimation error for various degrees of tilt, with maximum roll and pitch being 20° and 30° respectively. The graph shows that the mean heading angle estimation error is 2.5°, with 90th percentile error being less than 5°.

5.4.4 Computation Timing

While the output timing of the VLC AoA positioning algorithm is highly critical to the correct step length estimation, it is computationally the most complex part of the algorithm as it involves image processing and VLC ID decoding, which takes a relatively larger number of computations to complete. Therefore, it is imperative that the positioning result of the VLP algorithm from one captured camera frame is available before the camera captures the next frame. The frame capture rate of the smartphone camera is 30 frames per second, which leads

to an available interval of 33 ms for the image conversion, preprocessing, VLC ID decoding, and position and angle calculation. In order to verify the timing performance of the algorithm, we ran the VLC AoA computation algorithm for several instances while the person holding the smartphone was standing under the light and the positioning result was being consecutively output. We then recorded the average frame processing time with a moving average window of about 200 frames. The results are shown in Figure 5.18. They indicate that the average frame processing time is about 16 ms, which is about 50% of the available time and hence can safely meet the timing requirements for the position output rate.

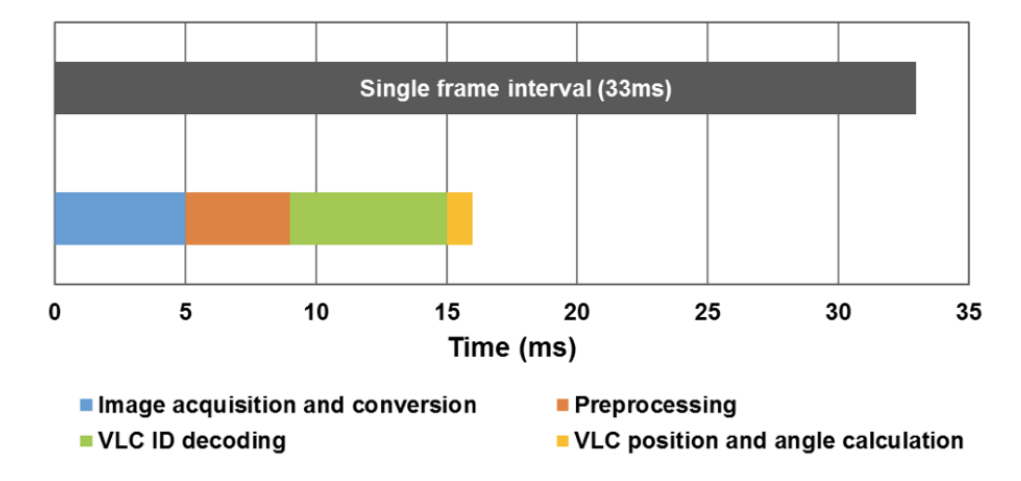


Figure 5.18 VLC AoA algorithm computation time.

5.4.5 Indoor Navigation Performance

The measurement of the VLC- and PDR-based combined positioning approach is performed in an area of 10 m x 10 m, as shown in Figure 5.19. The total path length is about 40 meters with one LED set for position, heading angle and step length calibration. The green box shows the area covered by the VLC light that indicates the range over which the PDR step length and heading direction are calibrated. The true path and the estimated path are shown in the map in blue and red respectively. It can be observed that the estimated path is very close to the ground truth with mean error less than 1 m.

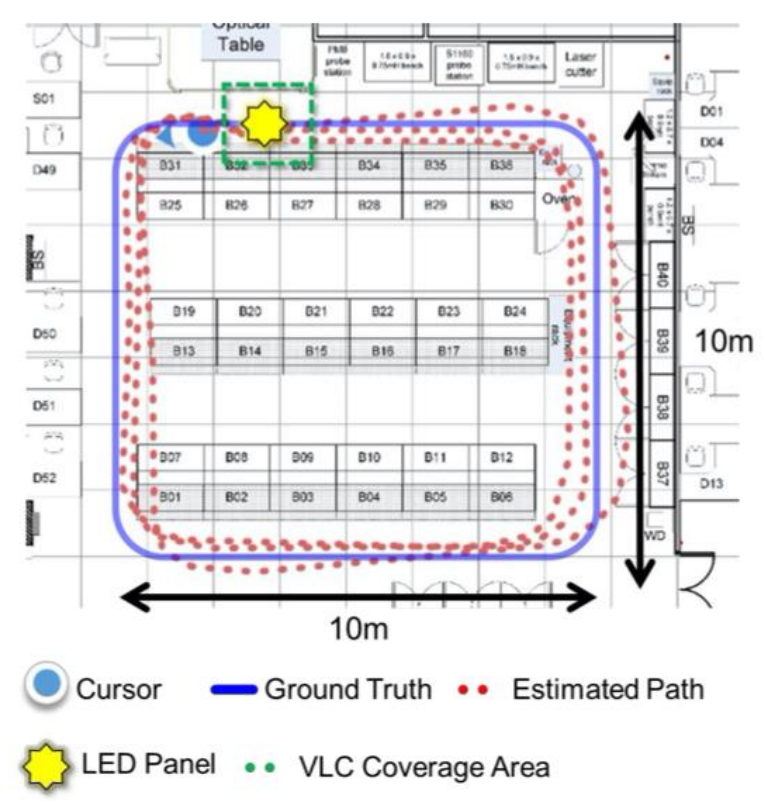


Figure 5.19 Measurement results of combined VLC and PDR combined algorithm in an area of $10~\mathrm{m} \times 10~\mathrm{m}$

5.5 Summary

In this chapter, a visible light communication-assisted pedestrian dead reckoning-based indoor navigation system is presented. Our proposed system, LiDR, uses a high-accuracy VLP location estimate for PDR calibration and step length estimation using the walking speed of the pedestrian as they pass under VLC-embedded smart LED lights. In addition, we use light shape and geometry features for heading angle calibration at a relatively low computation cost as compared to other sensor fusion-based methods proposed in the literature. We evaluated our LiDR system on an Android application, which has our system fully integrated with a digital map based front-end. The experiments conducted in our lab demonstrate that the proposed system can achieve precision of <1 m with a light density of as low as 1 light every 10 m.

In the current stage, we did not consider the scenario that the user keeps the phone in their pocket, which would essentially make LiDR rely only on PDR for navigation. In the future, we

plan to integrate a Bluetooth beacon-based location estimate for scenarios where VLC is not available for prolonged periods of time.

5.6 References

- [1] F. Zafari, I. Papapanagiotou, and K. Christidis, "Micro-location for Internet of Things equipped smart buildings," *IEEE Internet Things J.*, vol. 3, no. 1, pp. 96–112, Feb. 2016.
- [2] W. Kang and Y. Han, "SmartPDR: Smartphone-based pedestrian dead reckoning for indoor localization," *IEEE Sensors J.*, vol. 15, no. 5, pp. 2906–2916, May 2015.
- [3] Q. Tian, Z. Salcic, K. Wang, and Y. Pan, "A multi-mode dead reckoning system for pedestrian tracking using smartphones," *IEEE Sensors J.*, vol. 16, no. 7, pp. 2079–2093, Apr. 2016.
- [4] S. He and S.-H. G. Chan, "Wi-Fi fingerprint-based indoor positioning: Recent advances and comparisons," *IEEE Commun. Surveys Tuts.*, vol. 18, no. 1, pp. 466–490, 1st Quart., 2016.
- [5] R. Liu et al., "Collaborative SLAM based on WiFi fingerprint similarity and motion information," in *IEEE Internet Things J.*, vol. 7, no. 3, pp. 1826-1840, March 2020.
- [6] Y. Zhuang and N. El-Sheimy, "Tightly-coupled integration of WiFi and MEMS sensors on handheld devices for indoor pedestrian navigation," *IEEE Sensors J.*, vol. 16, no. 1, pp. 224–234, Jan. 2015.
- [7] L.-H. Chen, E. H.-K. Wu, M.-H. Jin, and G.-H. Chen, "Intelligent fusion of Wi-Fi and inertial sensor-based positioning systems for indoor pedestrian navigation," *IEEE Sensors J.*, vol. 14, no. 11, pp. 4034–4042, Nov. 2014.
- [8] Z. Chen, Q. Zhu, and Y. C. Soh, "Smartphone inertial sensor-based indoor localization and tracking with ibeacon corrections," *IEEE Trans. Ind. Informat.*, vol. 12, no. 4, pp. 1540–1549, Aug. 2016.
- [9] N. Yu, X. Zhan, S. Zhao, Y. Wu, and R. Feng, "A precise dead reckoning algorithm based on Bluetooth and multiple sensors," *IEEE Internet Things J.*, vol. 5, no. 1, pp. 336–351, Feb. 2018.

- [10] Y. Li, Y. Zhuang, H. Lan, Q. Zhou, X. Niu, and N. El-Sheimy, "A hybrid WiFi/magnetic matching/PDR approach for indoor navigation with smartphone sensors," *IEEE Commun. Lett.*, vol. 20, no. 1, pp. 169–172, Jan. 2016.
- [11] Y. Li, Y. Zhuang, H. Lan, P. Zhang, X. Niu, and N. El-Sheimy, "Selfcontained indoor pedestrian navigation using smartphone sensors and magnetic features," *IEEE Sensor J.*, vol. 16, no. 19, pp. 7173–7182, Oct. 2016.
- [12] H. Chen, F. Li, and Y. Wang, "SoundMark: Accurate indoor localization via peer-assisted dead reckoning," *IEEE Internet Things J.*, vol. 5, no. 6, pp. 4803–4815, Dec. 2018.
- [13] F. Gu, S. Valaee, K. Khoshelham, J. Shang and R. Zhang, "Landmark graph-based indoor localization," *IEEE Internet of Things J.*, vol. 7, no. 9, pp. 8343-8355, Sept. 2020.
- [14] A. Bose and C. H. Foh, "A practical path loss model for indoor WiFi positioning enhancement," in *Proc. 6th Int. Conf. Inf., Commun. Signal Process.*, Dec. 2007, pp. 1–5.
- [15] S. Schmitt, S. Adler, and M. Kyas, "The effects of human body shadowing in RF-based indoor localization," in *Proc. Int. Conf. Indoor Positioning Indoor Navigat.*, Oct. 2014, pp. 307–313.
- [16] L. Wan, G. Han, L. Shu, S. Chan, and N. Feng, "PD source diagnosis and localization in industrial high-voltage insulation system via multimodal joint sparse representation," *IEEE Trans. Ind. Electron.*, vol. 63, no. 4, pp. 2506–2516, Apr. 2016.
- [17] L. E. Diez, A. Bahillo, J. Otegui, and T. Otim, "Step length estimation methods based on inertial sensors: A review," *IEEE Sensors J.*, vol. 18, no. 17, pp. 6908–6926, Sep. 2018.
- [18] J. Qian, L. Pei, D. Zou, K. Qian, and P. Liu, "Optical flow based step length estimation for indoor pedestrian navigation on a smartphone," in *Proc. IEEE/ION Position Location Navig. Symp. (PLANS)*, 2014, pp. 205–211.

- [19] N. Roy, H. Wang, and R. R. Choudhury, "I am a smartphone and I can tell my user's walking direction," in *Proc. ACM MOBISYS*, 2014, pp. 329–342.
- [20] T. Komine and M. Nakagawa, "Fundamental analysis for visible light communication system using LED lights," *IEEE Trans. Consum. Electron.*, vol. 50, no. 1, pp. 100–107, Feb. 2004.
- [21] H. L. Yang, W. Zhong, C. Chen, A. Alphones, and P. Du, "QoS-driven optimized design-based integrated visible light communication and positioning for indoor IoT networks," *IEEE Internet Things J.*, vol. 7, no. 1, pp. 269–283, Jan. 2020.
- [22] LED Lighting Market to Grow to 70 Billion, LightED Mag., St. Louis, MO, USA, 2018.
- [23] S. Ma, Q. Liu, and P. C.-Y. Sheu, "Foglight: Visible light-enabled indoor localization system for low-power IoT devices," *IEEE Internet Things J.*, vol. 5, no. 1, pp. 175–185, Feb. 2018.
- [24] B. Hussain, C. Qiu and C. P. Yue, "Smart lighting control and services using visible light communication and Bluetooth," in 2019 IEEE 8th Global Conference on Consumer Electronics (GCCE), 2019.
- [25] M. F. Keskin, A. D. Sezer, and S. Gezici, "Localization via visible light systems," *Proc. IEEE*, vol. 106, no. 6, pp. 1063–1088, Jun. 2018.
- [26] C. Danakis, M. Afgani, G. Povey, I. Underwood, and H. Haas, "Using a CMOS camera sensor for visible light communication," in *Proc. 31th IEEE GLOBECOM Workshop*, 2012, pp. 1244–1248.
- [27] B. Hussain, et al.: JSAP-OSA Joint Symposia 2017 Abstracts, paper 6p_A409_6.
- [28] X. G. Liu, X. Wei, and L. Guo, "DIMLOC: Enabling high-precision visible light localization under dimmable LEDs in smart buildings," IEEE Internet Things J., vol. 6, no. 2, pp. 3912–3924, Apr. 2019.
- [29] Y. S. Kuo, P. Pannuto, K. J. Hsiao, and P. Dutta, "Luxapose: Indoor positioning with mobile phones and visible light," in *Proc. ACM MobiCom*, 2014, pp. 447–458.
- [30] R. Zhang, W.-D. Zhong, K. Qian, and S. Zhang, "A single LED positioning system based on circle projection," *IEEE Photon. J.*, vol. 9, no. 4, pp. 1–9, Aug. 2017.

- [31] Y. Hou et al., "Single LED beacon-based 3-D indoor positioning using off-the-shelf devices," *IEEE Photon. J.*, vol. 8, no. 6, pp. 1–11, Dec. 2016.
- [32] Z. Li, A. Yang, H. Lv, L. Feng, and W. Song, "Fusion of visible light indoor positioning and inertial navigation based on particle filter," *IEEE Photon. J.*, vol. 9, no. 5, Oct. 2017.
- [33] H. Huang et al, "Hybrid indoor localization scheme with image sensor-based visible light positioning and pedestrian dead reckoning," Appl. Opt., vol. 58, (12), pp. 3214-3221, 2019.
- [34] Y. Wang and H. Zhao, "Improved smartphone-based indoor pedestrian dead reckoning assisted by visible light positioning," *IEEE Sensors J.*, vol. 19, no. 8, pp. 2902–2908, Apr. 2019.
- [35] F. Gu, K. Khoshelham, C. Yu, and J. Shang, "Accurate step length estimation for pedestrian dead reckoning localization using stacked autoencoders," *IEEE Trans. Instrum. Meas.*, vol. 68, no. 8, pp. 2705–2713, Aug. 2019.
- [36] J. W. Kim, H. J. Jang, D.-H. Hwang, and C. Park, "A step, stride and heading determination for the pedestrian navigation system," *J. Global Position. Syst.*, vol. 3, nos. 1–2, pp. 273–279, Dec. 2004.
- [37] B. Huang, G. Qi, X. Yang, L. Zhao, and H. Zou, "Exploiting cyclic features of walking for pedestrian dead reckoning with unconstrained smartphones," in *Proc. ACM Int. Joint Conf. Pervasive Ubiquitous Comput. (UbiComp*), 2016, pp. 374–385.
- [38] H. Weinberg, "Using the ADXL202 in pedometer and personal navigation applications," *Anal. Devices*, vol. 2, no. 2, pp. 1–6, 2002.
- [39] H. Gao and P. D. Groves, "Context determination for adaptive navigation using multiple sensors on a smartphone," in *Proc. ION GNSS*+, Portland, OR, USA, Sep. 2016, pp. 1–15.
- [40] A. Martinelli, H. Gao, P. D. Groves, and S. Morosi, "Probabilistic context-aware step length estimation for pedestrian dead reckoning," *IEEE Sensors J.*, vol. 18, no. 4, pp. 1600–1611, Feb. 2018.

- [41] Q. Wang, L. Ye, H. Luo, A. Men, F. Zhao, and C. Ou, "Pedestrian walking distance estimation based on smartphone mode recognition," *Remote Sens.*, vol. 11, no. 9, p. 1140, May 2019.
- [42] Q. Wang, L. Ye, H. Luo, A. Men, F. Zhao, and Y. Huang, "Pedestrian stride-length estimation based on LSTM and denoising autoencoders," *Sensors*, vol. 19, no. 4, p. 840, Feb. 2019.
- [43] J. Hannink et al., "Mobile stride length estimation with deep convolutional neural networks," *IEEE J. Biomed. Health Inform.*, vol. 22, no. 2, pp. 354–362, Mar. 2018.
- [44] Q. Wang et al., "Personalized stride-length estimation based on active online learning," *IEEE Internet Things J.*, early access, Feb. 04, 2020, doi: 10.1109/JIOT.2020.2971318.
- [45] L. Zheng, X. Zhan, X. Zhang, S. Wang, and W. Yuan, "Heading estimation for multimode pedestrian dead reckoning," *IEEE Sensors J.*, vol. 20, no. 15, pp. 8731–8739, Aug. 2020.
- [46] F. Evennou, F. Marx, and E. Novakov, "Map-aided indoor mobile positioning system using particle filter," in *Proc. IEEE Wireless Commun. Netw. Conf.*, Mar. 2005, pp. 2490–2494.
- [47] L. L. Shen and W. W. S. Hui, "Improved pedestrian dead-reckoning-based indoor positioning by rssi-based heading correction," *IEEE Sensors J.*, vol. 16, no. 21, pp. 7762–7773, Nov. 2016.
- [48] Z. Li, X. Zhao, F. Hu, Z. Zhao, J. L. Carrera Villacrés and T. Braun, "SoiCP: A seamless outdoor–indoor crowdsensing positioning system," in *IEEE Internet of Things Journal*, vol. 6, no. 5, pp. 8626-8644, Oct. 2019.
- [49] R. Harle, "A Survey of indoor inertial positioning systems for pedestrians," in *IEEE Communications Surveys & Tutorials*, vol. 15, no. 3, pp. 1281-1293, Third Quarter 2013
- [50] A. R. Pratama and H. R. Widyawan, "Smartphone-based pedestrian dead reckoning as an indoor positioning system," in *Proc. Int. Conf. Syst. Eng. Technol. (ICSET)*, Sep. 2012, pp. 1–6.

[51] M. Holzl, R. Neumeier, and G. Ostermayer, "Analysis of compass sensor accuracy on several mobile devices in an industrial environment," in *Computer Aided Systems Theory - EUROCAST 2013*, R. Moreno-D'1az, F. Pichler, and A. Quesada-Arencibia, Eds. Berlin, Heidelberg: Springer Berlin Heidelberg, 2013, pp. 381–389.

CHAPTER 6 Conclusion, Future Work and Publications

6.1 Summary of Contributions

In this thesis, OCC-based Li-Fi system design is presented that enables IoT connectivity and location-based intelligence in optical devices and equipment including, LED lightings, signage, and displays. The key contributions of the thesis are divided in to three parts as follows:

- (1) On the transmitter side, a universal Li-Fi modulator design is presented that can enable OCC link in a wide variety of LED lighting, signage and displays. The proposed design is capable of handling a wide input voltage and power range, and features lower number of onboard components and implementation cost as compared to integrated Li-Fi driver designed proposed in the prior works. In addition, the modulator features a Bluetooth-based wireless control and iBeacon-based proximity sensing to support IoT connectivity and location-based geofencing. Measurement results are conducted to verify the modulators function, as well as performance and reliability including long-term impact on LED lightings power consumption, lumens and color temperature.
- (2) On the receiver side, an OCC system is realized using rolling shutter camera of a smartphone. The impact of various system parameters including light size, shape, color and smartphone camera hardware, on receiver's sensitivity and detection range is studied. Based on the analysis, practical OCC receiver design guidelines are established. Given the system specifications, modulation and coding scheme parameters are derived including frequency and packet size, etc., to achieve the target communication distance.
- (3) The transceiver design presented in the aforementioned two parts is utilized to build a Li-Fi and Bluetooth integrated smart lighting infrastructure to enable high accuracy indoor localization in large-scale venues. The high accuracy VLC-based indoor positioning algorithm using camera projection technique is implemented on smartphone, that is complimented with long-range non-LoS Bluetooth and inertial sensor-based pedestrian dead reckoning (PDR) algorithm to provide a continuous and smooth indoor positioning experience in various indoor

environment with varying density of lightings. The system is deployed in a $10m \times 10m$ area and is shown to achieve a positioning accuracy of < 0.5m.

6.2 Future Work

The high-accuracy indoor positioning and location-based information delivery system presented in the thesis will serve as a platform for further research in following key areas.

6.2.1 Indoor Farming Control and Management using VLC integrated Smart Grow Lights

Efficient utilization of resources including, energy, space, and labor cost, is critical for building sustainable indoor farms. Automation through status monitoring sensors can help to reduce the cost in conventional monoculture indoor farms that are growing a single type of crop. However, management and control of individual crops becomes highly challenging when a variety of crops are grown in a small area with each requiring different conditions and growth rate leading to a high maintenance cost.

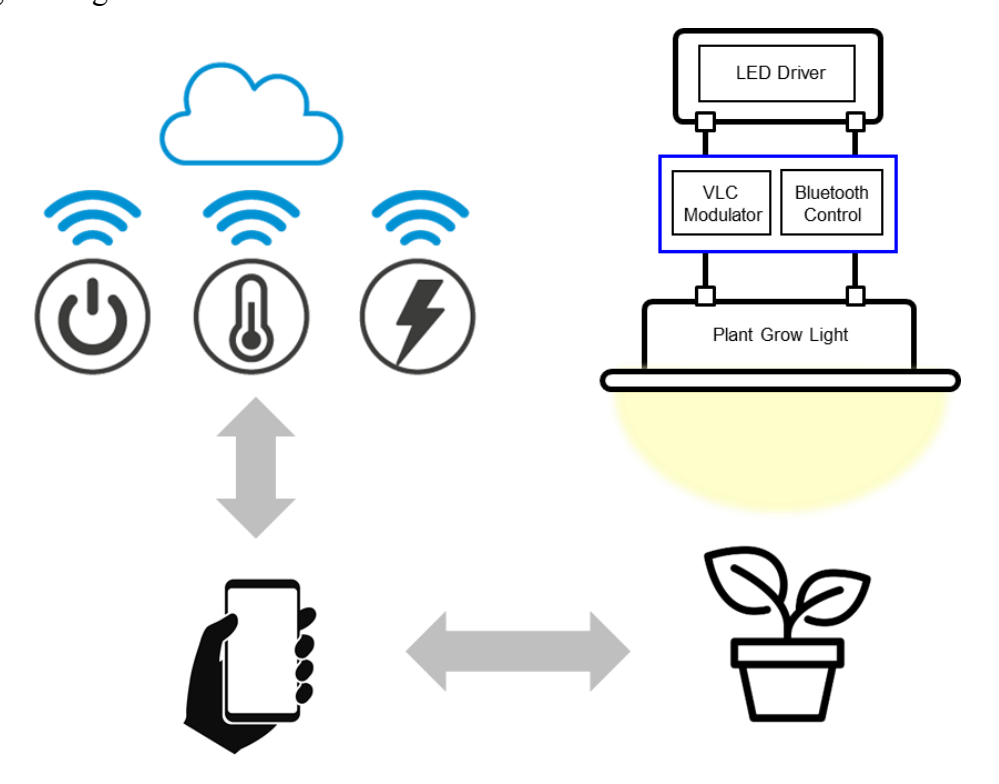


Figure 6.1 VLC-based Smart Farming System Architecture

In this research, an indoor farming control and management system will be proposed that utilizes the VLC-based high accuracy localization technology to address the above problem.

By integrating the VLC function in LED grow lights, the proposed system will use the line-of-sight property of VLC to uniquely identify, monitor and control the growth of each plant in an indoor farm by using a smartphone application. In addition, the integrated Bluetooth-based wireless control in grow RGB LED lights will be used for remotely controlling the lighting intensity and color temperature to excite specific growth hormones in plants for optimizing the plant growth. A cloud-based farm management and control platform will be built to collect and store the information about crops including temperature, water, humidity, and growth status. The data stored in the cloud will be used for building machine-learning models to continuously optimize the use of resources to achieve maximum growth. The system architecture is illustrated in Figure 6.1.

6.2.2 Smart Home Appliance Control and Location-Based Access

Smart home devices are becoming increasingly popular nowadays, with several well-known products in the market from Amazon, Google, and Xiaomi. Generally, a smart home device features either WiFi or Bluetooth and is controlled via a smartphone application, for instance, a smart light bulb, or a smart curtain. Controlling and managing one or two such devices is straightforward, however, as the number of devices continue to grow, connectivity and control becomes increasingly challenging. There could be several devices within the radio range of the smartphone, yet the user cannot filter the relevant devices based on his/her location due to the lack of location context and directionality in both appliances and smartphone.

In this research, a high-accuracy 3D localization system using a ceiling light will be proposed that can tell the location and the orientation of the smartphone within accuracy of 10 cm and 5 degrees, respectively. The proposed system will allow the user to control appliances using both location and orientation. For instance, the user could point the smartphone towards the TV to connect and control, or walk close to the door to automatically unlock the door.

6.3 Publications

6.3.1 Works under review

[1] **B. Hussain**, Y. Wang, J. Cheng, R. Chen, and C. P. Yue, "LiDR: Visible Light Communication-Assisted Dead Reckoning for Accurate Indoor Localization," *IEEE Internet of Things Journal (submitted and under review)*.

6.3.2 Published

- [1] **B. Hussain**, C. Qiu and C. P. Yue, "A Universal VLC Modulator for Retrofitting LED Lighting and Signage," *2019 IEEE 8th Global Conference on Consumer Electronics*, p. 1008-1009, Oct. 2019.
- [2] **B. Hussain**, C. Qiu and C. P. Yue, "Smart Lighting Control and Services using Visible Light Communication and Bluetooth," *2019 IEEE 8th Global Conference on Consumer Electronics*, p. 1-2, Oct. 2019.
- [3] **B. Hussain**, X. Li, C.Y. Lee, C. P. Yue, "Smart LCD displays with modulated LED backlights for Li-Fi enabled applications," *OPJ-OSA Joint Symposia on Optics*, paper 31aAJ4, Nov. 2018.
- [4] **B. Hussain**, C. Lau, C. P. Yue, "Li-Fi based secure programmable QR code (LiQR)," *JSAP-OSA Joint Symposia*, Sep. 2017.
- [5] **B. Hussain**, X. Li, F. Che, C. P. Yue, and L. Wu, "Visible Light Communication System Design and Link Budget Analysis," *IEEE/OSA Journal of Lightwave Technology*, vol. 33, no. 24, pp. 5201–5209, Dec. 2015.
- [6] **B. Hussain**, F. Che, F. Zhang, T. Yim, W.H. KI, L. Wu, C.P. Yue, "A fully integrated IEEE 802.15.7 visible light communication transmitter with on-chip 8-W 85% efficiency boost LED driver," *IEEE Symposium on VLSI Circuits*, Jun. 2015, pp. 216-217.

- [7] Y. Wang, **B. Hussain**, and C. P. Yue. "Arbitrarily tilted receiver camera correction and partially blocked LED image compensation for indoor visible light positioning," *IEEE Sensors Journal*, 2021 (early access). Doi: 10.1109/JSEN.2021.3057103.
- [8] X. Li, **B. Hussain**, J. Kang, H. S. Kwok and C. P. Yue, "Smart μLED display-VLC system with a PD-based / camera-based receiver for NFC applications," *IEEE Photonics Journal*, vol. 11, no. 1, Feb. 2019.
- [9] C. Qiu, **B. Hussain** and C. P. Yue, "Bluetooth Based Wireless Control for iBeacon and VLC Enabled Lighting," *2019 IEEE 8th Global Conference on Consumer Electronics*, p. 614-615, Oct. 2019.
- [10] X. Li, B. Hussain, L. Wang, J. Jiang and C. P. Yue, "Design of a 2.2-mW 24-Mb/s CMOS VLC receiver SoC with ambient light rejection and post-equalization for Li-Fi applications," *IEEE/OSA Journal of Lightwave Technology*, vol. 36, no. 12, pp. 2366– 2375, Jun. 2018.
- [11] X. Li, **B. Hussain**, J. Kang, H. S. Kwok and C. P. Yue, "Smart micro-LED display with synchronized information broadcast for enhanced user interaction," *International Display Workshops*. pp. 421–424, Dec. 2018.
- [12] L. Sun, X. Li, **B. Hussain** and C. P. Yue, "An adaptive threshold decoding algorithm for visible light communication data recovery from LED-based display systems," *IEEE Photonics Conference*, pp. 239-240, Oct. 2017.
- [13] L. Sun, **B. Hussain**, X. Li, G. Zhu and C. P. Yue, "A micro-LED driver with bandwidth expansion for visible light communications," *JSAP-OSA Joint Symposia*, paper 6p_A410_5, Sep. 2017.
- [14] X. Li, **B. Hussain**, L. Wang, J. Jiang and C. P. Yue, "A 2.2-mW 24-Mb/s CMOS LiFi receiver system-on-a-chip with ambient light rejection and post-equalization," *IEEE Photonics Conference*, pp. 29-30, Oct. 2017.
- [15] Xianbo Li, Liang Wu, Zhaojun Liu, **Babar Hussain**, Wing Cheung Chong, Kei May Lau, C Patrick Yue, "Design and Characterization of Active Matrix LED Microdisplays

- with Embedded Visible Light Communication Transmitter," *IEEE/OSA Journal of Lightwave Technology*, vol. 34, no. 14, pp. 3349–3457, Jul. 2016.
- [16] X. Li, W. K. Cho, **B. Hussain**, H. S. Kwok and C. P. Yue, "Micro-LED display with simultaneous visible light communication function," *SID Symposium Digest of Technical Papers*, vol. 49, no. 1, pp. 876–879, May 2018.
- [17] Fengyu Che, Liang Wu, **Babar Hussain**, Xianbo Li, and C. Patrick Yue, "A Fully Integrated IEEE 802.15.7 Visible Light Communication Transmitter With On-Chip 8-W 85% Efficiency Boost LED Driver," *IEEE/OSA Journal of Lightwave Technology*, vol. 34, no. 10, pp. 2419–2430, May 2016.
- [18] L. Wang, **B. Hussain**, X. Li and C. P. Yue, "Modulation optimization for visible laser light communication systems," IEEE Photonics Conference, pp. 301-302, Oct. 2017.
- [19] Y. Wang, W. Guan, B. Hussain, and C. Patrick Yue, "High Precision Indoor Robot Localization Using VLC Enabled Smart Lighting," the 2021 Optical Fiber Communication Conference and Exhibition (OFC), June 06-11, 2021.
- [20] Liang Wu, Xianbo Li, Wing Cheung Chong, Zhaojun Liu, Fengyu Che, **Babar Hussain**, Kei May Lau, C Patrick Yue,, "An AMLED microdisplay driver SoC with built-in 1.25Mb/s VLC transmitter," in *IEEE Symposium on VLSI Circuits*, pp. C328–C329, Jun. 2015.